Effects of Inorganic Carbon on Cyanobacterial Phycobiliprotein Fluorescence

LUKE SAMUEL MOORE

Effects of Inorganic Carbon on Cyanobacterial Phycobiliprotein Fluorescence

Luke Moore

Department of Biosciences, Durham University

For The Degree of Masters of Science

Supervised by Prof. Martin J. Cann & Dr. Lars- Palsson

06/09/2024

Table of Contents

Abbreviations

2-PG	2-phosphoglycolate
AEF	alternative electron flow
Apc	Allophycocyanin
ApcA	Allophycocyanin alpha subunit
ApcB	Allophycocyanin beta subunit
ATP	Adenosine triphosphate
CBB	Calvin-Bensson-Bassham cycle
CCM	carbon-concentration mechanism
Cpc	C-phycocyanin
CpcA	C-phycocyanin alpha subunit
CpcB	C-phycocyanin beta subunit
E. coli	*Escherichia coli*
EET	Electronic energy transfer
IMAC	Immobilised metal affinity chromatography
LA	Luria Agar
LB	Luria Broth
M_r	Relative Molar Mass
NADP	Nicotinamide adenine dinucleotide phosphate
NMR	nuclear magnetic resonance
PAGE	Polyacrylamide gel electrophoresis
PBP	Phycobiliprotein
PBS	Phycobilisome
PC	Phycocyanin
PE	Phycoerythrin
PET	photosynthetic electron transport
PSI	Photosystem I
PSII	Photosystem II
PTM	Post-translational modification
RFU	Relative fluorescence units
ROF	Reactive oxygen species
RPM	Rotations per minute
RuBisCO	ribulose-1,5-bisphosphate carboxylase/oxygenase
RuBP	1,5-ribulose bisphosphate
S. sp. 6803	*Synechocystis sp.* PCC *6803 / Kazusa*
S. sp. 7002	*Synechococcus sp.* PCC *7002*
SEC	Size exclusion chromatography
TEO	triethyloxonium tetrafluoroborate
UV-Vis-NIR	Ultraviolet-Visible-Near Infrared
WT	Wild type

Abstract

Cyanobacteria have the potential to be energy-efficient sources of biofuels and high-value chemicals. However, they are not currently viable as cell factories on industrial scales, because high-production strains need to be engineered. To unlock their industrial potential, one promising approach is to optimize their carbon-dioxide-based regulatory pathways. Previous research has demonstrated that reversible carbamylation of the phycobiliprotein allophycocyanin A of *Synechocystis* sp. PCC6803 regulates electronic energy transfer in the cyanobacterial phycobilisome. Using *in vitro* analysis of purified proteins, this study demonstrates that the phycobiliprotein c-phycocyanin may also experience enhancement of energy transfer due to carbamylation mediated by elevated carbon dioxide concentrations.

Introduction

Cyanobacteria

The currently employed technologies for producing renewable energy include biomass, wind, sunlight, and geothermal power (Farrokh et al., 2019). Cyanobacteria are a potential source of biofuels on an industrial scale. Another potential biofuel source that has been researched extensively for optimisation is lignocellulosic biomass (Raud et al., 2019). The major advantage of cyanobacteria for industrial biomass production is their photosynthetic ability to utilise atmospheric CO_2 as a carbon source and sunlight as an energy source. Their benefits include a much greater conversion of solar energy into biomass (9% for cyanobacteria compared with 0.5-3% for higher plants respectively) and the potential for growth of cyanobacteria in waste or salt water (Khan et al., 2019). However, cyanobacteria are not currently viable as cell factories on an industrial scale (Khan et al., 2019). Various studies have demonstrated the capacity of cyanobacteria to produce commercially relevant chemicals such as alcohols, fatty acids, diols, and organic acids (Table 1). A large body of research exists on strategies to improve cyanobacterial productivity. However, cyanobacteria are currently only used for limited-scale production. High-production strains must be genetically engineered to achieve commercial viability and inexpensive infrastructure must be developed to grow biomass and harvest the products (Khan et al., 2019). Research into the effects of CO_2 on photosynthetic apparatus is vital for understanding growth limitations that may currently be preventing the scaling-up of cyanobacteria growth and for engineering more efficient strains in the future (Novoveská et al., 2023).

Table 1: List of industrially important chemicals produced by cyanobacterial strains, engineering strategies used, and cultivation conditions. Table adapted from (Khan et al., 2019).

Host Strain	Chemicals	Production (mg/L)	References
S. elongatus UTEX 2973	Sucrose	35.5/h	(Song et al., 2016)
S. elongatus PCC 7942	Sucrose	36.1/h	(Ducat & Silver, 2012)
S. elongatus PCC 7942	Sucrose	28.3/d	(Weiss et al., 2017)
Synechocystis sp. PCC6803	Ethanol	212/d	(Gao et al., 2012)
S. elongatus PCC 7942	Squalene	7.08/OD_{730}	(Choi et al., 2017)

Carbon Availability and Photosynthesis

The first cyanobacteria could have arisen as long as 2.6-2.7 billion years ago (Shestakov & Karbysheva, 2017). The proportion of carbon dioxide (CO_2) in the Earth's atmosphere has varied greatly over the span of cyanobacterial life. Local CO_2 compositions in many biological niches also differ significantly from the majority of the atmosphere (Cummins et al., 2014). Generating organic materials by fixing inorganic carbon is one of the fundamental processes supporting all life on Earth. The Calvin-Bensson-Bassham cycle (CBB) is the primary pathway through which CO_2 is fixed into biomass, and it is mediated by enzymes from the family ribulose-1,5-bisphosphate carboxylase/oxygenase (RuBisCO). Several other pathways exist in prokaryotes. However, the CBB cycle is used by cyanobacteria and all photosynthesising plants (Fuchs, 2011). RuBisCO is responsible for the only quantitatively relevant conversion of inorganic to organic carbon (Iñiguez et al., 2020). It is believed that RuBisCO activity accounts for a large majority of atmospheric CO_2 fixation, as it can

comprise as much as 50% of total soluble protein within photosynthetic microbes and plant leaves (Andersson & Backlund, 2008).

RuBisCO catalyses the binding of CO_2 to the sugar 1,5-ribulose bisphosphate (RuBP), a major early step of carbon fixation (Kacar et al., 2017). RuBisCO I present in cyanobacteria, and its active site must be activated through sequential carbamylation of a particular lysine side chain and subsequent binding of Mg^{2+} (Blake & Cann, 2022). In addition to catalysing the carboxylation of RuBP, RuBisCO also catalyses a competing oxygenation reaction, producing one 3-phosphoglycerate and one 2-phosphoglycolate (2-PG) molecule. 2-PG inhibits central carbon metabolism, meaning the oxygenation reaction can reduce carbon fixation by as much as 50% (Blake & Cann, 2022).

Throughout RuBisCO's evolution, the atmospheric concentration of CO_2 decreased, and the concentration of O_2 has increased. The shift in the concentrations of RuBisCO's two substrates created a need for carbon-concentration mechanisms (CCMs), which likely co-evolved with RuBisCO kinetic characteristics (Iñiguez et al., 2020). The carboxysome is a compartment in bacteria that contains RuBisCO and carbonic anhydrase, which catalyses the reversible transformation of CO_2 to HCO_3^- (bicarbonate) (Hagemann et al., 2021). Other essential components of CCMs include active CO_2 uptake systems, HCO_3^- transport, and carbonic anhydrase (Forchhammer & Selim, 2020). When inorganic carbon is limited, CCMs are strongly upregulated (Forchhammer & Selim, 2020). CCMs involve multiple carbon uptake systems associated with NA^+ and H^+ gradients.

Post-translational modifications and carbamylation

Post-translational modifications (PTMs) of proteins are amino acid side chain modifications that occur after proteins are synthesised, which are essential for protein function. Experimental techniques for discovering PTMs are often labour-intensive and protracted (Ramazi & Zahiri, 2021).

CO_2 interacts with RuBisCO in two capacities, both as a substrate and cofactor through carbamylation of the active site. The carbamylation PTM is caused by nucleophilic attack by CO_2 on amino groups and significantly impacts the functionalities of RuBisCO (Linthwaite et al., 2018).

Carbamylation involves the attachment of CO_2 to lysine ε-amino- or N-terminal α-amino- groups (Figure 1, Figure 2). Other proteins that depend on carbamylation include haemoglobin, β-lactamase, ubiquitin, urease, and connexin 26 (Figure 3).

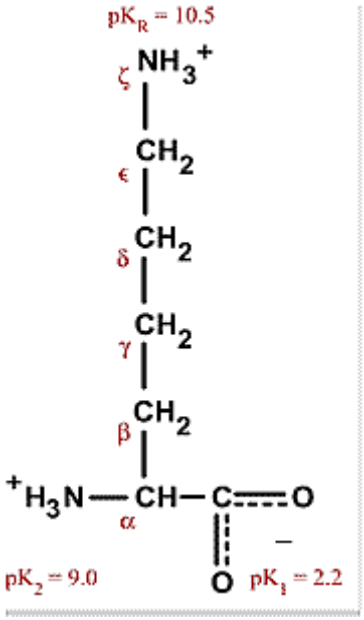

Figure 1: Lysine atomic structure with labelled amino groups. Figure copied from: (*Basic Amino Acids*, 2003)

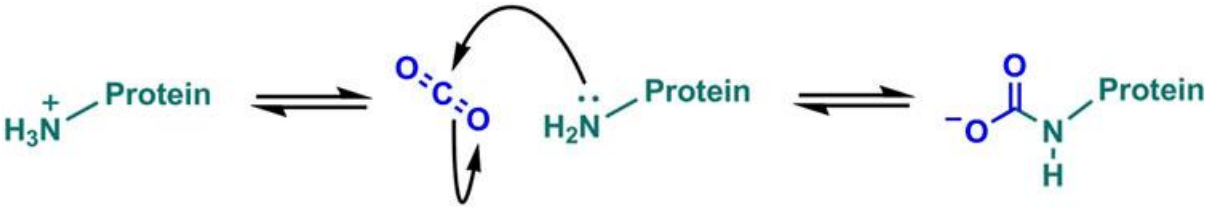

Figure 2: Carbamates can form due to a reversible interaction between neutral amino groups and CO_2. Figure copied from: (Blake & Cann, 2022).

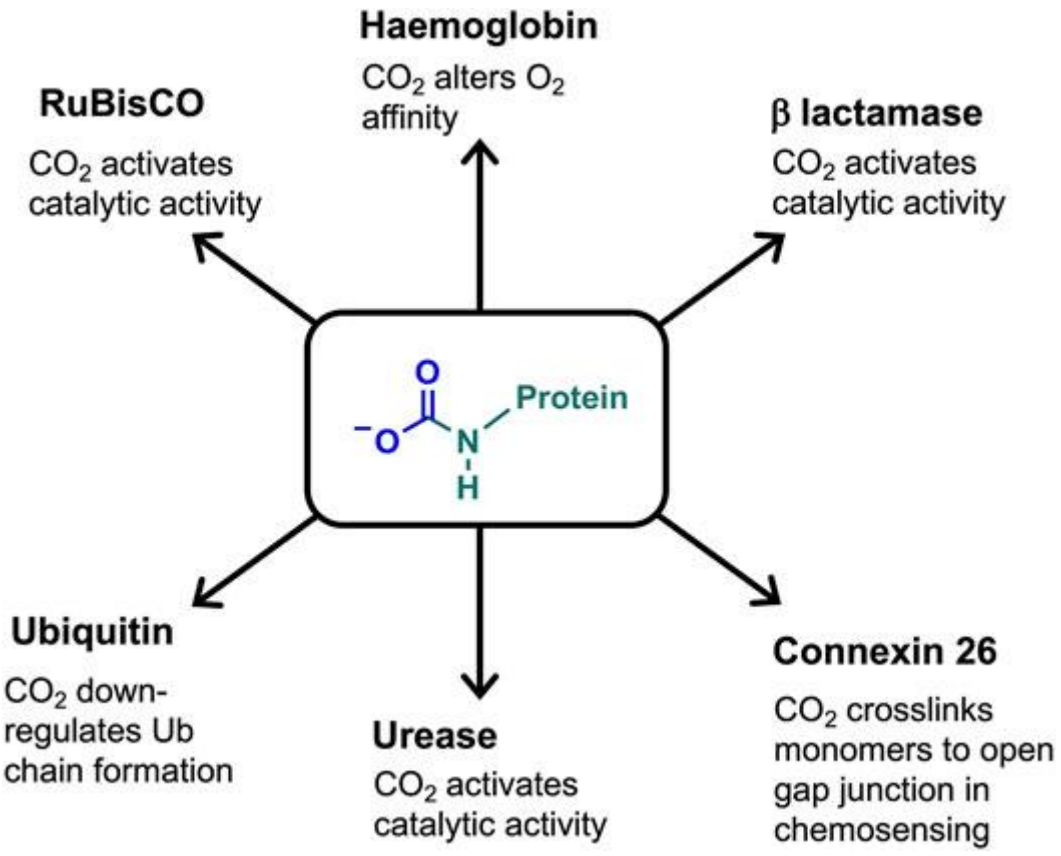

Figure 3: a selection of CO_2-binding proteins with previously described roles of the carbamate PTM. Figure copied from: (Blake & Cann, 2022).

Hypotheses regarding the involvement of carbamylation in protein regulation were first posed in the 1970s and 1980s. However, methods for trapping carbamates for a sufficient time to observe them directly did not exist at the time (Blake & Cann, 2022). Reversible carbamylation can be maintained by specific pH environments, such as those found within haemoglobin, or through stabilising reactions, such as those observed in RuBisCO (Linthwaite et al., 2018). Early attempts at identifying PTMs, such as carbamates, relied on electrospray ionisation mass spectrometry. They successfully demonstrated the presence of carbamates but could not locate the positions of such modifications (Terrier & Douglas, 2010). Recently, the Cann group developed a method for trapping carbamate PTMs on proteins, peptides, and amino acids. Their method involves selectively derivatising labile carbamates via ethylation, resulting in a sufficiently stabilised carbamate for downstream analysis (Linthwaite et al., 2018). The water-soluble Meerwein reagent triethyloxonium tetrafluoroborate (TEO) was investigated to alkylate labile CO_2 PTMs, thus trapping them. The TEO-based method was

validated by detecting the presence of a previously identified carbamylated site on haemoglobin. The same trapping and detection methodology was applied to denatured haemoglobin to demonstrate the need for the privileged pH environment in haemoglobin to exist for stable carbamates. Their methods can also be used for proteins within whole cells with identical results to the analysis of isolated proteins (Linthwaite et al., 2018). A major advantage of the TEO-based method is that it can identify carbamates under physiologically relevant conditions. Subsequently, another group developed a method for detecting lysine sites that undergo carbamylation using the CO_2 analogue isocyanic acid. Isocyanic acid competes with CO_2 at the carbamylation site in a concentration-dependent manner that allows quantitative detection of carbamylation sites, and this method mitigates the risk of false positives from non-specific probes (King et al., 2022).

Photosystem I and Photosystem II

During cyanobacterial photosynthesis, photosystem I (PSI) and photosystem II (PSII) within the thylakoid membrane absorb energy from photons and oxidise the chlorophyll reaction centres to propel photosynthetic electron transport (PET) from H_2O to $NADP^+$. Through multiple steps, electrons from H_2O are transferred to $NADP^+$ in the PET system. PET forms a proton gradient across the thylakoid membrane, which is necessary for ATP synthase function and, therefore, for ATP production. NADPH and ATP generated during PET function as energy donors in the CBB cycle (Shimakawa et al., 2016).

Under high light incidence or low CO_2 concentration conditions, $NADP^+$ regeneration is a rate-limiting step during PET unless a pathway for alternative electron flow (AEF) can be utilised. In *S. 6803* an AEF dependent on O_2 can be induced by low CO_2 concentration.

When $NADP^+$ regeneration is limited, the accumulation of electrons in the PET system can form reactive oxygen species (ROS). Accumulated electrons are transferred to O_2 on the electron acceptor side of PSI of the thylakoid membrane, which leads to the production of H_2O_2 and O_2^-. ROS production leads to oxidative stress and the inactivation of PSI (Shimakawa et al., 2016).

Phycobilisomes

Phycobilisomes (PBS) are large pigment-protein complexes embedded into the thylakoid membrane of cyanobacteria that house the various photosynthetic light-harvesting proteins. They may constitute up to 50% of the cell's soluble protein (*The Phycobilisome, a Light-Harvesting Complex Responsive to Environmental Conditions*, n.d.). They harvest incident light and transmit the energy through a network of pigments (bilins) to the chlorophyll in the photosynthetic reaction centres (Domínguez-Martín et al., 2022; Li et al., 2023). Phycobilisomes mainly comprise phycobiliproteins (PBPs) bound to linker proteins. Two predominant PBPs are phycoerythrin (PE) (which absorbs green light) and phycocyanin (PC) (which absorbs red light) (Montgomery, 2017). PC and PE are commercially valuable products with potential for use as food colourants, nutritional supplements, and immunological assays (Hsieh-Lo et al., 2019).

An important feature of PBS function is that pigments are bound to the phycobiliproteins in a structure that establishes a resonance energy cascade leading from the outer areas to the centre of the PBS, which ensures that the energy transfer is unidirectional towards the chlorophyll in the core, and eventually to the PSII reaction centre ((Domínguez-Martín et al., 2022; J.-Y. Lin et al., 2022). Phycobilisomes absorb wavelengths in the range of 450-650nm. Importantly, cyanobacterial PBSs can absorb solar light of specific wavelength ranges poorly absorbed by chlorophyll (Dartnell et al., 2011). Remarkably, at fluencies typically encountered during cyanobacterial growth, electronic energy transfer (EET) efficiency is estimated to be almost 100% (Adir et al., 2020). The disadvantage of these highly efficient light harvesting apparatuses is the deadly effect of excess energy transmitted in the cell when it is not utilised in photosynthesis. All photosynthetic organisms have mechanisms to dissipate excess energy into heat. In cyanobacteria, 60-80% of captured light energy undergoes non-photochemical quenching (Domínguez-Martín et al., 2022).

The structure of the cyanobacterial PBS has been determined using electron microscopy. It comprises a core of cylinders with attached rods that radiate outwards (Figure 4). The core cylinders

comprise allophycocyanin (Apc), and the rods are mainly phycocyanin (PC). The Apc α and β subunits are in a 1:1 molar ratio, each containing a chromophore called phycocyanobilin (MacColl, 2004). The blue pigmentation of the biliproteins is why cyanobacteria were previously called blue-green algae (Dartnell et al., 2011). In some cyanobacterial species, the distal segments of the PBS rods can accommodate other chromophores, such as PE or phycoerythrocyanin, to give them the capacity for chromatic adaptation. (Dartnell et al., 2011).

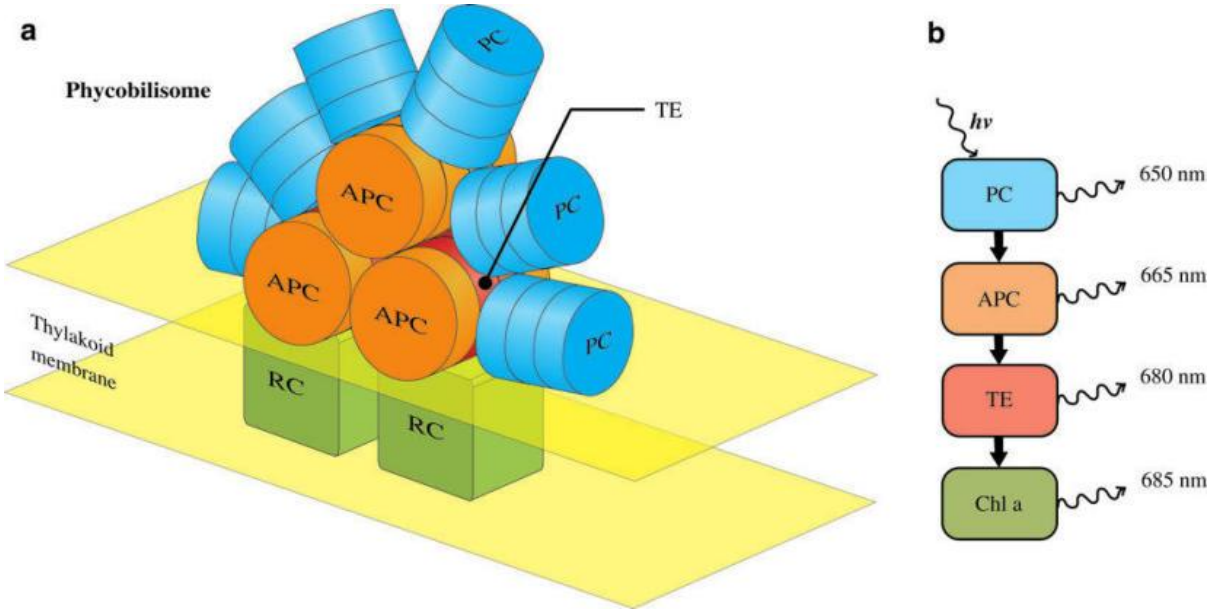

Figure 4: Phycobilisome structure of Synechocystis PCC 6803. *Six phycocyanin (PC) rods are bound to three central allophycocyanin (APC) cylinders. Terminal emitters (TE) transfer energy to the chlorophyll in the reaction centres (RC) implanted in the thylakoid membrane. Peak absorption and emission wavelengths are optimised to cause fast and efficient excitation energy transfer towards the RC. Excess energy is emitted as fluorescence at the wavelengths displayed for each unit. Figure copied from* (Dartnell et al., 2011).

One study performed a proteomic analysis of *S. sp. 6803* under conditions of inorganic carbon and light limitations. They found that light limitation dramatically impacted the proteome, while inorganic carbon limitation provoked a weaker effect. Interestingly, carbon assimilation proteins display a stronger response to light-intensity alterations than to inorganic carbon (Jahn et al., 2018).

The monomers used to assemble PBPs comprise individually produced α and β subunits. These αβ heterodimers constitute a single PBP subunit known as an αβ monomer, which is used to assemble $(\alpha\beta)_3$ trimers (Guillén-García et al., 2022). Two $(\alpha\beta)_3$ units can dimerise to form a PBP hexamer (Marx & Adir, 2013).

Allophycocyanin

Evidence from non-cyanobacterial models suggested that the availability and fixation of CO_2 are coupled with light harvesting. This prompted the Cann group to search for carbamylation sites on proteins related to photosynthesis in *S. 6803* and to assess the effects of carbamylation on EET in whole cells. Their results suggested that carbamylation at the K6 site of the allophycocyanin α-subunit (ApcA) enhanced EET within the PBS, resulting in a more effective transfer of electronic energy. Their work suggests that carbamylation at the ApcA K6 site enhances EET in whole cells (Guillén-García et al., 2022).

The light-harvesting complexes in live cells are composed of PBP trimers (Guillén-García et al., 2022). One method for distinguishing between Apc trimers and monomers could be the absorbance peaks. The absorption maximum of monomers is at 615nm, and the absorption maximum of trimers is at 650nm, accompanied by a shoulder at approximately 620nm (Figure 5). These data suggest that if purified Apc could be verifiably separated into monomers and trimers as a control, a method could be validated for differentiating monomer and trimer forms of Apc based on absorbance spectra. The limitation of this method would be that the amount of protein required to run statistically significant comparisons on assembled and non-assembled Apc would be labour-intensive to express and purify.

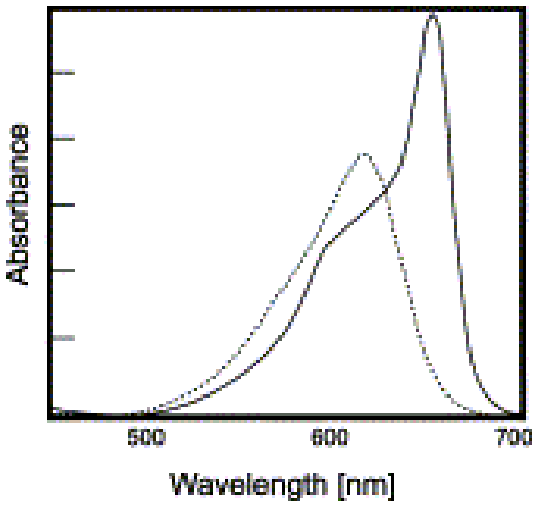

Figure 5: Absorption spectrum of allophycocyanin trimers (solid line) and monomers (dotted line). The trimer is in pH 6.0 sodium phosphate buffer at 0.10 ionic strength. The monomer is in pH 6.0 buffer plus 0.50 M NaSCN. Figure copied from (MacColl, 2004).

C-Phycocyanin

Like all PBPs, C-phycocyanin (Cpc) is composed of α and β subunits, which form αβ monomers, which in turn assemble into $(\alpha\beta)_3$ trimers. X-ray crystallography has determined Cpc's $(\alpha\beta)_6$ quaternary structure. It has been reported that while Cpc is in solution, the $(\alpha\beta)_6$ hexamer is only stable at high Cpc concentrations in high phosphate buffer concentrations, at a low or neutral pH. Because of this, purifying Cpc using column chromatography usually produces a mixture of Cpc hexamers, trimers, and monomers. The composition of this mixture will depend on pH and the concentrations of Cpc and the buffer (Minato et al., 2021). Phycocyanin in solution can be reversibly assembled and disassembled between monomeric, trimeric, and hexameric states (Berns & MacColl, 1989). However, this study did not attempt to convert PBP monomers or trimers into hexamers for analysis.

Experimental Plan

Allophycocyanin and C-phycocyanin

Relatively little research has been performed on inorganic carbon in the form of CO_2 or HCO_3^- as a regulator of photosynthesis. It has been established that the concentration of atmospheric CO_2 is a regulator of photosynthesis due to the competing carboxylation and oxygenation reactions catalysed by RuBisCO. Carbon concentration in photosynthetic organisms has also been researched previously. The alternative pathways cells use to avoid damage from absorbing excess light energy is a matter of ongoing research. However, the mechanisms of photosynthetic regulation through transient interactions with carbon CO_2, such as carbamylation, are poorly understood. The importance of carbamylation in regulating photosynthesis is still a matter of ongoing debate, which must be researched to understand environmental processes that impact human health, such as cyanobacterial blooms (Ma & Wang, 2021), and for optimising the growth of cyanobacteria for use in biofuel production (L. Wang et al., 2020).

The Cann group previously demonstrated that ApcA is a CO_2 receptor in the cyanobacterial PBS and that the carbamylation of ApcA plays a role in regulating photosynthetic EET. They observed that

elevated CO_2 concentrations enhanced EET *in vitro* and in live cells (Guillén-García et al., 2022). They also generated *E. coli* strains that produced the mutant $ApcAB^{K6A}$ (Apc K6A) mutated at the carbamylation site and would not undergo carbamylation (Guillén-García et al., 2022). It was subsequently hypothesised that Cpc could also be a CO_2 receptor that regulates EET through carbamylation. This project aimed to identify any Cpc sites that undergo reversible carbamylation by observing differences in Cpc emission cause by elevated CO_2 concentrations. This was achieved by expressing Cpc in recombinant *Escherichia coli* (*E. coli*) strain BL21 cells using methods adapted from a paper published in 2010 (Biswas et al., 2010). The Cann lab had previously produced *E. coli* strains BL21 and DH5α carrying plasmids for the expression of Cpc. Three plasmids are required for proper recombinant expression in *E. coli,* and these plasmids were transformed into a single *E. coli* BL21 strain. Protein yield was optimised by modifying culture conditions. Cpc was purified from *E. coli* and analysed *in vitro* to identify carbamylation sites. *In vitro* analysis involved steady-state fluorescence analysis of the proteins in the presence of added inorganic carbon and a negative control for added carbon.

Previous work in the Cann group identified four potential sites of Cpc carbamylation. Four mutant Cpc genes were generated to replace the charged lysine with uncharged alanine on both the α subunit (CpcA) and the β subunit (CpcB): CpcA-K2A, CpcA-K137A, CpcB-K36A, and CpcB-K135A. These mutant strains generated previously were used as a source of modified proteins in this study. When putative carbamylation sites are identified, ^{13}C-NMR spectroscopy can be used to confirm CO_2-binding sites, however NMR analysis was not performed in this study. Because the Cann group has previously demonstrated that carbamylation of ApcA is a regulator of EET, ApcA can be used as a positive control for the methods used with Cpc.

After carbamylation sites are identified, strains of *S. 6803* with mutated Cpc simulating conditions of full carbamylation and no carbamylation at the identified carbamylation sites could be engineered in the future. These engineered strains can be used to assess the effects of Cpc carbamylation on EET

and the growth of whole cells. The carbamylated lysine can be mutated to arginine to simulate a state of no carbamylation while maintaining a charged state at that amino acid position, and a strain where the lysine is replaced with glutamate to represent the local carbamate charge state at 100% occupancy. It would also be necessary to ensure that the mutated Cpc proteins display similar secondary structures to the wild-type Cpc by generating and comparing circular dichroism spectra. Measuring the effects of carbamylation on EET would involve a similar methodology to the previous analysis of Apc, measuring fluorescence quantum yield as an indicator of energy transfer within the PBS.

Methods

Plasmid Construction

The pCpcBA plasmid was used as a template for site-directed mutagenesis. The vector, insert, and four variable insert sequences were submitted to GenScript. Four mutant plasmids were produced: pCpcBA (α-chain K2A), pCpcBA (α-chain K137A), pCpcBA (β-chain K36A), and pCpcBA (β-chain K135A).

Cpc and Apc Expression

A multiplasmid coexpression system was required to produce functional phycobiliproteins in *E. coli* (Table 2). The Apo-Apc subunits (ApcA and ApcB) are produced by the *apcA* and *apcB* genes (Chen et al., 2016). Haem is produced by most organisms, including *E. coli* (Ge et al., 2023). In *E. coli*, haem can be converted to biliverdin IX by the exogenous haem oxygenase Ho1 enzyme. Biliverdin IX can be converted to phycocyanobilin (phycocyanobilin) by PCB ferredoxin oxidoreductase *PcyA* enzyme. In this study, a plasmid encoding both the Ho1 and a histidine-tagged PcyA enzyme was transformed into *E. coli*. The holo-Apc subunits are formed by adding PCB to apo-ApcA and apo-ApcB, catalysed by bilin lyases (Chen et al., 2016). CpcT attaches Cys-153 of CpcB to PCB in cyanobacteria. CpcU and CpcS attach Cys-82 of CpcB and the equivalent Cys residues of Apc subunits to PBPs (Biswas et al., 2010).

Table 2: Recombinant proteins used in this study, their species of origin, their expression vectors, and the antibiotics used for their growth selection in this study.

Plasmid	Protein Produced	Vector	Antibiotic Resistance
UTS	*Synechococcus sp*. PCC 7002 CpcU, CpcT, and CpcS coexpressed on one mRNA	pCOLA	Kanamycin
Ho1 and HT-PcyA	Synechocystis *sp*. PCC 6803 Ho1 and Synechococcus *sp*. PCC 7002 HT-PcyA	pACYC Duet	Chloramphenicol
HT-CpcB and CpcA	*Synechococcus sp*. PCC 7002 HT-ApcA and ApcB	pCDF Duet	Spectinomycin
CpcA-K2A	*Synechococcus sp*. PCC 7002 HT-CpcA-K2A and CpcB	pCDF Duet	Spectinomycin
CpcA-K137A	*Synechococcus sp*. PCC 7002 HT-CpcA-K137A and CpcB	pCDF Duet	Spectinomycin
CpcB-K36A	*Synechococcus sp*. PCC 7002 HT-CpcA and CpcB-K36A	pCDF Duet	Spectinomycin
CpcB-K135A	*Synechococcus sp*. PCC 7002 HT-CpcA and CpcB-k135A	pCDF Duet	Spectinomycin
ApcAB	*Synechococcus sp*. 7002 HT-ApcA and ApcB	pET100	Ampicillin
K6A apcAB	*Synechoccocus sp.* PCC 7002	pET100	Ampicillin

Plasmid DNA extraction

Plasmids were extracted from storage strains of *E. coli* DH5α using the Monarch® Plasmid Miniprep Kit (New England Biolabs) according to the manufacturer's instructions.

Competence

To produce competent stocks of *E.* coli DH5α and BL21 strains, cells were incubated in LB broth for 16 hours at 37°C and shaking at 180 RPM. After incubation, cultures were diluted by a factor of 1:100 in fresh LB broth and incubated under identical conditions until the OD_{600} of cultures was 0.5. Cultures were incubated on ice for 20 minutes and then centrifuged to pellet cells. The supernatant was discarded, and cells were resuspended in 0.1M $CaCl_2$ and then incubated on ice for 30 minutes. Cells were pelleted again and resuspended in a solution of 0.1M $CaCl_2$ and 15% v/v glycerol, then stored at -80°C.

Transformations

Plasmid DNA was added to chemically competent *E. coli* and incubated on ice for 30 minutes. Cell preparations were incubated shocked at 42°C for 10 seconds and subsequently incubated on ice for 5 minutes. Preparations were then diluted by a factor of 1:19 with room-temperature Super Optimal Broth with Catabolite repression (SOC) broth and incubated at 37°C for 60 minutes at 180 RPM. Cells were spread onto agar plates containing appropriate antibiotics to select plasmid-carrying strains (Table 3).

Table 3: Concentrations of antibiotics used for selection of plasmid-carrying strains

Kanamycin 50 µg/ml	Chloramphenicol 34 µg/ml	Spectinomycin 50 µg/ml	Ampicillin 100 µg/ml

To produce *E. coli* strains encoding more than one plasmid, plasmids were transformed individually. Plasmid-carrying strains were made competent, as described previously, for subsequent transformations of other plasmids.

Recombinant Protein Expression

E. coli BL21 cells stored at -80°C were streaked onto Luria agar (LA) plates containing appropriate antibiotics to select desired strains and grown for 16 hours at 37°C. Single colonies were inoculated into 100 ml Luria broth (LB) with antibiotics and incubated for 16 hours at 37°C while shaking at 180 RPM to produce seed cultures. 1 ml of seed culture was centrifuged, and pellets were visually examined for colour indicative of basal expression before seeding expression cultures. When Cpc or Apc was expressed, *E. coli* cell pellets appeared blue. To determine optimal expression parameters, 10 ml-100 ml seed culture was transferred to 1L LB with antibiotics for protein expression. Cultures for expression were grown at 37°C while shaking at 150 RPM until their OD_{600nm} was 0.6-0.8. Then isopropyl-β-d-1-thiogalactopyranoside (IPTG) was added to achieve a final concentration of 0.5 mM in expression cultures to induce protein expression. The incubator temperature was then reduced to 18°C, and cultures were incubated for approximately 14 hours while shaking.

After incubation, cultures were centrifuged in 1L tubes at 4,000 RPM in Beckman Coulter Avanti Hi-Speed JLA 8.1000 rotors centrifuges at 4°C for 30 minutes to pellet cells. Pellets were transferred to 50 ml conical centrifuge tubes and centrifuged in a benchtop centrifuge at 4,000 RPM for 10 minutes to separate residual media. Pellets were subsequently frozen and stored at -80°C.

Protein Purification

Pellets were thawed and resuspended in 'Nickel Buffer A' (150 mM NaCl, 30 mM Tris, 5% v/v glycerol, pH 7.9) with one Roche protease inhibitor cocktail tablet. Cells were lysed by sonication (SONICS Vibracell 10 rounds of 15 seconds pulse on and 15 seconds off at an amplitude of 45%). The lysate was clarified by centrifugation using an Avanti Hi-Speed JA-25.50 at 20,000 RPM for 40 minutes.

Where one or two proteins were purified at a time, the clarified lysate was purified using a 5ml Cytiva HisTrap Ni Sepharose High-Performance column with either a Gilson MINIPULS® 3 peristaltic pump or an ÄKTA™ Start and protein was eluted using increasing imidazole concentrations, up to a maximum of 0.5 M imidazole. When purifying three to five distinct proteins simultaneously, Poly-Prep columns (Bio-Rad) containing 1ml Ni Sepharose 6 Fast Flow resin (Cytiva) and purifications were performed under gravity flow for higher simultaneous throughput. Due to the higher resin volume and higher binding capacity of HisTrap columns compared to polyprep columns, HisTrap columns were used preferentially when visual observations of cell pellets indicated a high protein yield was present in the sample.

Cpc and Apc could be visually observed in eluted fractions. Polyacrylamide gel electrophoresis was performed to confirm protein presence using a 15% acrylamide separating gel. PageRuler Plus Protein ladder (Thermo Fisher Scientific) was used as a sizing standard. In some cases, protein detection in eluted chromatography fractions was based on visual observations alone.
Protein-containing fractions were concentrated using Vivaspin® 20 Ultrafiltration Unit with a 10 kDa molecular weight cut-off. The concentrated protein solution was dialysed overnight into 150 mM NaCl, 30 mM Tris, pH 7.9 in 3.5 KDa MWCO SnakeSkin™ tubing. For some, but not all, assays, protein

preparations were purified using gel filtration chromatography using a 120 cm size-exclusion column (HiLoad® 16/600 Superdex® 200 pg, Cytiva) was carried out on an ÄKTA™ Start.

Size Exclusion Chromatography Calibration

To calibrate the HiLoad® 16/600 Superdex® 200 pg, the column elution volume was determined using Blue dextran 2000 (Cytiva) separately from protein standards to find the void volume. The protein standards were eluted through the column in two separate elutions of three proteins each to produce clear and well-separated peaks. The resulting data was used to calculate the average distribution constant, K_{av} (Figure 6), which was then plotted against the $\log_{10}$ of each protein's relative molar mass (M_r). The elution volume for each protein was calculated using Microsoft Paint 22H2 to determine the X-coordinate of each protein peak on the bitmap file generated by the ÄKTA™ Start, accurate to one pixel. The volume corresponding to each protein peak was also calculated to an accuracy of one pixel.

$$K_{av} = \frac{V_e - V_0}{V_c - V_0}$$

Figure 6: Average distribution constant, K_{av}, formula. V_e: protein elution volume, V_c: column volume, V_o: void volume.

Excitation-Emission Spectra

Two instruments were used for measuring steady-state fluorescence: a Jobin Yvon Horiba Fluorolog 3 and a Synergy H4 plate reader. The fluorolog was used with quartz cuvettes for individual excitation and/or emission measurements of 3ml total liquid volume. When using the fluorolog for excitation and/or emission analysis, a Cary 5000 Ultraviolet-Visible-Near Infrared (UV-Vis-NIR) was used to measure sample absorbance. The H4 plate reader was used with 96-well plates for higher-throughput analysis of samples with a total liquid volume of 100 µl each. For standardisation of protein concentration before fluorescence analysis, protein absorbance spectra were measured, and optical densities of protein were standardised to 0.1 absorbance units at their absorbance maxima.

The H4 plate reader was used to measure absorbance (in transparent 96-well plates) in cases where it was used for fluorescence analysis (performed in black 96-well plates).

Steady-state fluorescence analysis of proteins was compared between protein preparations containing final concentrations of 20 mM sodium bicarbonate ($NaHCO_3$) and 20 mM sodium chloride (NaCl). $NaHCO_3$ and NaCl buffers were prepared daily, and the pH of both buffers differed by less than 0.1. Solutions for emission analysis were prepared up to a final volume of 3ml or 100 µl using the appropriate volume of the protein's dialysis buffer or 0.1M MOPS within 0.1 pH units of the NaCl and $NAHCO_3$ buffers. All buffers used when analysing protein were within 0.1 pH units between pH 7.35-7.50 for all analyses after the data for (Figure 17, Figure 18) were obtained. Measurements were taken for each protein preparation only once to prevent photo-degradation, except in the cases of repeat measurements to estimate instrument error and excitation-emission analysis after 60-hour incubations with NaCl and $NaHCO_3$ (Table 4, Table 5).

Table 4: Synergy H4 Plate reader analysis parameters

H4			
	Absorbance	Excitation	Emission
Starting wavelength (nm)	550	450 ± 9	610 ± 9
End wavelength (nm)	700	660	750
Increment increase (nm)	1	1	1
Excitation wavelength (nm)	N/A	N/A	590 ± 9

Table 5: Fluorolog and UV-Vis analysis parameters

Fluorolog			
	Absorbance	Excitation	Emission
Starting wavelength (nm)	400	350	600
End wavelength (nm)	800	700	800
Increment increase (nm)	1	1	1
Excitation wavelength (nm)	N/A	N/A	590 (Apc) and 595 (Cpc)

Data Analysis

Absorbance and concentration

The spectra were imported into Microsoft Excel from the Cary or H4 plate reader. Peak absorbance values were identified, and the sample volume required to achieve an absorbance peak of 0.1 in the same total volume of liquid was calculated. Where there was insufficient protein for each replicate to have an absorbance value of 0.1, reaction volumes were standardised to lower amounts. In the case of the Cpc WT and CpcB-K36A hexamer samples (Figure 53, Figure 54), excitation spectra were used to standardise protein concentration due to insufficient samples for absorbance measurements.

Protein Emission

$NaHCO_3$ was used as a source of CO_2, and NaCl was used as a negative control for adding CO_2 or other forms of inorganic carbon. $NaHCO_3$ dissolves in water to produce CO_2 gas according to the following equation (Janković, 2009):

$$2NaHCO_3 \longrightarrow Na_2CO_{3\,(s)} + CO_{2\,(g)} \uparrow + H_2O_{\,(l)}$$

The exact concentration of CO_2 present in the reaction solutions was unknown, as the equipment necessary to determine the exact CO_2 concentrations in reaction volumes as low as 100 µl was not available. However, for the purposes of these experiments, it was only necessary to see a qualitative significant response to elevated CO_2, and future work should include quantitative analysis of any dose-dependent responses that might occur.

The spectra were imported into Microsoft Excel. The maximum values of each emission spectrum were identified, and the variance between replicates was calculated. Peaks were normalized based on the first recorded fluorescence intensity value to account for differing quantities of active protein in each sample, i.e. peak emission values were divided by the first recorded emission values (at 600 nm in the Fluorolog and 610 nm in the H4 Plate Reader). A two-tailed *T-test* assuming equal variance in both samples was performed on the original and normalized values to determine the significance of differences caused by inorganic carbon.

Due to differing levels of variance between samples where *T-test*s were performed, a combined coefficient of variance was obtained by adding the squares of variance coefficients for both test states (NaCl and $NaHCO_3$) and obtaining the square root of the resulting number using the following formula:

$$Combined\ variance = \sqrt{((coefficient\ of\ variance\ NaCl)^2 + (Coefficient\ of\ variance\ NaHCO3)^2)}$$

Results

It was hypothesised that carbamylation of phycobiliproteins mediated by elevated CO_2 concentrations regulates photosynthetic energy transfer in live cells. An increase in the emission of purified phycobiliproteins was expected in the presence of elevated inorganic carbon. Because multiple rounds of protein purification and excitation-emission analysis were performed, purification data is presented beside excitation-emission data for each round of purification.

Protein Expression

Growth Curves

During most expressions of Apc and Cpc proteins in *E. coli*, it was not feasible to generate growth curves, as a combination of Erlenmeyer flask styles (baffled and non-baffled flasks) were often used at once. However, data is presented (Figure 7) from one Apc WT and Apc K6A expression where all flasks were of the 'Pyrex® Erlenmeyer flask, and narrow neck baffled' design (Sigma Aldrich). After the final reading (115 minutes post-inoculation), recombinant protein expression was induced using IPTG.

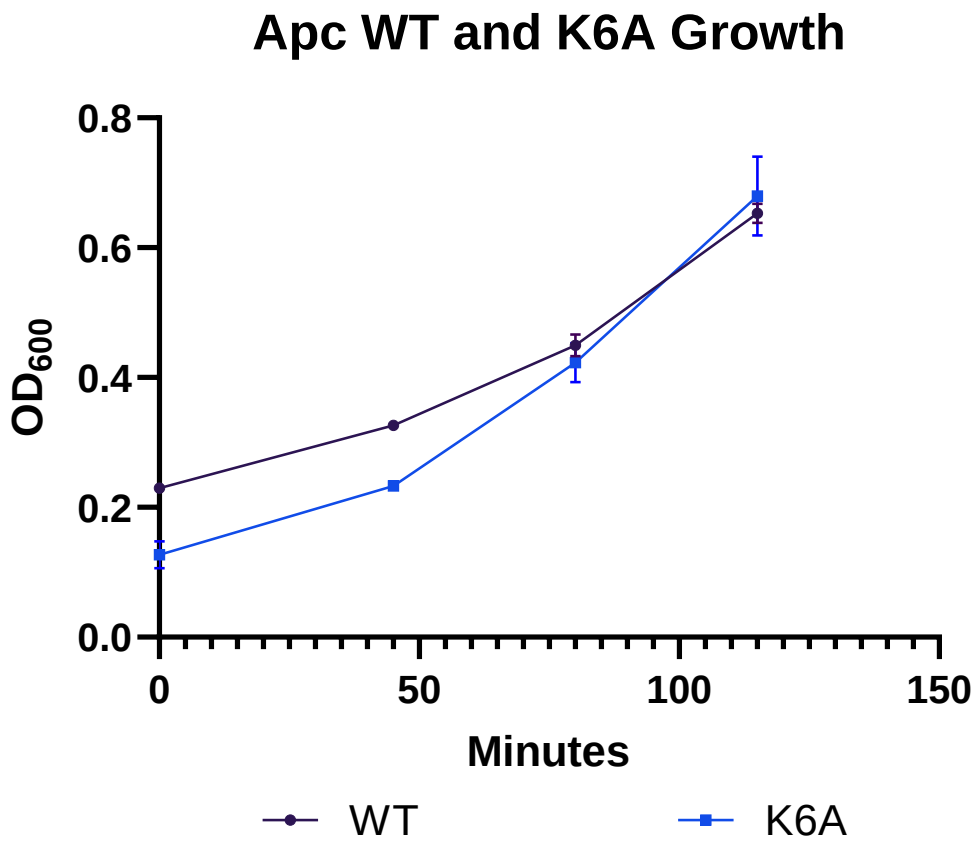

Figure 7: Growth curves of E. coli *expression cultures for Apc WT and Apc K6A from the point of inoculation with seed culture to the point of expression. Optical densities at a wavelength of 600 nm (OD_{600}) were measured at 0, 45, 80, and 115 minutes post-inoculation. 45 ml seed culture was inoculated into 1L Luria Broth (LB) containing appropriate antibiotics and incubated in 2L baffled Erlenmeyer flasks at time 0. N=3.*

Protein Detection in Purified Lysates

Immobilised Metal Affinity Chromatography

Calculated using UniProt (The UniProt Consortium, 2023), CpcA from *Synechocystis sp.* strain PCC 6803 / Kazusa has a molecular weight of 17,586.60 Da and CpcB has a molecular weight of 18,126.47 Da. The $(\alpha\beta)_3$ trimer was expected to have a size of approximately 107.1 kDa. The Cpc hexamer was expected to be 214.2 kDa. ApcA has a mass of 17,355 Da, and ApcB has a mass of 17,216 Da in the

species *Synechocystis sp.* (strain PCC 6803 / Kazusa). The $(\alpha\beta)_3$ trimer was expected to be 103.7 kDa. The hexamer was expected to be 207.4 kDa.

Size Exclusion Chromatography

The data used to generate the HiLoad® 16/600 Superdex® 200 pg column calibration curve (Table 6) and the calibration curve (Figure 8) are displayed below. The calibration curve's R^2 value of 0.9967 indicates a high correlation between elution time and the Log_{10} of the protein's M_r.

Table 6: Protein standards and their elution volumes for HiLoad® 16/600 Superdex® 200 pg column calibration

Protein	log(Mr)	Elution volume (ml)	Calibration Run
Aldolase	5.198657	70.2	2
Conalbumin	4.875061	76.2	1
Ovalbumin	4.633468	81.25	2
Carbonic anhydrase	4.462398	86.5	1
Ribonuclease	4.136721	93.73	2
Aprotinin	3.812913	100.5	1
Blue dextran (void volume)	N/A	46.4	0

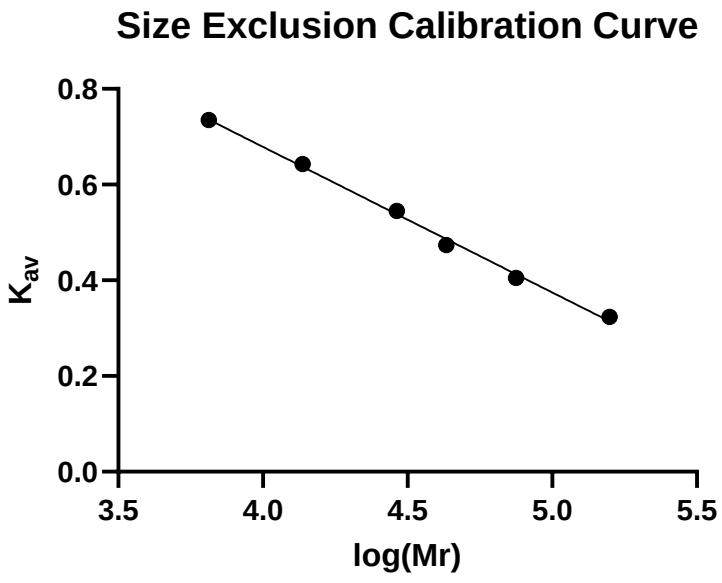

Figure 8: Calibration curve of HiLoad® 16/600 Superdex® 200 pg column used in Size Exclusion Chromatography (SEC). Protein standards used were from both high and low molecular weight Gel Filtration Calibration Kits (Cytiva). Proteins used were Aldolase, Conalbumin, Ovalbumin, Carbonic anhydrase, Ribonuclease, and Aprotinin. R^2 was calculated based on a simple linear regression trendline: 0.9967. Trendline formula: y = -0.3043x + 1.896.

Based on the calibration curve, the expected elution volumes for Apc were 73.5 ml and 52.7 ml for the trimer and hexamer forms, respectively. Expected elution volumes for Cpc were 73.3 ml and 52.4 ml for the trimer and hexamer forms, respectively.

Analysis of Purified Protein

Excitation Spectra

For Apc WT, excitation spectra were measured using a Fluorolog (N=1) and a Synergy H4 Plate Reader (N=3). Calculated using the Fluorolog, the maximum excitation was achieved at 609 nm (Figure 9). Calculated using the H4 Plate Reader, the Excitation maximum of Apc was between 616-620 nm (Figure 10). A difference of approximately 10 nm is relatively small, and there are a number of possible explanations. The excitation analysis performed in the Fluorolog was performed without replicates, and therefore, it is possible that taking more measurements would yield results that are precisely aligned with the H4. The protein preparations used to measure excitation in the Fluorolog and H4 were expressed and purified on different dates, and one possible reason for the small differences in excitation maxima is that there may have been different proportions of Apc hexamers, trimers, monomers, and αβ subunits in the different protein preparations.

Additionally, the preparation used in the Fluorolog went through IMAC. In contrast, the preparation in the H4 went through both IMAC and SEC, indicating that the H4 preparation may experience significantly fewer non-specific interactions than the Fluorolog preparation. Different buffers were also used; the Fluorolog analysis used 30 mM Tris 150 mM NaCl, while the H4 analysis used 100 mM MOPS, which could account for differing non-specific interactions. It is unlikely that pH played a role in the differences between Fluorolog and H4 data, as the pH of NaCl buffers differed by <0.1 between the Fluorolog and H4 analyses.

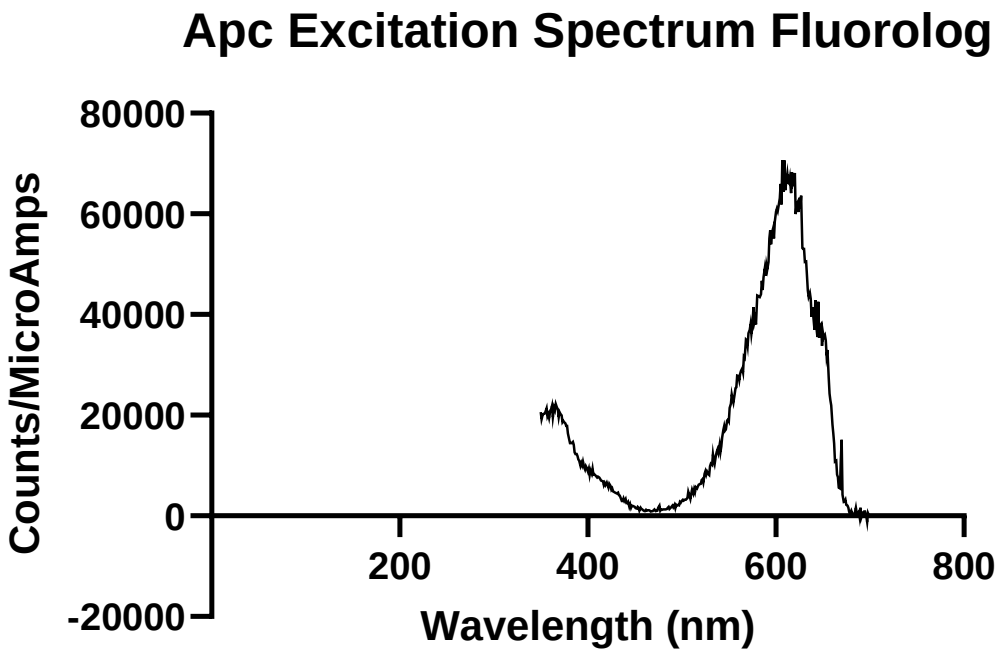

Figure 9: Apc excitation spectrum measured in buffer composed of 30 mM Tris 150 mM NaCl. Emission was monitored at 680 nm, and excitation was analysed between 350-700 nm. N=1

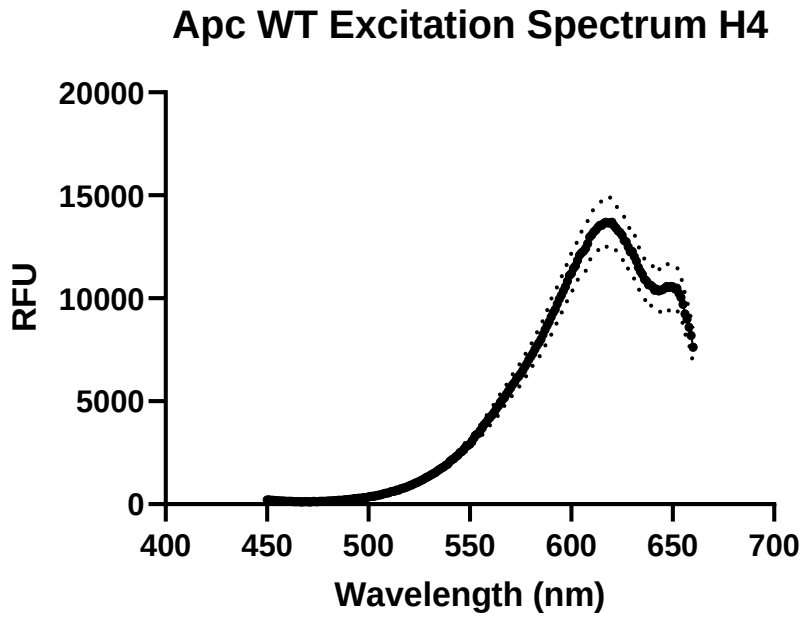

Figure 10: Apc WT excitation spectra obtained using H4 Synergy plate reader with standard deviation denoted by dotted lines. Emission was analysed at 680 nm, and excitation was measured between 450-660 nm. N=3.

The Cpc WT excitation maximum was 622 nm, and the CpcB-K36A excitation maximum was 627 nm (Figure 11, Figure 12). Both were purified using IMAC followed by SEC and measured in a buffer of 100 mM MOPS. For both Cpc excitation spectra, the sample size was N=1. Excitation maxima for Cpc monomers and trimers were not identified as part of this study.

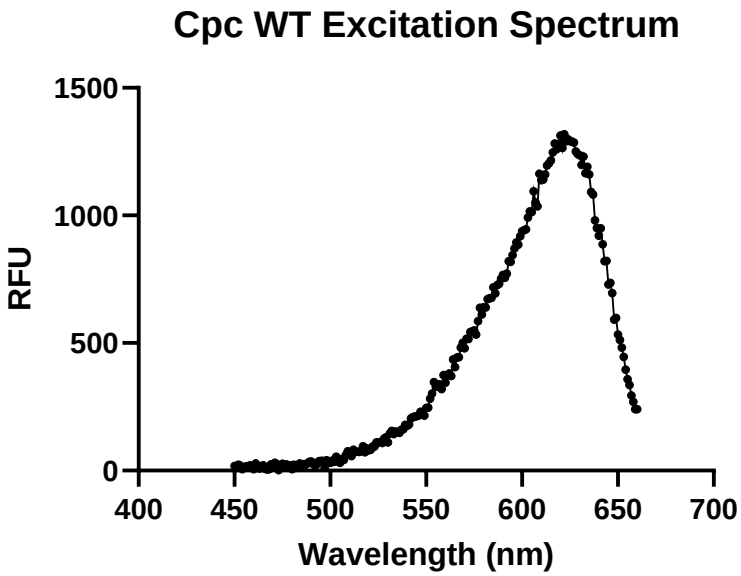

Figure 11: Cpc WT purified using IMAC followed by SEC excitation spectrum. Emission was analysed at 680 nm, and excitation was measured between 450-660 nm. N=1. RFU: relative fluorescence units

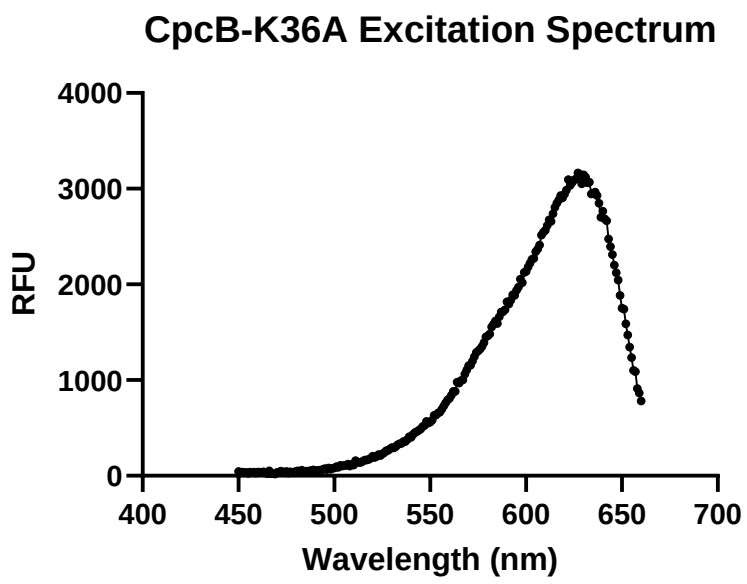

Figure 12: CpcB-K36A SEC purified excitation spectrum. Emission was analysed at 680 nm, and excitation was measured between 450-660 nm. N=1. RFU: relative fluorescence units.

Emission Spectra

Inorganic Carbon Suppressed Fluorescence in Cpc Purified with IMAC Only

Excitation-emission analysis was performed on Cpc WT to confirm that the methods used in this study produce enhanced fluorescence in the presence of inorganic $NaHCO_3$, when compared to NaCl.

A denaturing SDS-PAGE was run on the IMAC elution fractions used for excitation-emission analysis (Figure 13). Most of the protein present appeared as two bands between 15 and 25 kDa. This is consistent with the expected size of α and β subunits. This suggests that Cpc was successfully purified by IMAC, however a denaturing SDS-PAGE cannot indicate whether the subunits were assembled into functional protein before analysis.

Cpc WT excitation-emission spectra were compared in 20 mM NaCl and 20 mM $NaHCO_3$ (Figure 14) where biological replicates N=10. Cpc WT displayed a suppression of fluorescence in the presence of inorganic carbon. A two-tailed *t*-test with equal sample variance was used to analyse the differences between the NaCl and $NaHCO_3$ populations at 646 nm, the emission maximum. The result of p=0.014 suggests significant differences between the populations, however there were large variances between the emission maxima between biological replicates. All replicates were obtained from the

same preparation and the same tube of purified protein. The peak values were normalised to the first emission reading to account for differences in quantities of active Cpc between tests. The limitation of this normalisation method was that the baseline emission at 600 nm was likely affected by the presence of $NaHCO_3$. The *t*-test on the normalised data returned p=0.925. However, this only indicates that the differences between 600 nm and 646 nm emissions were not significantly lower in the $NaHCO_3$ samples than in the NaCl samples. The combined coefficients of variance of the emission maxima before and after normalisation were 6.7% and 5.7%, respectively.

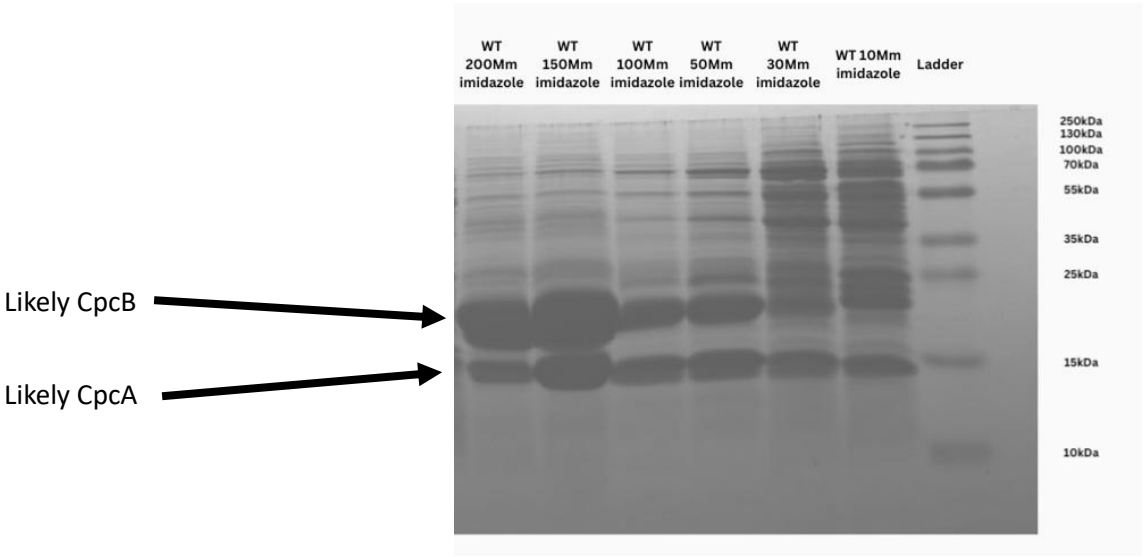

Figure 13: SDS PAGE gel on HisTrap purified fractions of Cpc wild type (WT). Fractions of 50 mM imidazole – 200 mM imidazole inclusive were concentrated for excitation-emission analysis.

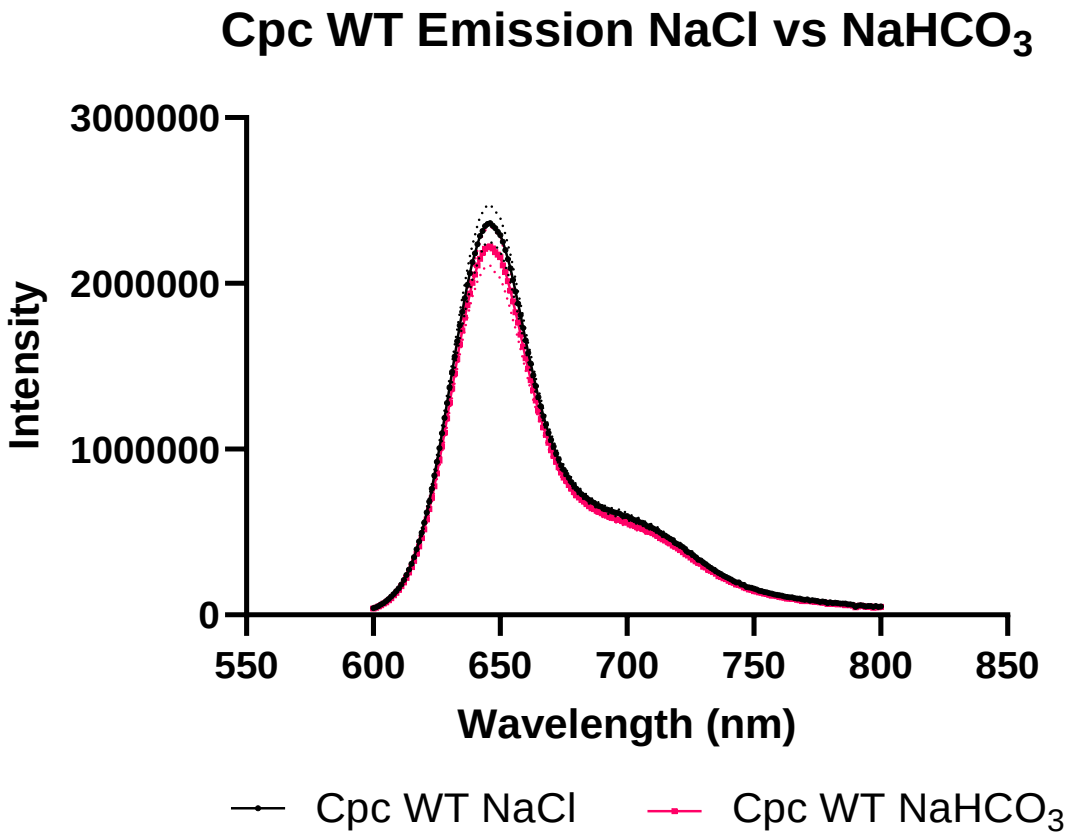

Figure 14: Excitation-emission spectra of Cpc WT when incubated with 20 mM NaCl or 20 mM $NaHCO_3$. The standard deviation is displayed as dotted lines. Data was obtained using a Fluorolog. N=10

The unexpected suppression of Cpc fluorescence in the presence of $NaHCO_3$ suggested that either the methods used for analysis were flawed and / or that inorganic carbon could reduce Cpc fluorescence in the presence of inorganic carbon.

Inorganic Carbon Failed to Suppress Fluorescence in Apc WT Purified using IMAC Alone

The unexpected suppression of IMAC-purified Cpc suggest that flaws existed in the methods used for the excitation-emission analysis. The excitation-emission analysis was performed using a positive control to validate the experimental method for Cpc analysis. Apc was used as a positive control for the analysis, as inorganic carbon's increase in EET in Apc has been previously demonstrated (Guillén-García et al., 2022).

Apc WT was expressed in recombinant *E. coli* and purified using IMAC. Excitation-emission analysis was performed on the purified protein. There were no significant differences between NaCl and $NaHCO_3$ conditions (Figure 15). *t*-test resulted in $p>0.05$ in both the original data and after emission peak data had been normalised to starting emission intensity. In this case, the combined variance coefficients were 3.7% and 1.7% before and after normalisation.

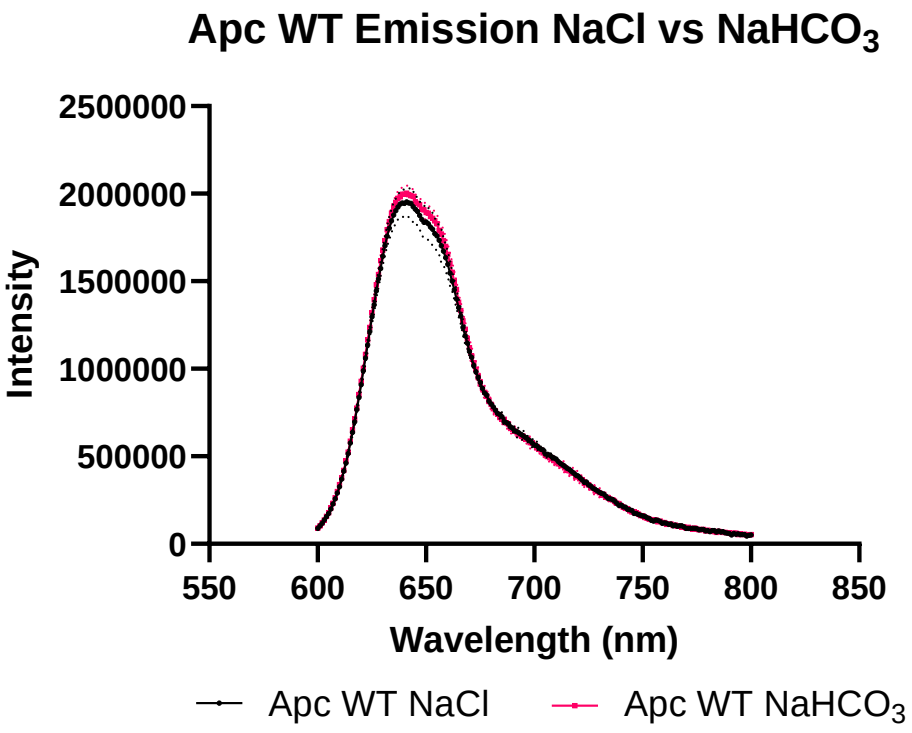

Figure 15: Excitation-emission spectra of Apc WT when incubated with 20 mM NaCl and 20 mM $NaHCO_3$. The standard deviation is displayed as dotted lines. N=3. Data was obtained using a Fluorolog.

The unexpected suppression of Cpc WT fluorescence in the presence of inorganic carbon and the absence of a significant Apc WT response confirmed that the methods used for the PBP fluorescence analysis described above were possibly flawed.

Modifying Tris Buffer pH Did Not Cause a Significant Apc Response to $NaHCO_3$

Because the data presented in Figure 15 did not validate the experimental method, potential sources of error in the experiment were identified and removed. The preparation of Apc WT used for the previous analysis was used again for excitation-emission analysis. The method was modified to

include adding HCl to the dilution buffer composed of 30 mM Tris, 150 mM NaCl immediately before analysis, to ensure that the pH of the reaction solution was between 7.40 and 7.50. The pH of the dilution buffer used during the previous analysis had not been modified and was approximately 7.9.

The data for this analysis is displayed in Figure 16. p>0.05 for the original data and when emission maxima were normalised to starting fluorescence. The combined variance coefficients of the emission maxima were 5.5% and 2.4% before and after normalisation, respectively.

There was also a notable difference in the variances of the NaCl conditions and the $NaHCO_3$ conditions. In the original data at the emission maximum wavelength, the variance was 5.3% for the $NaHCO_3$ condition but only 1.2% for NaCl.

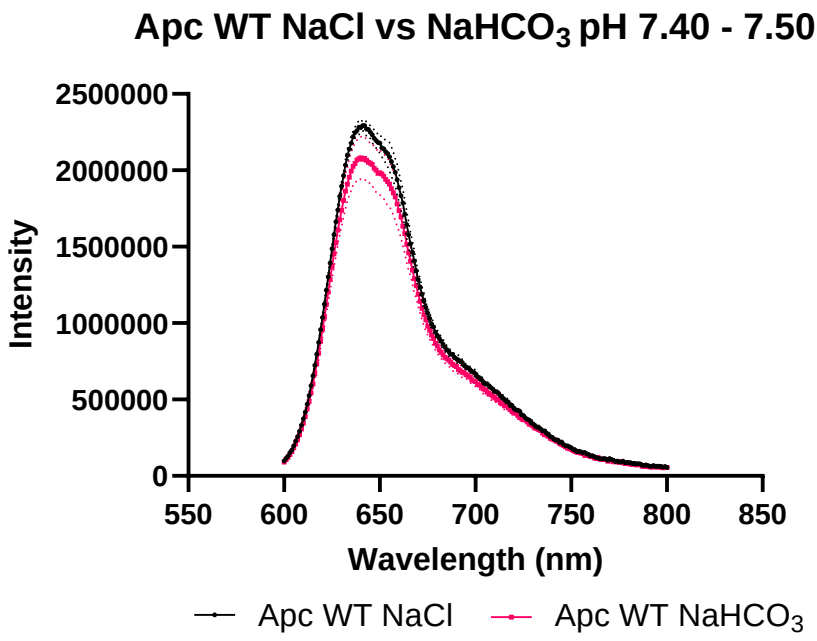

Figure 16: Excitation-emission spectra of Apc WT when incubated with 20 mM NaCl or 20 mM $NaHCO_3$. Buffer pH was modified to prevent $NaHCO_3$ degassing. Dilution buffer pH: 7.39, NaCl buffer pH: 7.45, $NaHCO_3$ buffer pH: 7.54. The standard deviation is displayed as dotted lines. N=3. Data was obtained using a Fluorolog.

The modified method did not cause Apc WT to respond significantly to $NaHCO_3$ when compared to the NaCl control. A greater variance was observed between $NaHC0_3$ replicates than NaCl replicates, which could indicate that different forms of Apc WT (subunits, monomers, trimers) to respond differently to $NaHCO_3$ depending on the relative concentration of each form in the reaction mixture.

Modified MOPS Buffer pH Did Not Cause a Significant Apc Response to $NaHCO_3$.

The results of the previous experiment demonstrated that modifying the pH of the Tris buffer used for dilution did not cause Apc WT fluorescence to respond significantly to $NaHCO_3$.

The same preparation of Apc WT was used again for excitation-emission analysis under different buffer conditions. To control the pH of the protein more precisely during emission analysis, the buffer used to dilute samples was changed. This removed the temperature dependence of the pH associated with Tris buffers and reduced the likelihood of inorganic carbon degassing from the sample. MOPS buffers have a low pH range, and NaOH was to be added to the MOPS buffer to reach a pH around 7.4 rather than the HCl, which was added to Tris buffers to reduce the pH from an unmodified pH of approximately 7.9. The NaCl and $NaHCO_3$ buffers were made in 0.1 M MOPS as well.

NaCl / $NaHCO_3$ buffer final concentrations were 0.1 M NaCl / $NaHCO_3$ and 0.1 M MOPS. All buffers were between pH 7.39 – 7.48, and buffer pH was tested immediately before excitation-emission analysis.

No significant differences existed between NaCl and $NaHCO_3$ conditions before or after normalisation (Figure 17). The combined coefficients of variance were 5.6% and 3.0% before and after normalisation, respectively.

In this case, the variance coefficients alone may be misleading, and therefore, the graph displaying individual replicates of $NaHCO_3$ conditions is displayed below (Figure 18). Three replicates had emission maxima at 641 nm or 642 nm. However, two replicates on the graph display shoulders with emission maxima at 656 nm and 657 nm, respectively. The reasons for these unexpected peaks are unknown, and all protein used in this experiment was purified together and stored in the same tube before analysis.

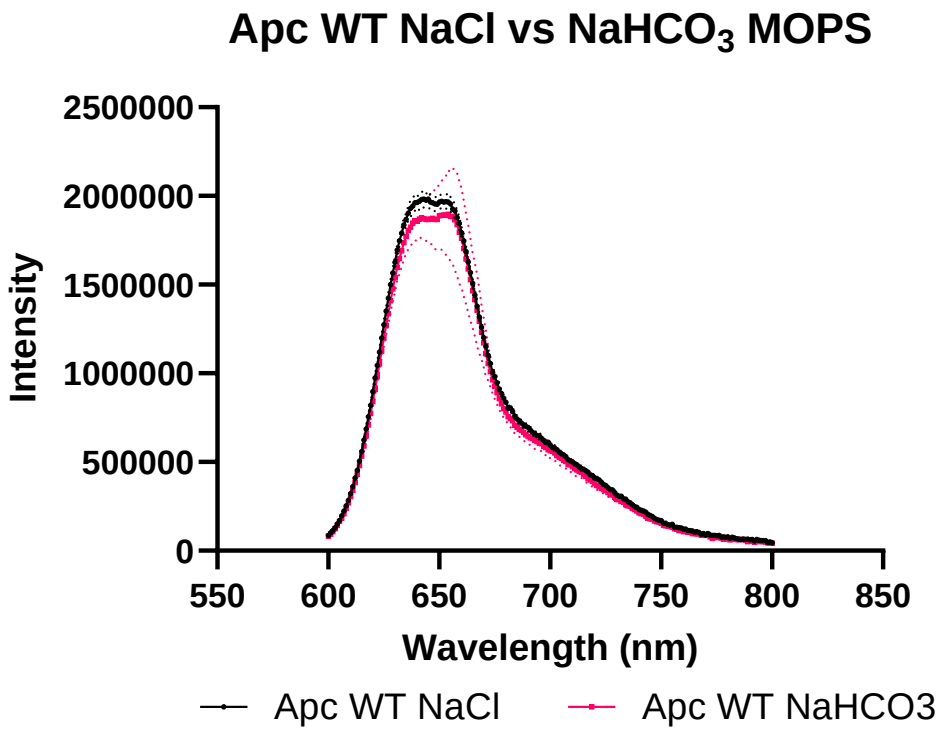

Figure 17: Excitation-emission spectra of Apc WT in 0.1 M MOPS and 20 mM NaCl or 20 mM $NaHCO_3$, with standard deviation denoted by dotted lines. $NaHCO_3$ N=5, NaCl N=3. Data was obtained using a Fluorolog.

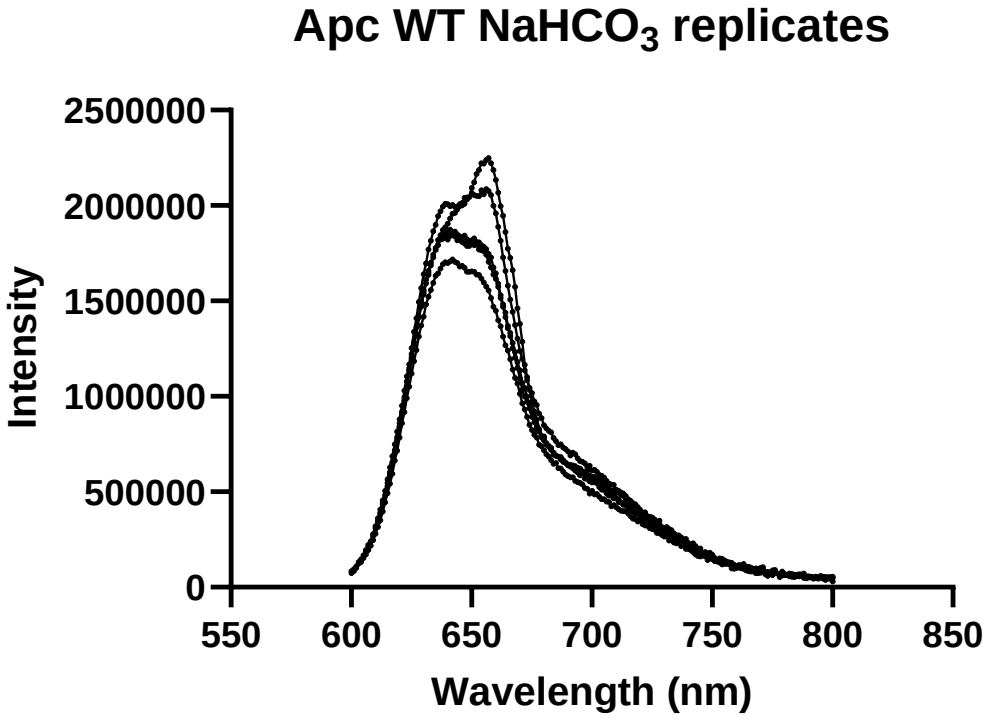

Figure 18: Individual replicates of excitation-emission spectra of Apc WT in a buffer of 20 mM $NaHCO_3$ and 0.1 M $MOPS_3$.

Despite precisely controlling buffer pH and changing the buffer used for diluting the sample and for creating 20 mM $NaHCO_3$ and 20 mM NaCl buffers to reduce the risk of CO_2 present in the $NaHCO_3$ buffer degassing, the methods used did not cause Apc WT fluorescence to change significantly in the presence of inorganic carbon. Additionally, some replicates of Apc WT analysis under $NaHCO_3$ conditions displayed unexplained, higher-than-expected emission maxima.

Excitation-Emission Analysis can Be Performed with a H4 Plate Reader

Apc WT did not respond significantly to the presence of inorganic carbon under several types of buffer conditions in the previous analyses. To increase the number of PBP analysis replicates that could be performed as part of a single experiment, the instrument used for excitation-emission analysis was changed. The first comparison of Apc WT under NaCl and $NaHCO_3$ conditions run using the new instrument was performed using the same protein preparation and the same sample pH and buffering method as the analysis displayed in (Figure 17).

The H4 plate reader allowed a much higher throughput of samples at a much lower volume, allowing the potential for greater sample numbers than the fluorolog. Method optimisation also allowed protein conservation due to the lower sample volumes required in a 96-well plate rather than the 3 ml cuvette.

Figure 19 displays the results of emission analysis of Apc WT when comparing NaCl with $NaHCO_3$ conditions. While significant differences were not observed between the test conditions (p>0.05 both before and after normalisation), the results aligned with previous analyses of Apc WT using the fluorolog. The combined coefficients of variance were 12.4% and 1.4% before and after normalisation, respectively.

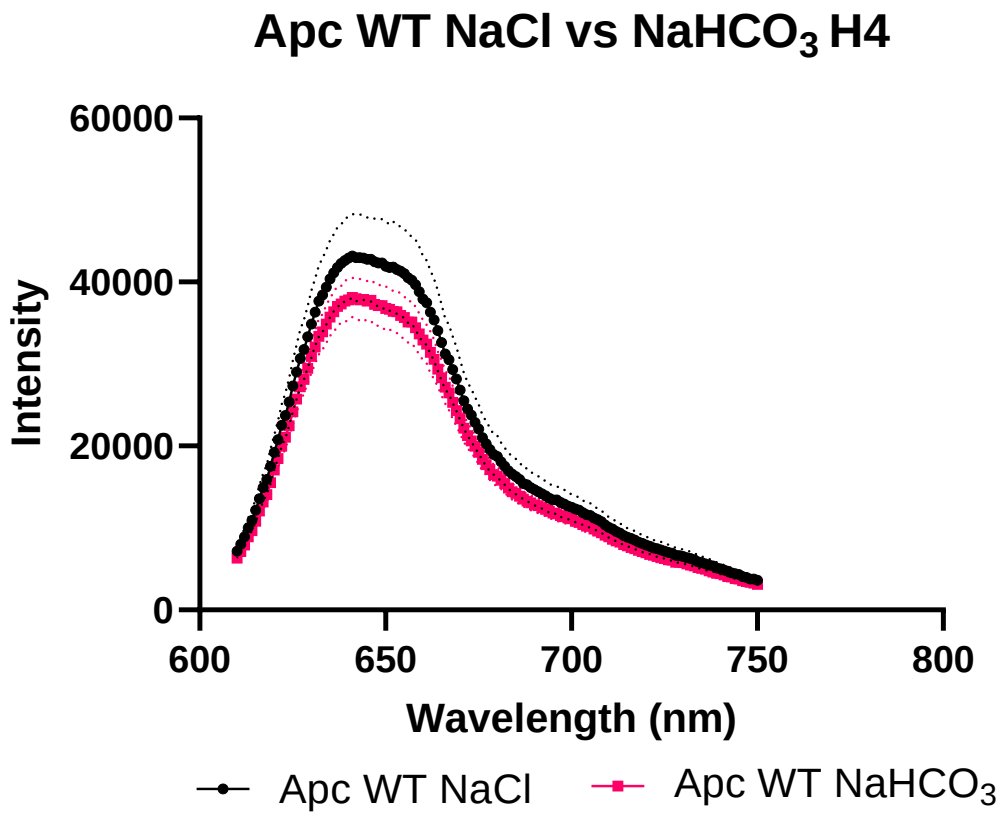

Figure 19: Excitation-emission spectra of Apc WT with 0.1 M MOPS and 20 mM NaCl or 20 mM $NaHCO_3$. Dotted lines denote standard deviation. N=5. Data was obtained using a H4 plate reader.

Apc WT Displayed Significant, Dose-Dependent Response to Inorganic Carbon

The first analysis using the H4 plate reader did not produce significant differences in Apc WT fluorescence between NaCl and $NaHCO_3$ conditions. A dose-dependent analysis was performed without modification to the method. However, more replicates (N=8) were used for dose-dependent analyses than previous analyses (N=5 or N=3). These results were obtained using the same protein preparation as all previous analyses of Apc WT using the fluorolog and H4 (Figure 15, Figure 16, Figure 17, Figure 19). The protein preparation had been purified over three weeks before the date of this analysis and stored at 4°C.

Apc WT analysis was performed in 5 mM and 20 mM concentrations of $NaHCO_3$ and NaCl (Figure 20, Figure 21). Data obtained showed significant (p<0.05) differences between NaCl and $NaHCO_3$ at concentrations of 5 mM and 20 mM, both in the original data (Table 7) and after peak values had

been normalised to starting emission (Table 8). There was a very high variance in the original data for both concentrations of NaCl and $NaHCO_3$ before normalising (Table 9).

When examining the raw data, 5 mM $NaHCO_3$ appears to reduce emission intensity. However, after normalising peak emission to starting fluorescence, 5 mM $NaHC0_3$ appears to increase the difference between peak and starting emission intensities (Table 10). A similar effect was not observed at the 20 mM concentration: 20 mM $NaHCO_3$ resulted in lower emission intensity than NaCl before and after normalisation to starting intensity.

When comparing 5 mM $NaHCO_3$ to 20 mM $NaHCO_3$ using a two-tailed unpaired *t*-test with Welch's correction, p=0.0003 and the 20 mM $NaHCO_3$ concentration has a lower emission intensity than 5 mM $NaHCO_3$ (Figure 22). No significant differences were observed between 5 mM NaCl and 20 mM NaCl conditions using a two-tailed unpaired *t-test* with Welch's correction (p=0.30). This would suggest a dose-dependent reduction in Apc emission mediated by adding $NaHCO_3$. However, it was expected that a dose-dependent increase in Apc emission would be observed, as it was demonstrated previously that increased carbon dioxide concentrations enhance the fluorescence of Apc *in vitro* and in live cells (Guillén-García et al., 2022).

It has previously been reported that absorbance spectra can be used to differentiate between Apc monomers and trimers (MacColl, 2004). This study did not aim to detect Apc trimers based on absorbance spectra because a method for measuring Apc assembly based on absorbance spectra could not be validated until functional Apc trimers were verifiably produced. However, even though a method for measuring Apc assembly using absorbance spectra had not been validated, the absorbance spectra may be used to indicate whether Apc trimers were present. The peak at 615 nm would suggest that most of the Apc units in the protein sample were monomers, and the shoulder visible at approximately 650 nm may represent a small amount of Apc trimers (Figure 23).

When interpreting these data, it is important to consider that the protein used had been purified three weeks before the experiment date and stored at 4^{o}C in a buffer composed of 30 mM Tris, 150

mM NaCl, and the proportion of fully assembled Apc hexamers was not quantified before analysis. It is unlikely that a quantitatively relevant number of Apc hexamers was present in the sample.

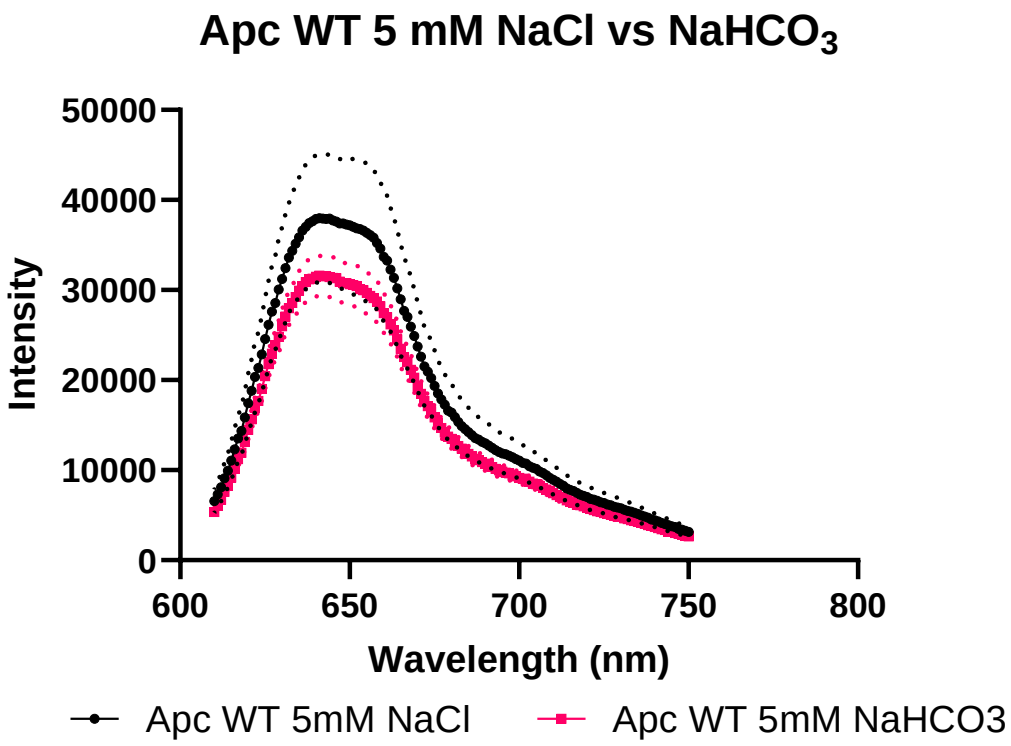

Figure 20: Excitation-emission spectra of Apc WT in 0.1 M MOPS and 5 mM NaCl or 5 mM $NaHCO_3$, with standard deviation denoted by dotted lines. N=8. Data was obtained using a H4 plate reader.

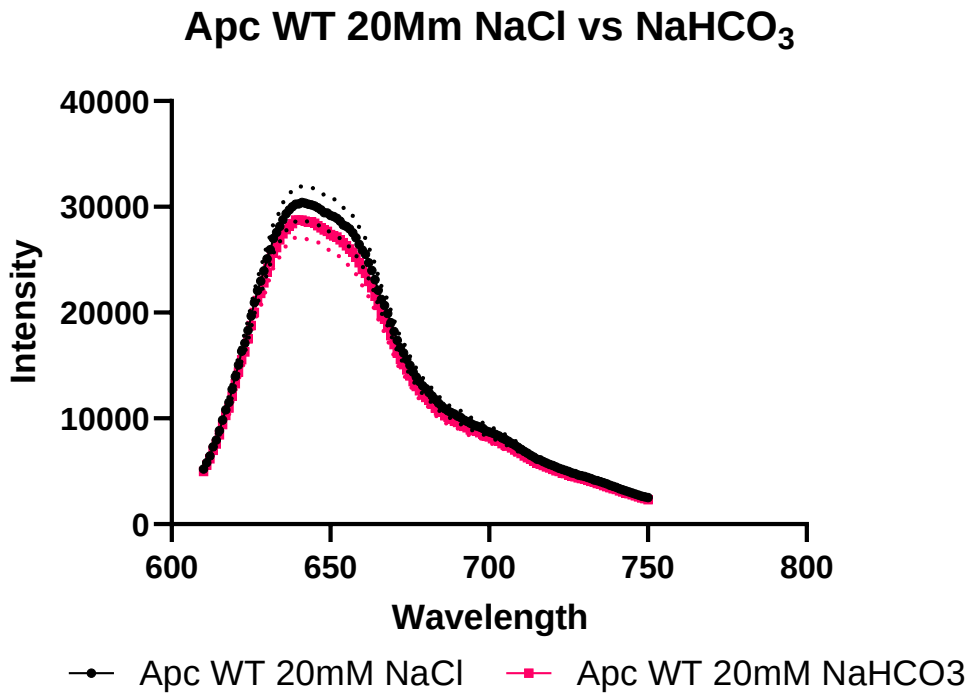

Figure 21: Excitation-emission spectra of Apc WT in 0.1 M MOPS and 20 mM NaCl or 20 mM $NaHCO_3$, with standard deviation denoted by dotted lines. N=9. Data was obtained using a H4 plate reader.

Table 7: Emission intensity (arbitrary units) of NaCl and $NaHCO_3$ conditions at concentrations of 5mM and 20mM.

641nm	5 mM NaCl	5 mM NaHCO3	20 mM NaCl	20 mM NaHCO3
Average	37,993	31,586	30,429	28,764
Standard deviation	6,572	2,027	1,500	1,549

Table 8: Average values and standard deviations of normalised NaCl and $NaHCO_3$ conditions at concentrations of 5mM and 20mM.

Normalised to 610nm	5 mM NaCl	5 mM NaHCO3	20 mM NaCl	20 mM NaHCO3
Average	5.81	5.89	5.85	5.78
Standard deviation	0.08	0.05	0.03	0.03

Table 9: Coefficients of variance for raw and normalised data for analysis of 5mM and 20mM NaHCO3 on Apc WT emission.

	5 mM NaCl / NaHCO3	20 mM NaCl / NaHCO3
Raw data	18.4%	7.3%
Normalised	1.6%	0.8%

Table 10: Comparison of 5mM averages before and after normalisation

	5 mM NaCl	5 mM NaHCO3	5 mM NaCl	5 mM NaHCO3
Average	37,993	31,586	5.814	5.892
Standard deviation	6,572	2,027	0.078	0.052
Variance	0.173	0.064	0.013	0.009
p-value	0.027		0.048	

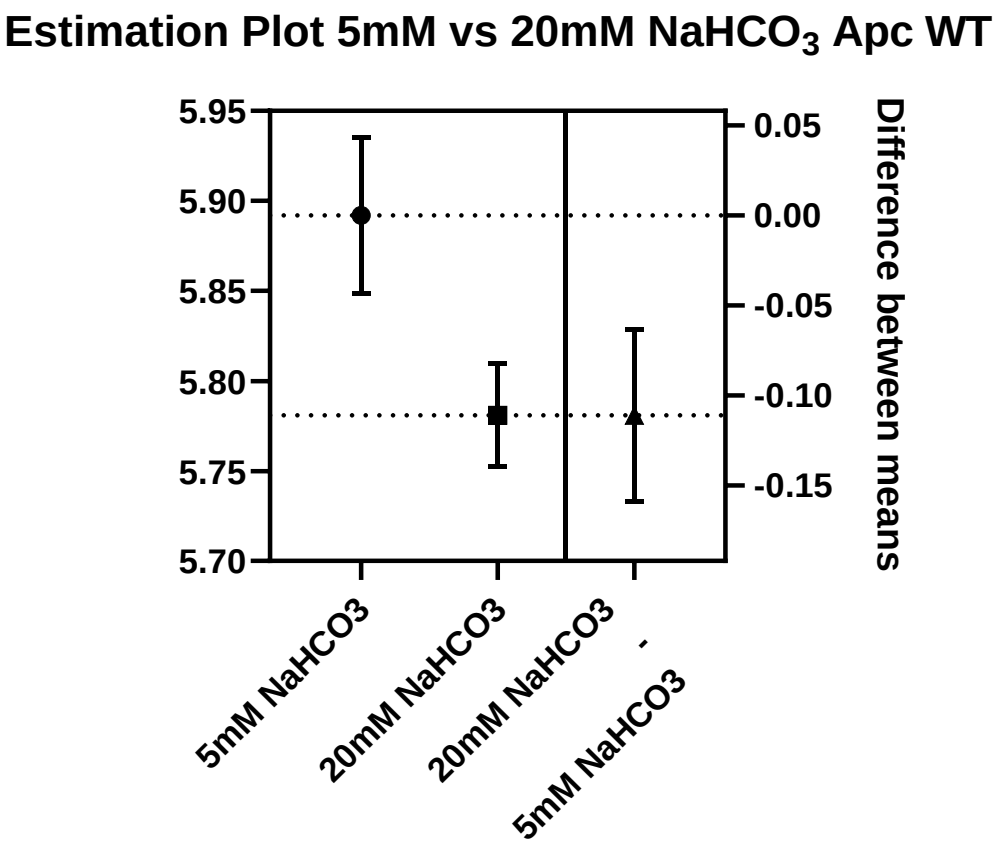

Figure 22: Estimation plot displaying the normalised mean values and standard deviations of Apc WT treated with 5mM $NaHCO_3$ and 20mM $NaHCO_3$ and the difference between the means.

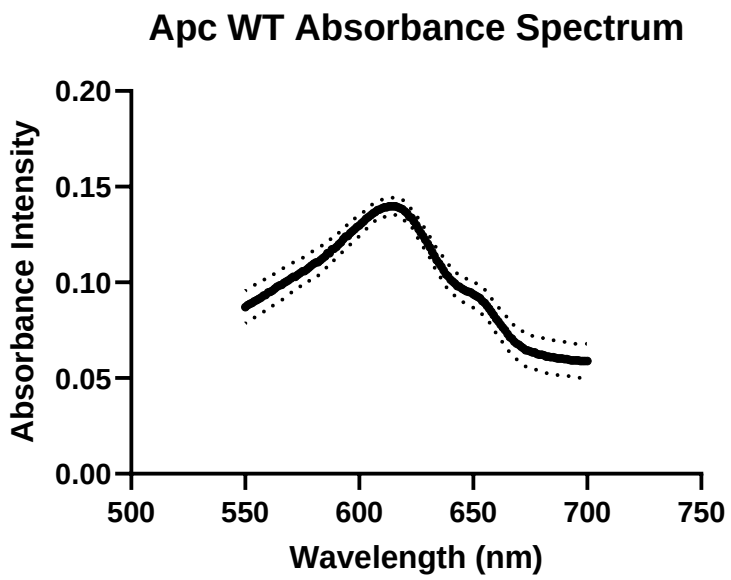

Figure 23: Apc WT absorbance spectrum with standard deviation denoted by dotted lines. N=3.

The data suggests that with a sufficiently high sample number (N=8), a dose-dependent suppression of Apc WT fluorescence is caused by the addition of inorganic carbon.

Significant Apc WT Response to Inorganic Carbon Was Not Reproduced

Once a dose-dependent response of Apc WT to $NaHCO_3$ was observed, Apc WT and Apc K6A was freshly expressed, purified, and analysed again to confirm the response observed in Apc WT and to determine whether the mutation at the K6A carbamylation site affected this response.

The SDS PAGE gel displayed bands (Figure 24). For the WT and the K6A mutant, there were two large bands between 15kDa and 25kDa, indicating that the majority of protein purified came from the recombinantly expressed APC proteins.

The excitation-emission analysis results of Apc WT and Apc K6A in the presence of 20 mM NaCl and $NaHCO_3$ were unexpected. (Figure 25, Figure 26). The raw data from the Apc K6A mutant shows a significant ($p=0.009$) decrease between peak fluorescence in the presence of 20 mM $NaHCO_3$ compared with 20 mM NaCl. After normalising the Apc K6A peak data to emission at 610 nm, $p=0.071$. Apc WT did not display significant differences between $NaHCO_3$ and NaCl conditions in the original or normalised data. The data generated using the Apc K6A mutant was consistent with data

previously generated using Apc WT, and the data generated using the Apc WT sample was consistent with the expected data from Apc K6A. The similarity between the K6A mutant and previously generated data with Apc WT raised the possibility that human error during purification or experimental set-up resulted in the Apc WT sample being labelled 'Apc K6A' and vice versa. Additionally, the emission maxima occurred at a higher wavelength than usual, at approximately 655nm, when it was expected to be approximately 643nm for both K6A and the WT. For variance coefficients, see (Table 11).

The absorbance spectra for Apc WT and Apc K6A show the peak at 615 nm with a shoulder at 650 nm. However, the Apc WT displays a much more pronounced shoulder at 650 nm (Figure 27, Figure 28). As previously stated, this suggests that the protein sample was made chiefly of monomers with few trimers. However, a method for differentiating between PBP monomers and trimers was not validated for these experiments.

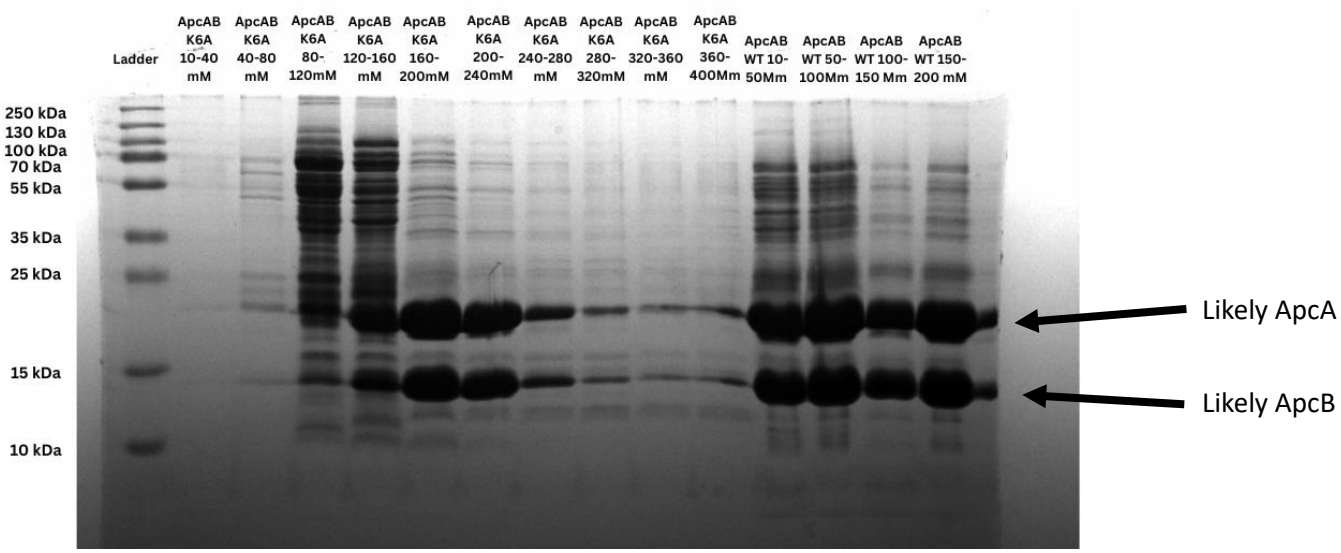

Figure 24: Apc WT and K6A HisTrap purified using ÄKTA™ Start on a gradient increase of imidazole concentration up to 400 mM for ApcAB^{K6A} and up to 500 mM for ApcAB WT. Concentrated ApcAB WT 10 mM – 200 mM imidazole (all ApcAB WT fractions on gel) for excitation emission analysis. Concentrated ApcAB-K6A 160 mM – 240 mM imidazole for excitation-emission analysis.

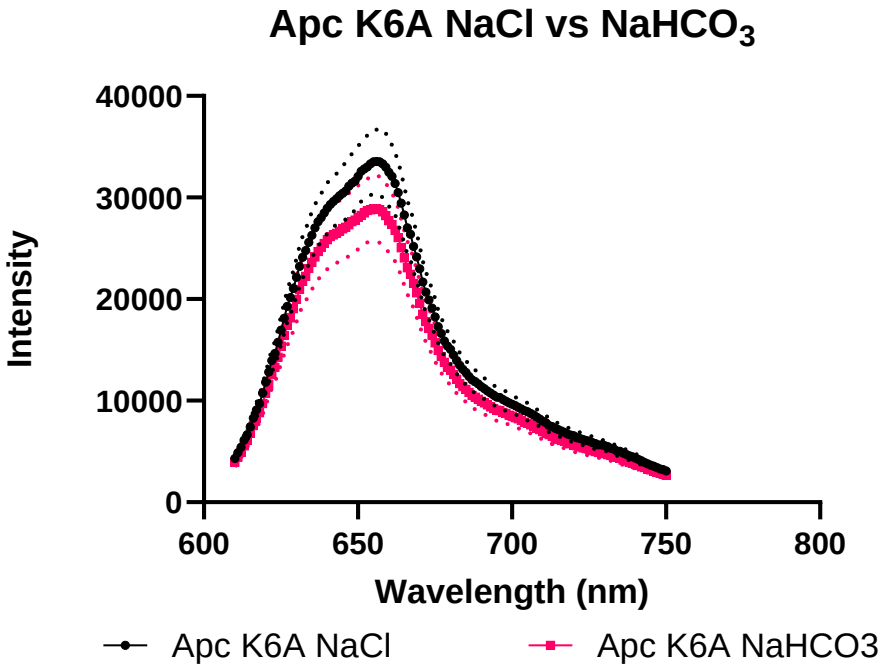

Figure 25: Excitation-emission spectra of Apc K6A in 0.1 M MOPS and 20 mM NaCl or 20 mM $NaHCO_3$. Dotted lines denote standard deviation. N=9. Data was obtained using a H4 plate reader.

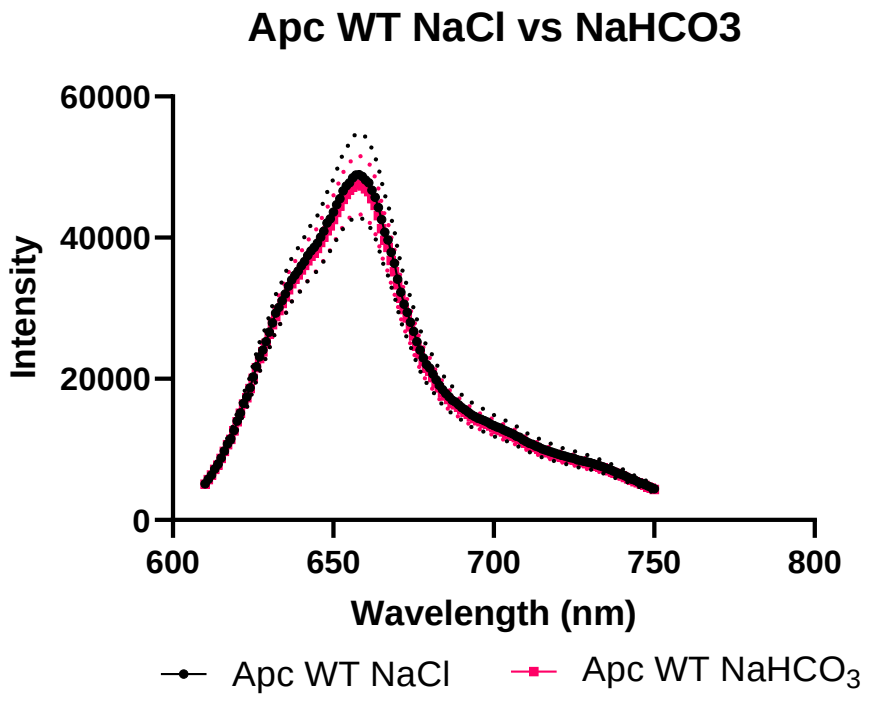

Figure 26: Excitation-emission spectra of Apc WT in 0.1 M MOPS and 20 mM NaCl or 20 mM $NaHCO_3$. Dotted lines denote standard deviation. N=10. Data was obtained using a H4 plate reader.

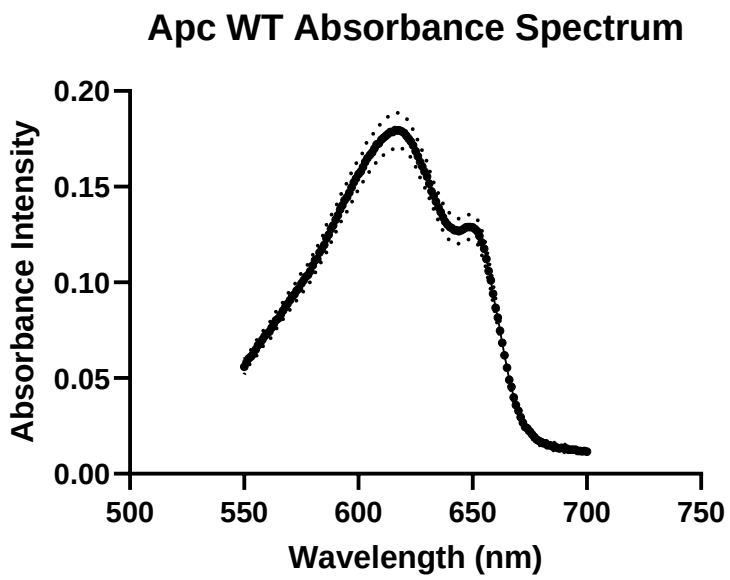

Figure 27: Apc WT Absorbance Spectrum. Dotted lines denote standard deviation. Data was obtained using a H4 plate reader N=3.

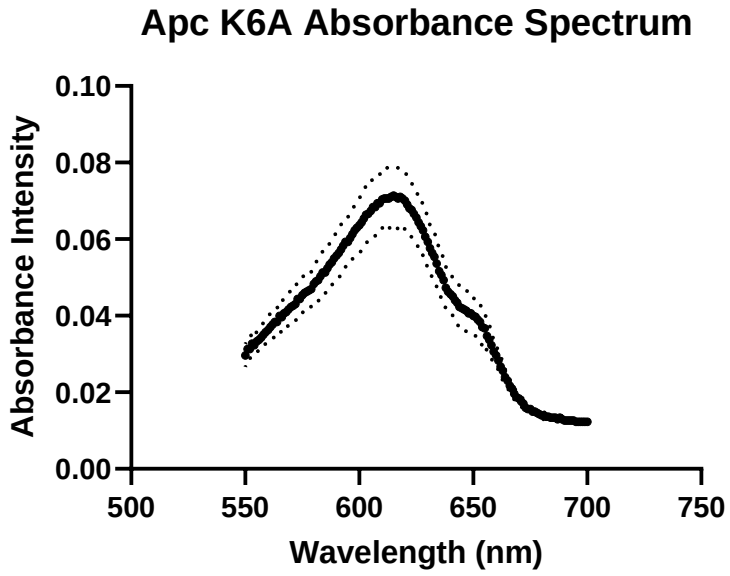

Figure 28: Apc K6A Absorbance Spectrum. Dotted lines denote standard deviation. Data was obtained using a H4 plate reader N=3.

Table 11: Combined coefficients of variance for Apc WT and Apc K6A before and after normalising emission peaks to emission at 610nm

	Apc WT	**Apc K6A**
Raw	14.3%	14.0%
Normalised	5.4%	11.5%

Due to the unexpected response of Apc K6A to $NaHCO_3$, and the unexpected lack of a response of Apc WT to $NaHCO_3$, no conclusions could be drawn from this analysis. Additionally, the unexpectedly

high wavelength of the emission peaks for both Apc WT and Apc K6A suggested that the proteins may not have functioned properly at the time of analysis.

Significant Apc WT Response to Inorganic Carbon Was Not Reproduced, Again

The previous analysis of Apc WT did not result in any differences between emission in the presence of $NaHCO_3$ and NaCl, and the peak emission wavelength was unexpectedly high. Another analysis of the same protein preparation was performed to assess if the unexpected similarity between the NaCl and $NaHCO_3$ conditions in the sample labelled 'Apc WT' resulted from human error on the day of analysis.

There was no significant difference between Apc WT under NaCl and $NaHCO_3$ conditions (p=0.22). Peak emission occurred again at a higher-than-expected wavelength (657±1 nm) (Figure 29).
The combined variance before and after normalisation was 7.6% and 3.3%, respectively.

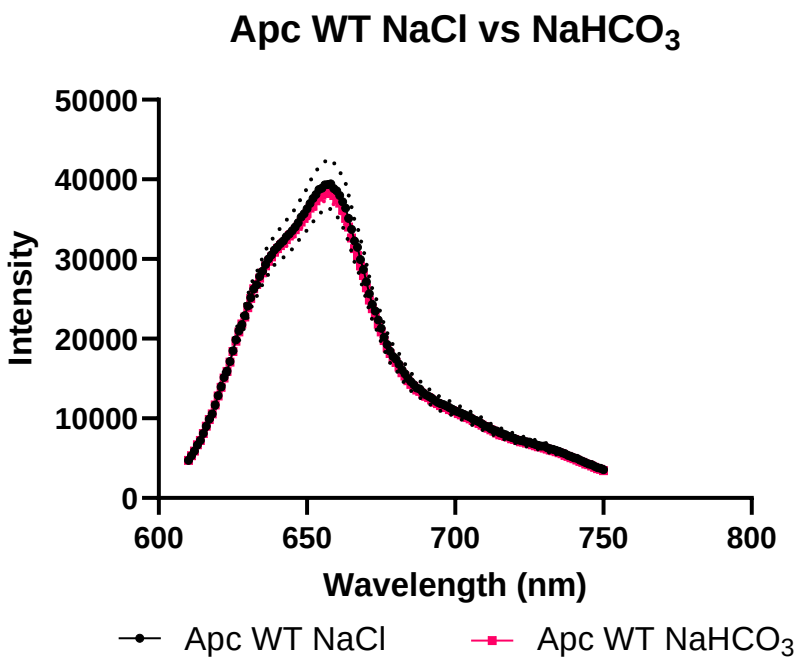

Figure 29: Repeat comparison between Apc WT under NaCl and $NaHCO_3$ conditions using the 'Apc WT' protein from the previous analysis to see if the pattern from the previous analysis was repeated. N=5. Data was obtained using a H4 plate reader.

The absence of a response of Apc WT to $NaHCO_3$ was repeated in this analysis. It was likely that the two protein preparations had not been mislabelled at the time of the previous analysis.

Apc WT Purified with IMAC followed by SEC Did Not Respond to Inorganic Carbon

Due to the unexpected absence of differences between Apc WT under NaCl and $NaHCO_3$ conditions, Apc WT and Apc K6A were purified using IMAC followed by SEC. The protein preparations used (Figure 25, Figure 26, Figure 29) were discarded. The excitation-emission analysis was performed again using the same method used to generate the data displayed in (Figure 25, Figure 26, Figure 29).

To reduce the risk of non-specific interactions, fresh purifications of Apc WT and K6A were produced using both IMAC and SEC (Figure 34, Figure 35), unlike previous preparations, which employed only IMAC.

The chromatograms produced by the ÄKTA™ Start during SEC suggest that there may have been few Apc WT trimers and no Apc WT hexamers, given the absence of separated peaks at the expected elution volume of trimers (73 ml) and no peak at the expected elution volume of the hexamer (52 ml) (Figure 30). The K6A mutant displayed three peaks. However, there was little separation between the larger peaks at approximately 75 ml and 80 ml (Figure 31), indicating little separation between Apc K6A αβ monomers (expected elution at >73 ml) and trimers (expected elution at 73 ml). A small peak eluted at approximately 50 ml from the Apc K6A sample, which may have corresponded to αβ hexamers that were expected to elute at 52 ml. However, this fraction was not used for further analysis due to insufficient sample size. The fractions containing both larger peaks were pooled together and used in the protein emission analysis. For variance, see (Table 12).

The Apc WT PAGE gel of SEC fractions (Figure 32) displays large bands of dissociated α and β subunits between 15 kDa and 25 kDa. In the PAGE gel of Apc K6A SEC fractions (Figure 33) also displayed large bands of dissociated α and β subunits between 15 kDa and 25 kDa. For both Apc WT and Apc K6A, the gels indicate that large quantities of recombinant Apc proteins were present in purified fractions.

The absorbance spectra display the peak at approximately 615 nm with a shoulder at 650 nm. This could indicate that the samples are mostly monomers with some trimers (Figure 36, Figure 37).

There were no significant differences between peak emission between the NaCl and $NaHCO_3$ states for the WT before or after normalising peak emission intensity to intensity at 610 nm. However, when comparing the NaCl to $NaHCO_3$ state for K6A, the *t*-test of the original data resulted in $p>0.05$, but after normalisation to starting emission intensity, $p=0.0053$. Despite purifying fresh protein and adding SEC during purification, the proteins analysed displayed the same problems as the previous set of analyses, i.e. the 'K6A' but not 'WT' mutant responded to inorganic carbon, and the emission maxima were between 655-658nm for both WT and K6A Apc. During this experiment, the K6A mutant displayed a much greater and more significant response to inorganic carbon than in the previous experiment, suggesting that the lack of significant results from analysis of the previous K6A analysis may have been a result of large inter-replicate variance (Table 11, Table 12). These data indicate that the unexpected data previously generated using the protein samples were introduced during protein expression or storage at -80°C.

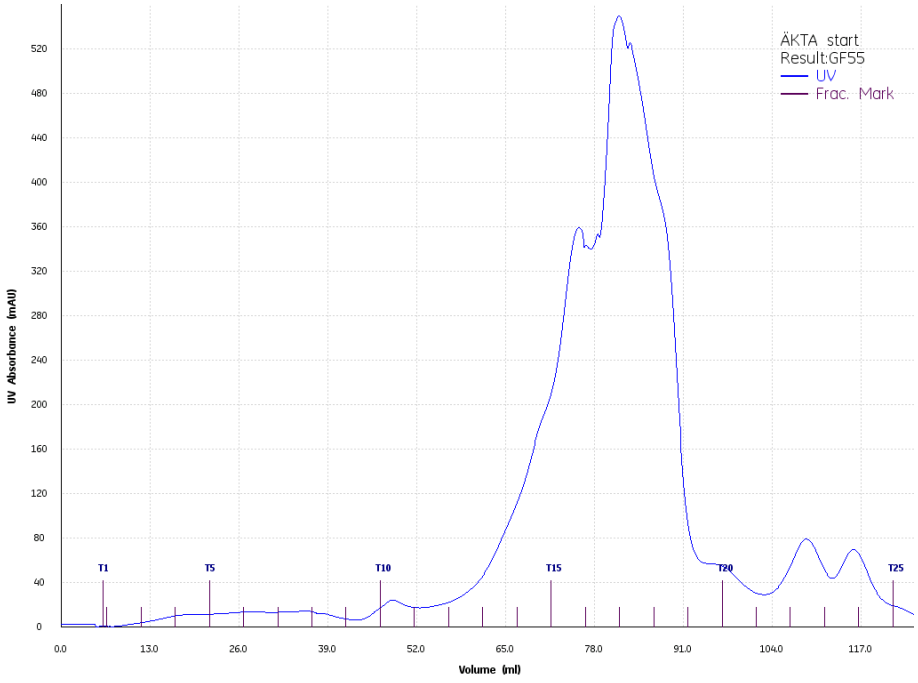

Figure 30: Chromatogram produced by ÄKTA™ Start of Apc WT SEC purification displaying elution of the fractions in which protein was eluted. Protein concentration was determined using UV absorbance measurements taken by the instrument. Fractions 14-18 were used for excitation-emission analysis.

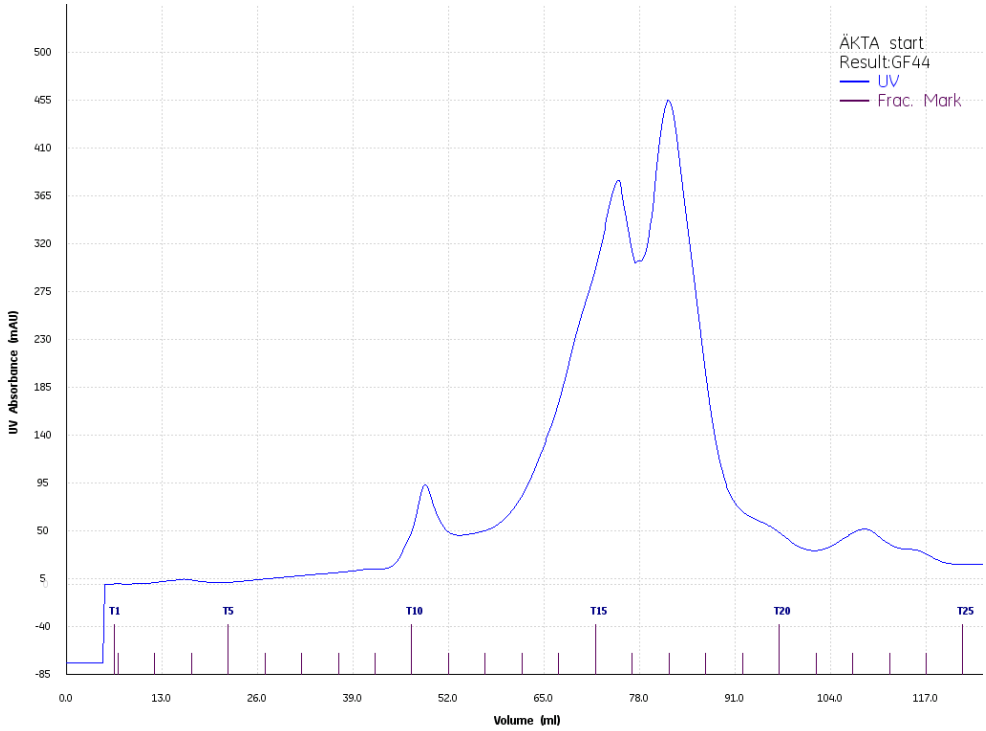

Figure 31: Chromatogram produced by ÄKTA™ Start of Apc K6A SEC purification displaying elution of the fractions in which protein was eluted. Protein concentration was determined using UV absorbance measurements taken by the instrument. Fractions 14-17 were used for excitation-emission analysis.

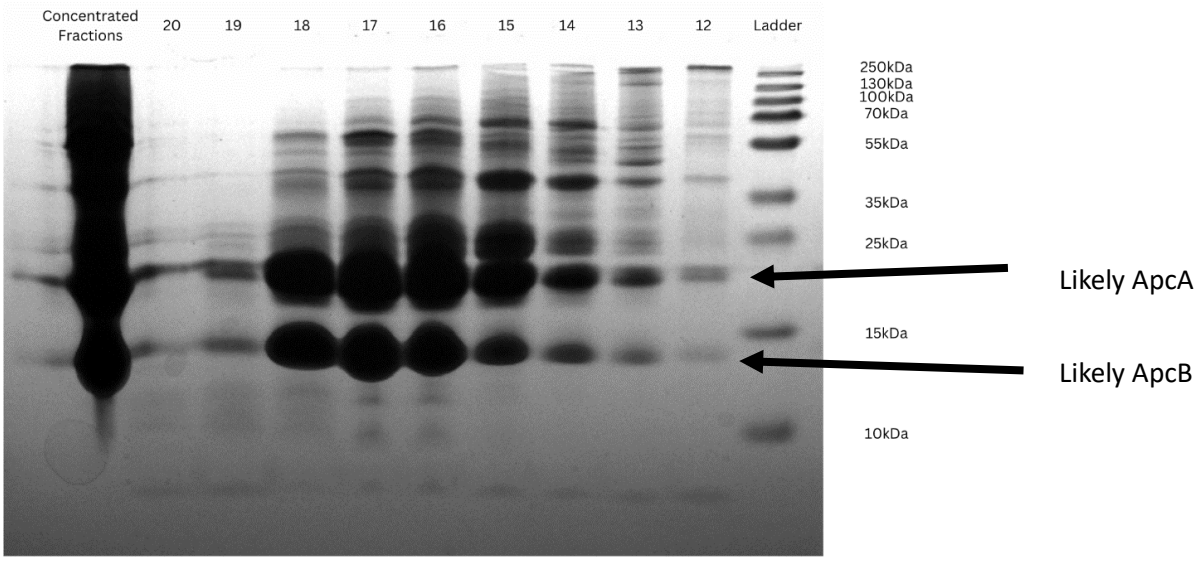

Figure 32: PAGE gel of purified Apc WT SEC fractions and concentrated combined fractions. Fractions 14-18 inclusive were concentrated for excitation-emission analysis.

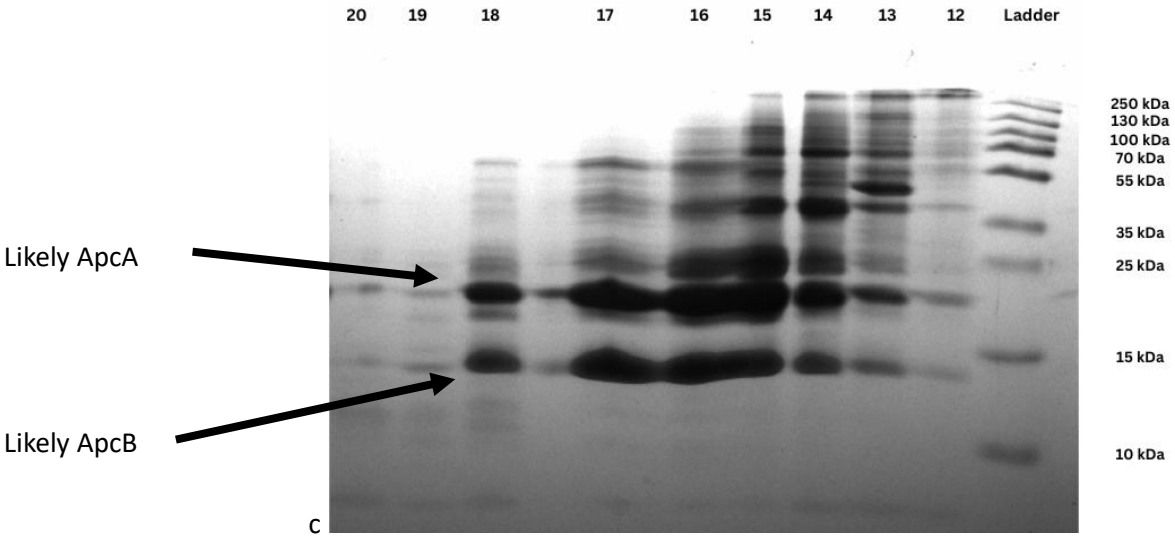

Figure 33 PAGE gel of Apc K6A SEC fractions. Fractions 14-17 inclusive were concentrated for excitation-emission analysis.

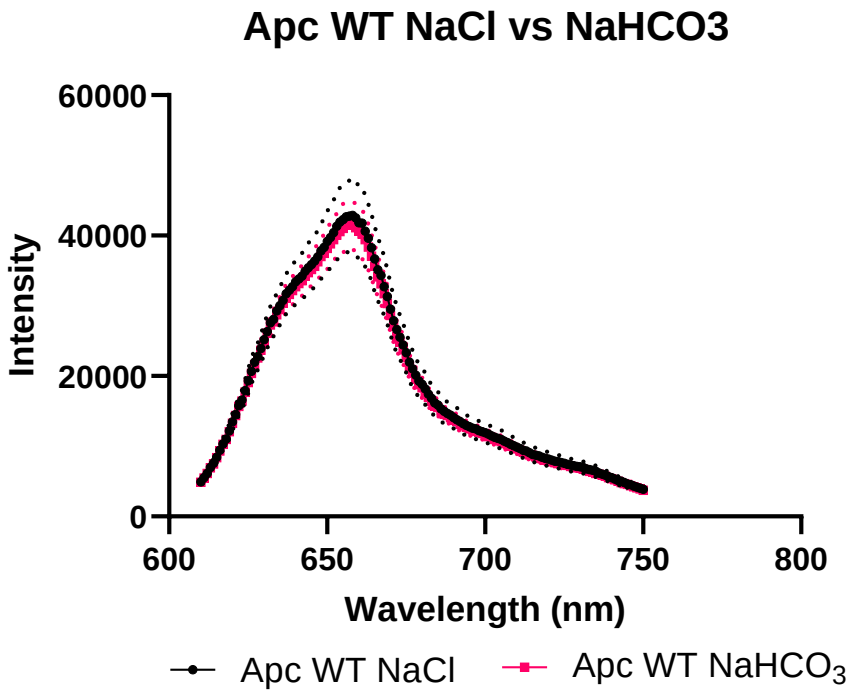

Figure 34: Excitation-emission spectra of Apc WT in 0.1M MOPS and 20 mM NaCl or 20 mM $NaHCO_3$, with standard deviation denoted by dotted lines. Apc WT was purified with IMAC and SEC before analysis. N=5. Data was obtained using a H4 plate reader.

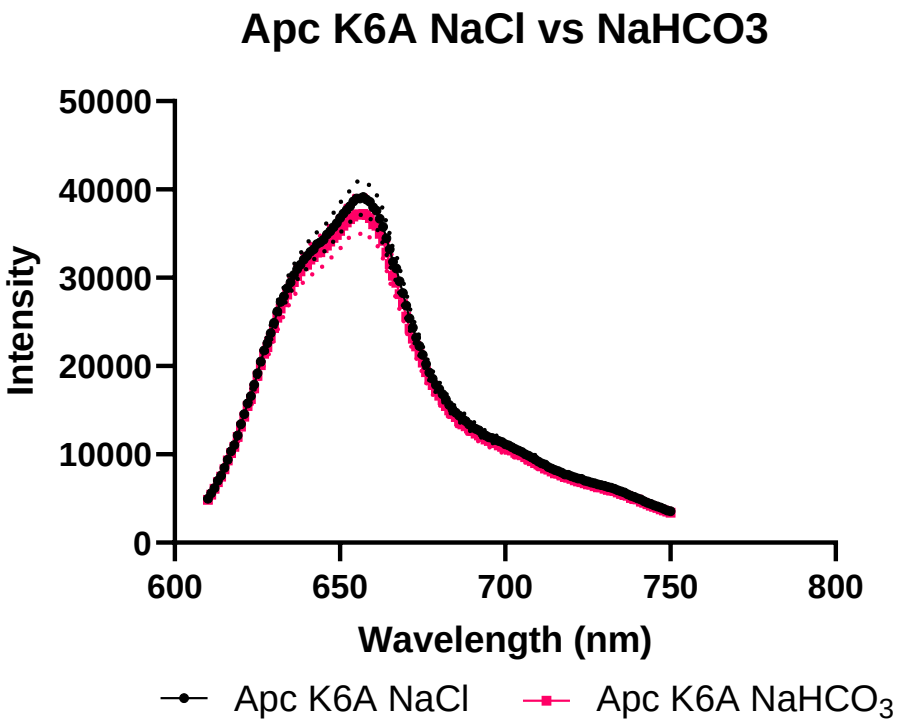

Figure 35: Excitation-emission spectra of Apc K6A mutant in 0.1 M MOPS and 20 mM NaCl or 20 mM $NaHCO_3$, with standard deviation denoted by dotted lines. Apc K6A was purified with IMAC and SEC before analysis. N=5. Data was obtained using a H4 plate reader.

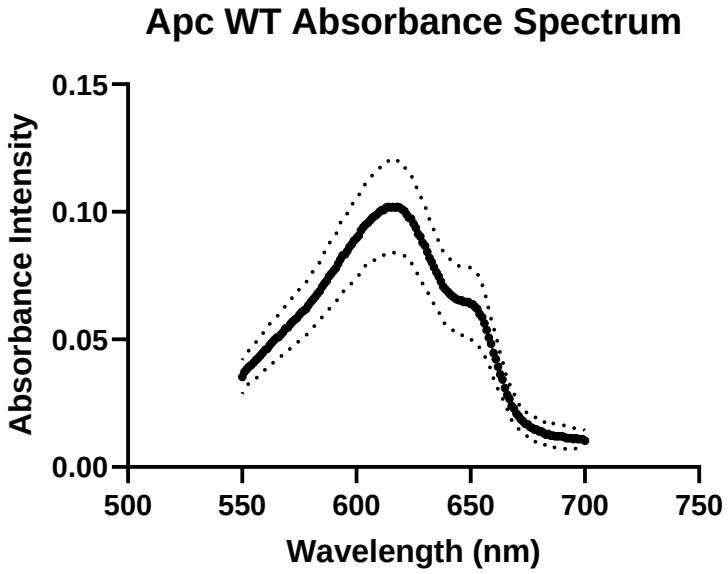

Figure 36: Absorbance Spectrum of Apc WT with standard deviation denoted by dotted lines. N=3. Data was obtained using a H4 plate reader. The analysed protein was in a solution of 0.1 M MOPS at a pH between 7.35 and 7.50.

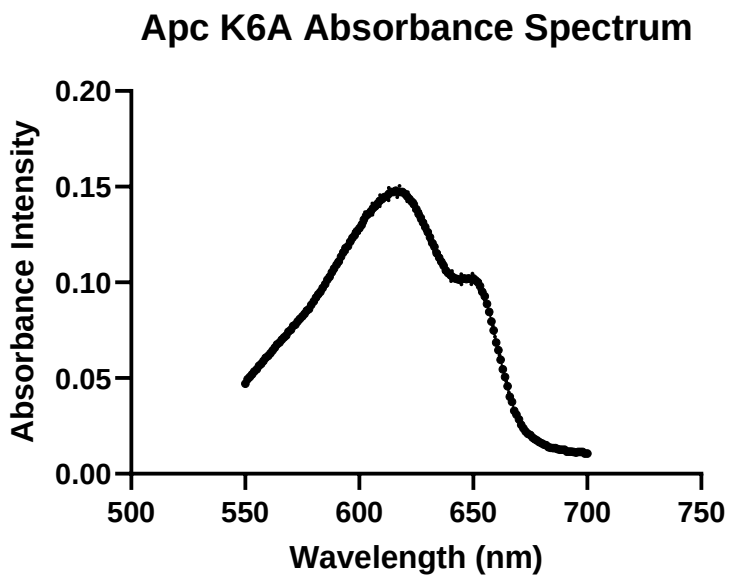

Figure 37: Apc K6A Absorbance Spectrum. Dotted lines denote standard deviation. N=3. Data was obtained using a H4 plate reader. Analysed protein was in a solution of 0.1 M MOPS at a pH between 7.35 and 7.50.

Table 12: Combined variance coefficients for Apc WT and Apc K6A samples before and after normalising peak emission intensity to intensity at 610 nm.

	Apc WT	**Apc K6A**
Raw	12.7%	6.3%
Normalised	3.7%	1.5%

Despite freshly purifying Apc WT and Apc K6A, neither protein preparation responded to $NaHCO_3$ as expected. Apc WT displayed no significant response to $NaHCO_3$, and Apc K6A displayed a significant difference between its emission maximum and emission at 610 nm. Both Apc K6A and Apc WT displayed higher-than-expected emission wavelength maxima. Additionally, the protein preparations used for both analyses likely consisted chiefly of αβ monomers and trimers.

Apc WT and Apc K6A αβ Trimers Did Not Respond Significantly to Inorganic Carbon

The previous three analyses had returned unexpected results that were most likely caused by unknown problems that occurred during protein expression or storage. To avoid, these problems, Apc WT and Apc K6A were expressed and purified again. Before purification of this protein batch, a calibration curve for the SEC column used was created to identify fractions likely to contain assembled Apc, as previous research demonstrated that enhanced Apc fluorescence was observed in

assembled Apc hexamers (Guillén-García et al., 2022). SEC was used to isolate Apc WT and Apc K6A trimer fractions for the excitation-emission analysis, which was performed without modifications.

The fresh preparation of Apc WT and K6A was expressed and purified using IMAC followed by SEC. The chromatogram produced during SEC corresponding to the Apc WT (Figure 38) shows that some hexamers may have been eluted at approximately 50 ml. However, there was insufficient sample in those fractions for further analysis. A clear peak at approximately 73 ml corresponded to the expected elution volume of Apc WT trimers. This peak was purified and analysed separately from the adjacent peak at approximately 85 ml, which was not analysed further. In the chromatogram for the Apc K6A purification (Figure 39), nothing eluted at 52 ml, suggesting a complete absence of hexamers. The peak at approximately 73 ml was bigger than the peak at approximately 85ml, implying that there was a greater quantity of αβ trimers than αβ monomers in the sample. The fraction corresponding to the trimers was used for further analysis.

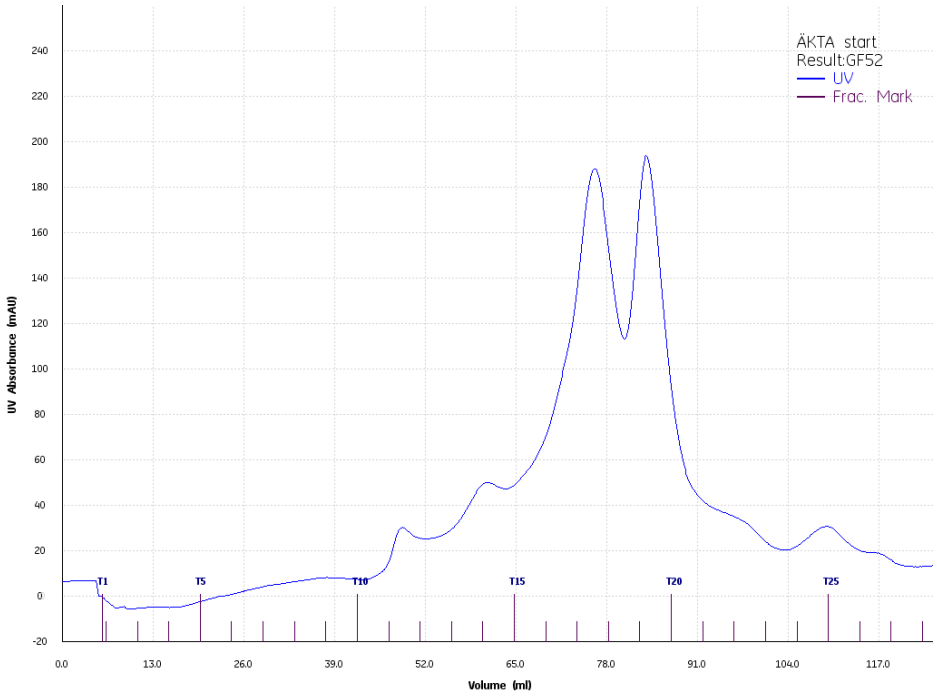

Figure 38: Chromatogram of Apc WT SEC purification displaying the fractions in which protein was eluted. Protein concentration was determined using UV absorbance measurements taken by the instrument. Fractions 14, 15, and 16 were concentrated for excitation-emission analysis.

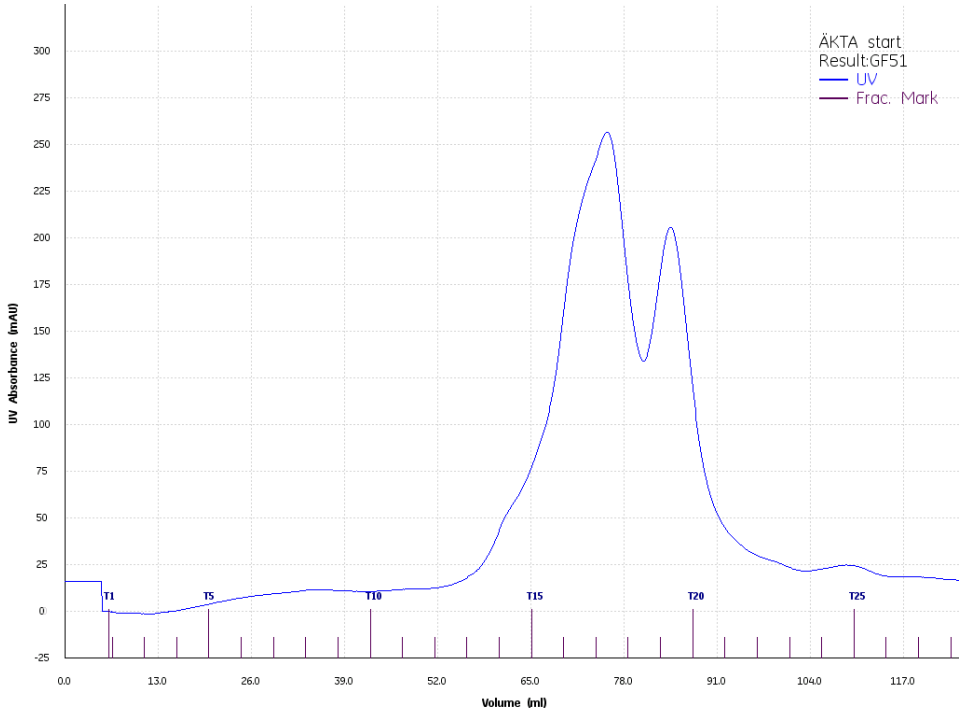

Figure 39: Chromatogram of Apc K6A SEC purification displaying the fractions in which protein was eluted. Protein concentration was determined using UV absorbance measurements taken by the instrument. Fractions 14, 15, and 16 were purified for excitation-emission analysis.

Interestingly, the K6A peak emission was around 640 nm (Figure 41) using this batch, but the WT peak emission was still approximately 656 nm (Figure 40). There were no significant differences between NaCl and $NaHCO_3$ conditions in the raw data or after normalising to emission at 610 nm for Apc WT or the K6A mutant. Combined variance coefficients are displayed in (

Table 13). Additionally, to demonstrate that the variance observed between replicates was not a result of the H4 plate reader's error, (Figure 42) displays the mean values and standard deviations of each biological replicate when measured three times in quick succession. The coefficient of variance for each replicate ranged from 0.9% to 2.0% for the six replicates at their emission maxima.

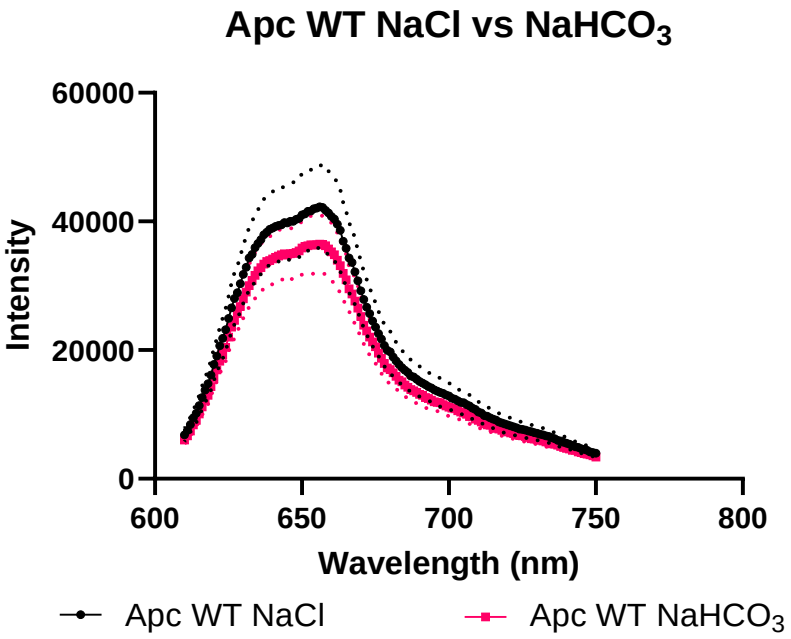

Figure 40: Excitation-emission spectra of Apc WT in 0.1 M MOPS and 20 mM NaCl or 20 mM $NaHCO_3$, with standard deviation denoted by dotted lines. Apc WT was purified with IMAC and SEC before analysis. N=3. Data was obtained using a H4 plate reader.

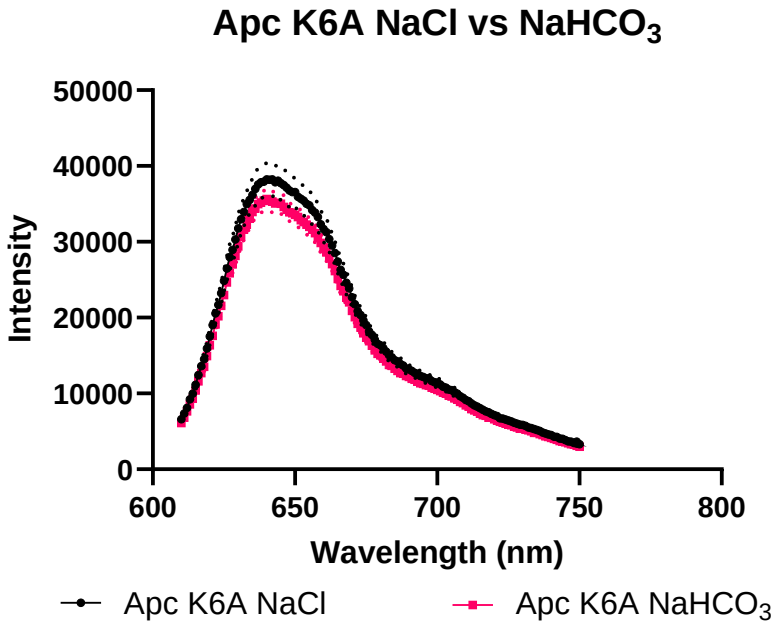

Figure 41: Excitation-emission spectra of Apc K6A mutant in 0.1 M MOPS and 20 mM NaCl or 20 mM $NaHCO_3$, with standard deviation denoted by dotted lines. Apc K6A was purified with IMAC and SEC before analysis. N=3. Data was obtained using a H4 plate reader.

Table 13: Combined variances of NaCl and $NaHCO_3$ conditions before and after normalisation of Apc WT and Apc K6A peak emission intensity to intensity at 610 nm.

	Apc WT	Apc K6A
Raw	15.8%	5.8%
Normalised	2.0%	0.6%

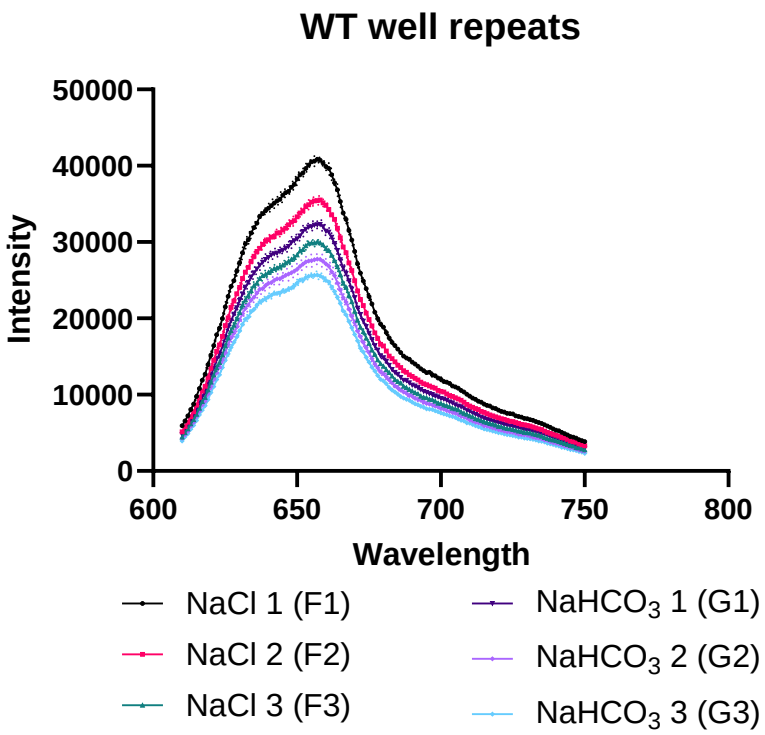

Figure 42: Repeat measurements (N=3) of each well used to analyse Apc WT protein variations in emission intensity measurements. Data was obtained using a H4 plate reader.

Apc WT and Apc K6A trimer fractions did not respond to $NaHCO_3$, in contrast with the dose-dependent significant response observed for Apc WT purified using IMAC alone in (Figure 21, Figure 20). Additionally, the variance between repeated measurements of the same samples using the H4 plate reader demonstrated that the absence of significant differences in Apc WT was not due to instrument error.

60-hour Incubation of Apc WT and Apc K6A with $NaHCO_3$ Caused Significant Fluorescence Decrease

Apc WT and Apc K6A displayed no significant difference in fluorescence for either protein in the presence of $NaHCO_3$. To assess if long-term exposure to $NaHCO_3$ affected fluorescence intensity, the samples used for the previous analysis (Figure 40, Figure 41) were incubated in the 20 mM NaCl or 20 mM $NaHCO_3$ buffers for approximately 60 hours at 4°C and then analysed again with no modifications to the analysis method.

After incubation, the K6A mutants displayed significant differences between NaCl and $NaHCO_3$ conditions when analysing the raw data (p=0.00023) (Figure 43), however after normalising peak emission intensity to emission at 610 nm, the difference between test conditions was not significant (p=0.71). This is in contrast with the WT, which had significant differences both before (p=0.026) and after (p=0.0032) normalisation to emission at 610nm (Figure 44). However, the pH in the two test conditions might have been altered significantly over time due to the differing buffering capacities of NaCl and $NaHCO_3$. For variance analysis, see (Table 14).

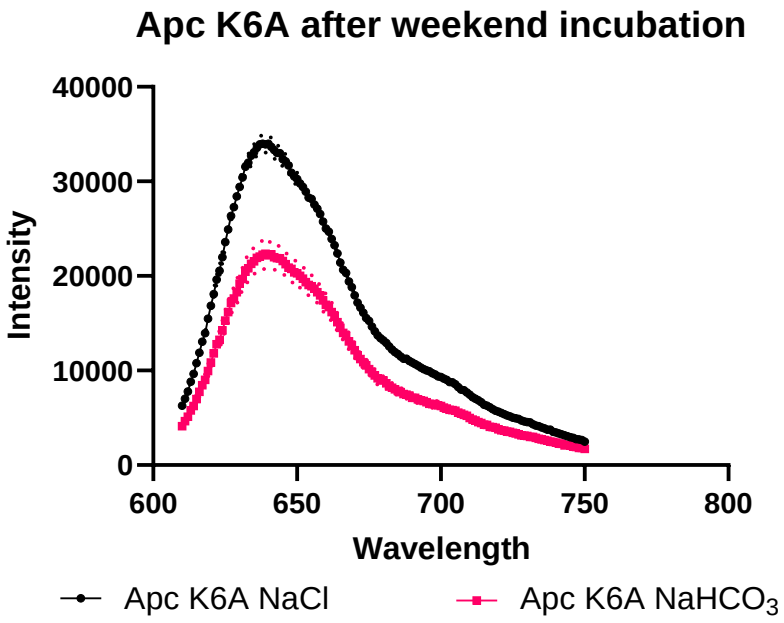

Figure 43: Excitation-emission spectra of Apc K6A mutant when incubated with 20 mM NaCl or 20 mM $NaHCO_3$, with standard deviation denoted by dotted lines. Apc K6A was purified with IMAC and SEC before analysis and then incubated for approximately 60 hours in NaCl or $NaHCO_3$ buffers. N=3. Differences in peak intensity are not significant after normalisation to emission at 610nm. Data was obtained using a H4 plate reader.

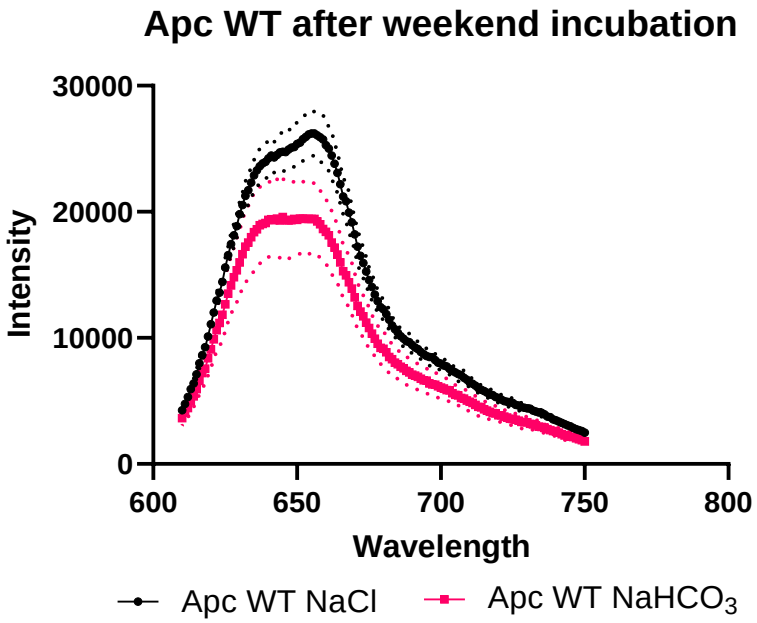

Figure 44: Excitation-emission spectra of Apc WT when incubated with 20 mM NaCl or 20 mM $NaHCO_3$, with standard deviation denoted by dotted lines. Apc WT was purified with IMAC and SEC before analysis and then incubated for approximately 60 hours in NaCl or $NaHCO_3$ buffers. N=3. Differences are significant both before and after normalisation. Data was obtained using a H4 plate reader.

Table 14: Combined variances for Apc WT and Apc K6A before and after normalisation of peak emission intensity to intensity at 610 nm

	Apc WT	**Apc K6A**
Raw	13.0%	5.3%
Normalised	3.0%	1.9%

Significant differences were observed between Apc WT and Apc K6A emission intensity raw data in the presence of $NaHCO_3$. There were significant differences in Apc WT fluorescence in the presence of $NaHCO_3$ after normalisation, but not in Apc K6A. It was unclear if the differences were caused by interactions between CO_2 and the proteins or if the differences were caused by the pH differences between the samples incubated with $NaHCO_2$ and NaCl.

Effects of pH 7.61 and 7.40 on Apc WT and Apc K6A fluorescence

The Apc WT preparation responded significantly to 60-hour incubation with $NaHCO_3$ both before and after normalisation, and Apc K6A responded significantly to $NaHCO_3$ before normalisation only. However, the stock 100mM $NaHCO_3$ buffer had a pH value of 7.60 after 60 hour incubation and the

100mM NaCl buffer had a pH of 7.40. Incubation with 20 mM $NaHCO_3$ can increase the pH of the reaction solution, and it was necessary to measure the effect that pH values of approximately 7.40 and 7.60 would have on Apc WT and Apc K6A fluorescence. To assess the effects of the pH difference on Apc emission intensity, the protein was dialysed into buffers at pH 7.40 and pH 7.61. The protein was subsequently subjected to excitation-emission analysis using a H4 plate reader.

For the K6A mutant, there were significant increases in emission with higher pH both in the raw data and after the emission peaks had been normalised to emission at 610 nm (Figure 46). For the WT, the difference between pH conditions was barely above the p-value required to be considered significant in the raw data (p=0.057). However, in the peak data normalised to emission at 610 nm, there were no significant differences (p=0.80) (Figure 45). These data suggest that the pH difference between the NaCl and $NaHCO_3$ conditions after 60-hour incubation likely affected the Apc K6A mutant's emission intensity but did not necessarily affect the Apc WT. For variance, see (Table 15).

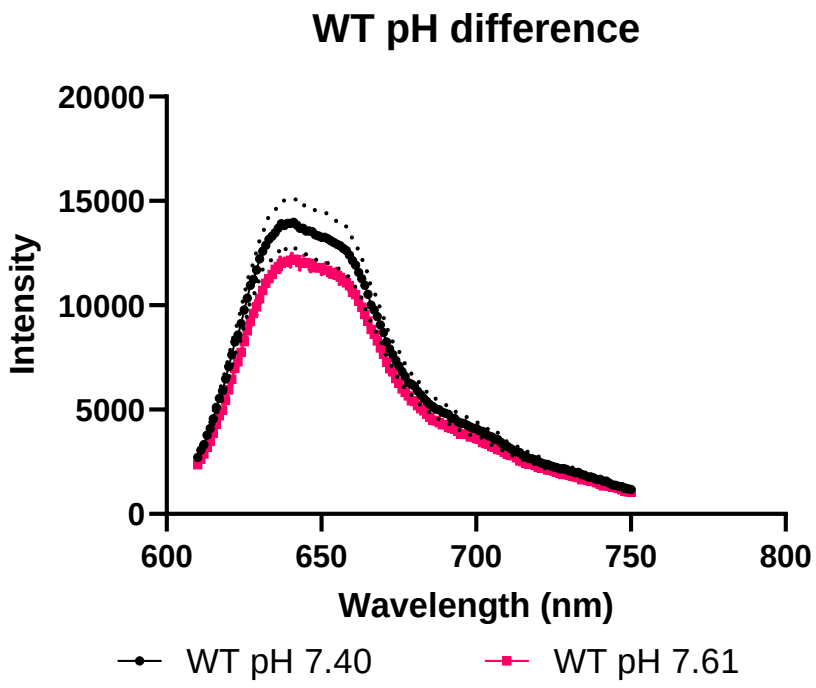

Figure 45: Excitation-emission spectra of Apc WT at pH 7.40 and pH 7.61. Differences are not significant in raw or normalised data. N=3. Data was obtained using a H4 plate reader.

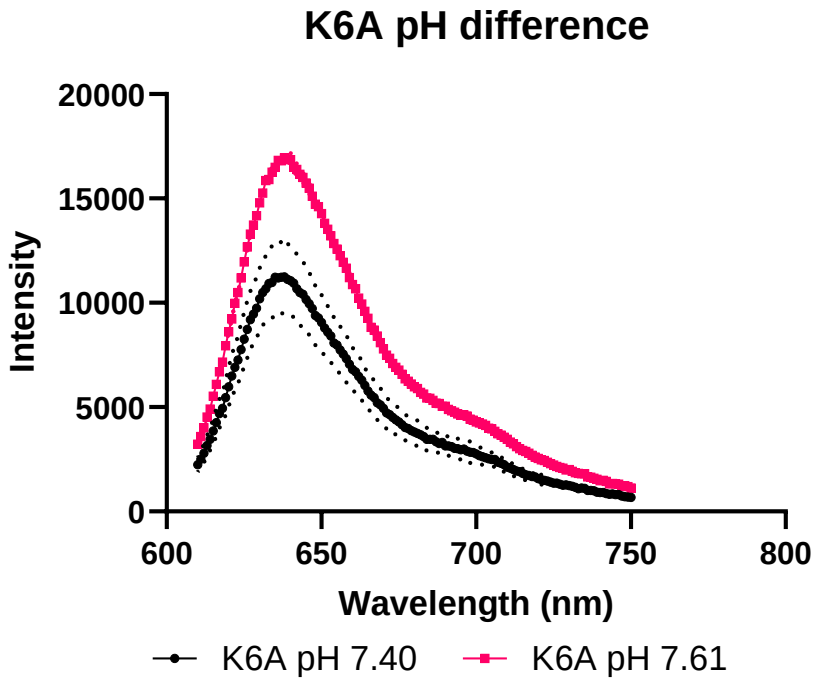

Figure 46: Excitation-emission spectrum of Apc K6A mutant at pH 7.40 and pH 7.61. Differences were significant before and after normalisation to starting fluorescence. N=3. Data was obtained using a H4 plate reader.

Table 15: Combined variance coefficients of pH 7.40 and 7.61 comparisons for Apc WT and Apc K6A in raw data and after normalising peak emission intensity to intensity at 610 nm.

	Apc WT	**Apc K6A**
Raw	6.7%	13.5%
Normalised	2.4%	1.6%

The data suggests that Apc WT fluorescence intensity can be significantly lower in 20 mM $NaHCO_3$ than in 20 mM NaCl after 60-hour incubation as a result of interactions between Apc WT and inorganic carbon, when using the trimer-containing SEC elutions.

Cpc WT and CpcB-K36A Hexamers Respond Significantly to Inorganic Carbon

The method developed on Apc WT can be used to demonstrate significant differences in Apc WT fluorescence intensity in the presence of $NaHCO_3$, either immediately after the addition of $NaHCO_3$, or after incubation with $NaHCO_3$ and NaCl buffers. The methods were applied to Cpc WT and two of its mutants.

Cpc WT, CpcB-K36A, and CpcA-K137A were purified for analysis. Purification of CpcA-K137A failed to produce enough protein for analysis.

The PAGE gel of Cpc WT SEC fractions (Figure 47) show small bands between 15 and 25 kDa, which may be α and β subunits of Cpc.

There was much less protein present in the CpcA-K137A fractions. For visualisation of the amount of excess protein removed by SEC, (Figure 47) can be compared with the products of IMAC alone (Figure 48).

The PAGE gel of CpcB-K36A IMAC fractions show that after SEC there is far less excess protein visible on the gel, however the bands are still not clearly defined (Figure 49).

For all three purifications, the chromatograms generated by the ÄKTA™ Start displayed peaks at approximately 52 ml, corresponding to the expected elution volume of αβ hexamers (Figure 50, Figure 51, Figure 52). For all three purifications, the fractions expected to contain only hexamers of PBPs were used for further analysis.

The raw data for the WT and CpcB-K36A displays significantly greater emission in the presence of $NaHCO_3$ (Figure 53, Figure 54). However, peak data normalised to emission at 610nm for both samples show non-significant differences. For variance, see (Table 16). The p-value before normalisation for the Cpc WT p=0.00033 and CpcB-K36A p=0.024.

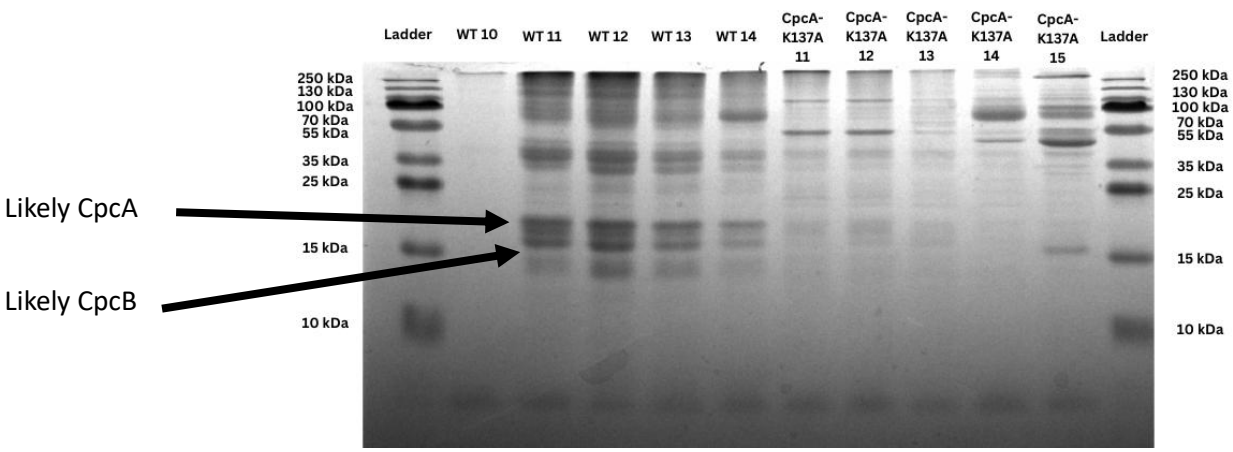

Figure 47: PAGE gel of Cpc WT and K-137A SEC fractions. WT fractions 10-14 inclusive and CpcA-K137A 11-15 inclusive were concentrated for excitation-emission analysis.

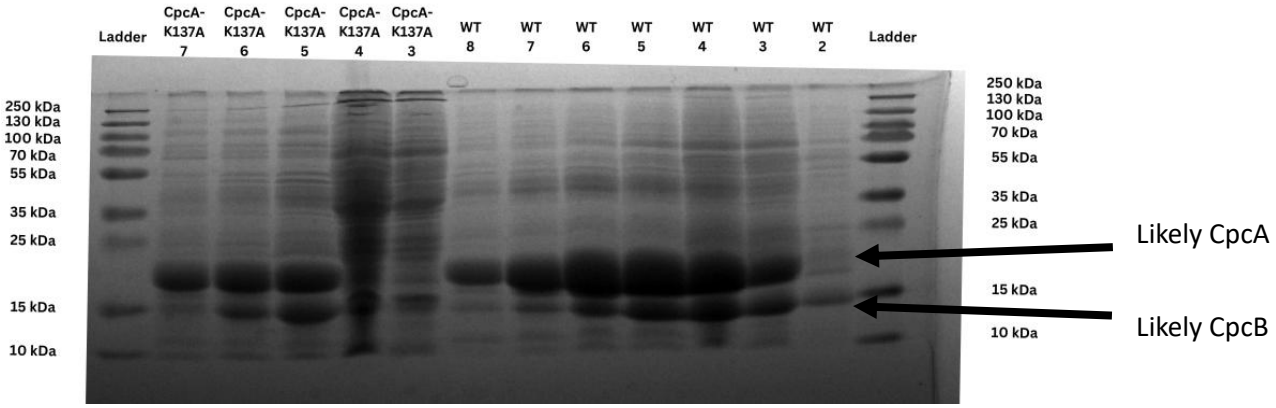

Figure 48: PAGE gel of Cpc WT and 1286 IMAC purification fractions. CpcA-K137A fractions 4-7 inclusive and Cpc WT fractions 3-7 inclusive were concentrated for further purification.

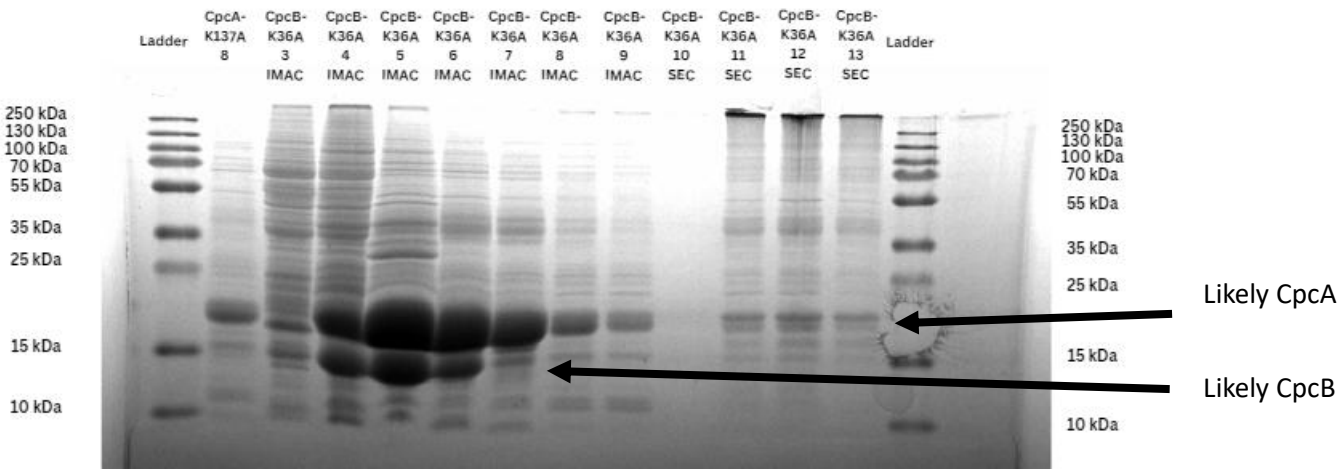

Figure 49: PAGE gel of CpcA-k137A IMAC fraction 8, CpcB-K36A IMAC fractions, and CpcB-K36A SEC fractions. CpcB-K36A IMAC fractions 4-7 inclusive were used for SEC, and CpcB-K36A SEC fractions 11 and 12 were used for excitation-emission analysis.

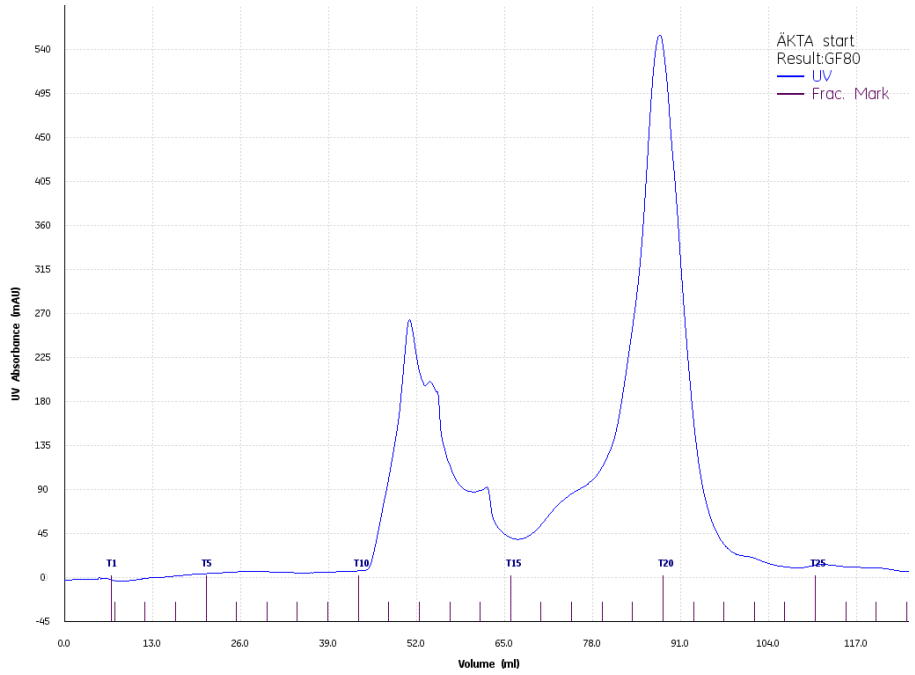

Figure 50: Chromatogram of Cpc WT SEC results displaying elution of the fractions in which protein was eluted. Protein concentration was determined using UV absorbance measurements taken by the instrument. Fractions 10-14 inclusive were concentrated for excitation-emission analysis.

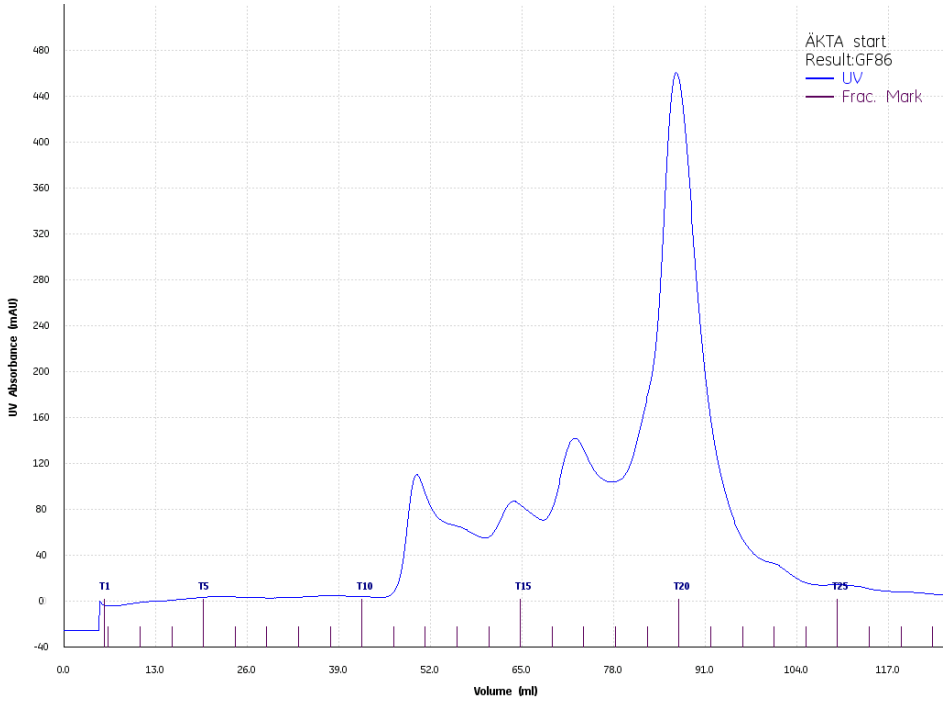

Figure 51: Chromatogram of CpcA-K137A (1286) SEC results displaying the fractions in which protein was eluted. Protein concentration was determined using UV absorbance measurements taken by the instrument. Fractions 11-15 inclusive were concentrated for excitation-emission analysis.

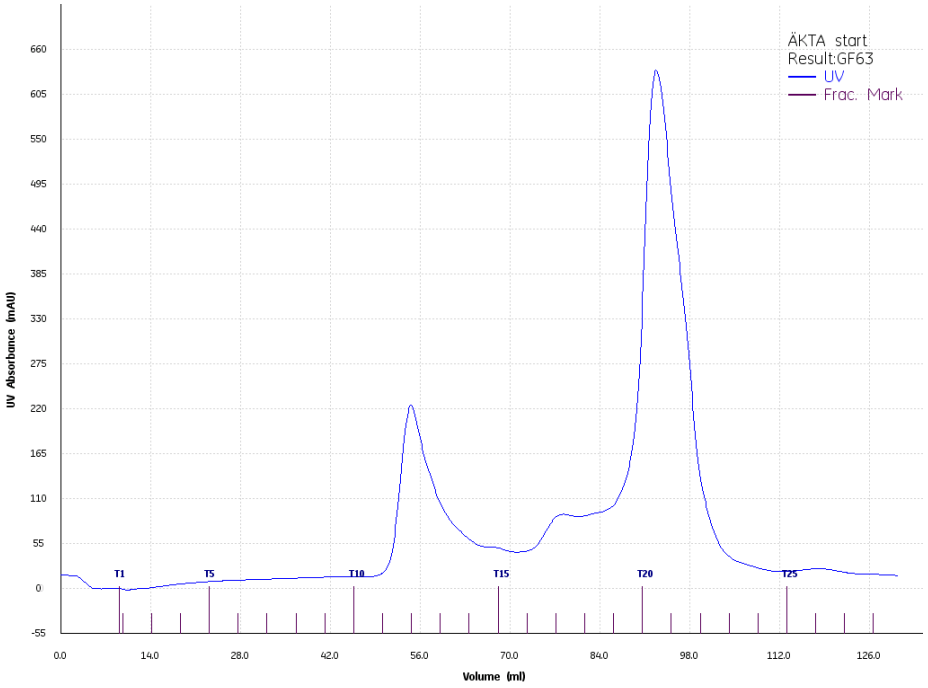

Figure 52: Chromatogram of CpcB-K36A results displaying the fractions in which protein was eluted. Protein concentration was determined using UV absorbance measurements taken by the instrument. Fractions 11 and 12 were concentrated for excitation-emission analysis.

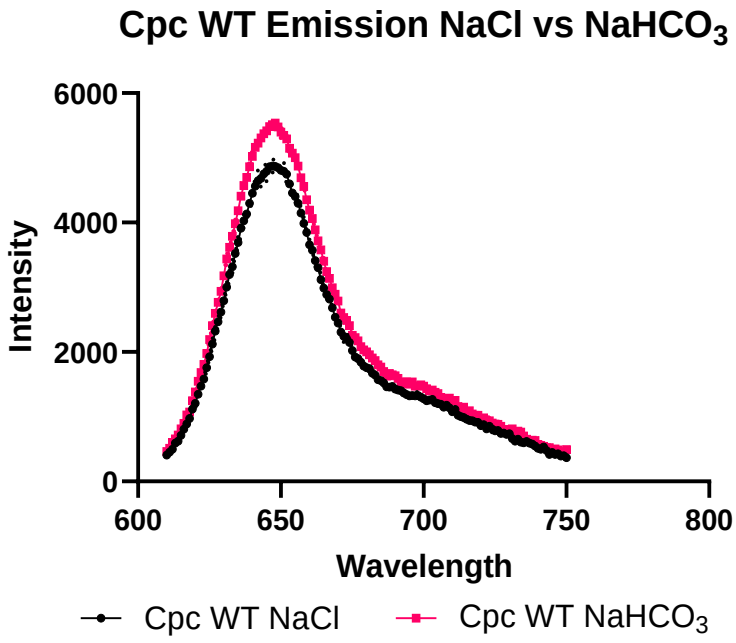

Figure 53: Excitation-emission spectra of Cpc WT in a buffer composed of 0.1M MOPS and 20mM NaCl or 20mM $NaHCO_3$, with standard deviation denoted by dotted lines. Cpc WT was purified with IMAC and SEC before analysis. N=3. Data was obtained using a H4 plate reader.

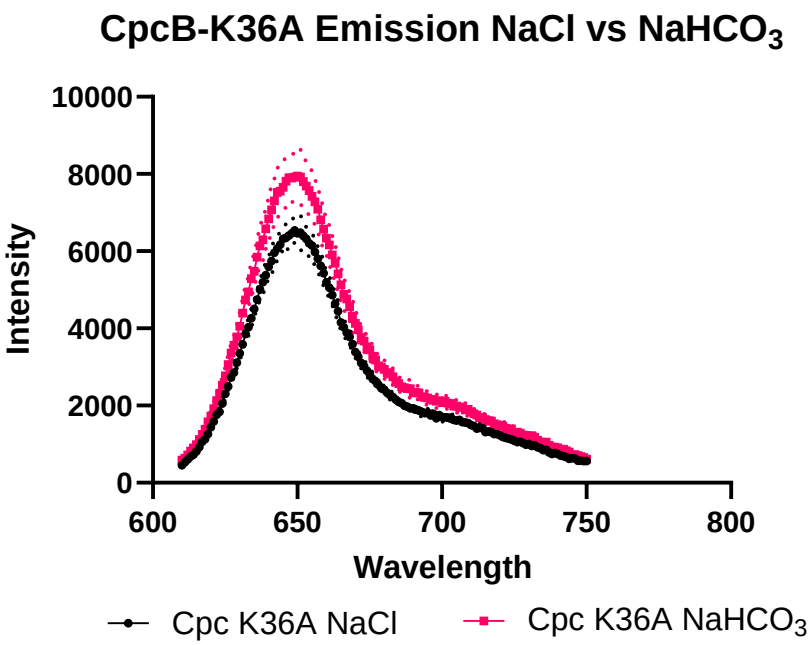

Figure 54: Excitation-emission spectra of CpcB-K36A in a buffer of 0.1 M MOPS and 20 mM NaCl or 20 mM $NaHCO_3$, with standard deviation denoted by dotted lines. CpcB-K36A was purified with IMAC and SEC before analysis. N=3. Data was obtained using a H4 plate reader.

Table 16: Variance analysis of NaCl vs $NaHCO_3$ analysis for Cpc WT and CpcB-K36A.

	Cpc WT	**CpcB-K36A**
Original	5.7%	10.7%
Normalised	4.6%	4.4%

This data suggests that the protein preparations used for excitation-emission analysis contained a high proportion of αβ hexamers. The analysis shows that 20 mM $NaHCO_3$ enhances the fluorescence of Cpc WT and CpcB-K36A compared to a 20 mM NaCl control with no added inorganic carbon. The peak data normalised to starting fluorescence did not display significant differences between $NaHCO_3$ and NaCl samples. However, this only means that the difference in emission intensity between 610 nm and the emission maxima is not significantly different between samples with added inorganic carbon and the controls.

Discussion

Emission Spectra and Method Optimisation

The excitation-emission analysis performed was based on previous work that demonstrated significant increases in Apc emission intensity in the presence of inorganic carbon (CO_2/HCO_3^-) when compared with controls (NaCl) (Guillén-García et al., 2022). The analysis of Apc and Cpc was expected to align precisely with the previous findings. The Cann group had also previously identified four possible sites where carbamylation was likely to occur on Cpc, and plasmids encoding mutant Apc and Cpc strains in *E. coli* that would not be able to carbamylate those putative sites had been created. Unfortunately, the expected increases in Cpc and Apc emission in the presence of inorganic carbon were not initially observed. There were two major differences between the expected results and the data obtained; there were large levels of variation between biological replicates, and the data indicated that inorganic carbon may reduce emission rather than increase it.

Proteins Purified Using IMAC Alone

Analyses Performed without Modifying Dilution Buffer pH

The first experiments in this project were performed on Cpc and Apc, purified with IMAC alone. The results of crudely purified protein were expected to align with previously obtained results.

One of the first experiments run on Cpc WT purified using IMAC alone was expected to have a sufficiently high sample number (N=10) to achieve small standard deviations and to display significant increases in fluorescence in the presence of inorganic carbon. A fluorolog was used to generated excitation-emission spectra of PBPs. When comparing the emission peaks, a significant decrease in emission intensity in the presence of $NaHCO_3$ was observed ($p=0.014$). However, there were large inter-replicate variations. After peak emissions were normalised to starting fluorescence to account for the 6.7% combined coefficients of variance for the NaCl and $NaHCO_3$ conditions, significant differences were not observed between the NaCl and $NaHCO_3$ conditions (Figure 14). The limitation of this normalisation method was that the baseline emission at 600 nm was likely affected

by the presence of $NaHCO_3$. Significant differences in the normalised data would only have indicated that the addition of $NaHCO_3$ caused a greater increase in fluorescence between emission at 600 nm and the emission maxima at approximately 646 nm. The negative effect of $NaHCO_3$ on Cpc WT fluorescence had two likely explanations: the method may have been flawed and / or inorganic carbon could decrease Cpc WT fluorescence.

Due to the unexpected decrease in emission intensity in the presence of inorganic carbon and the failure of the normalisation to account for the decrease, the experimental method was tested using Apc as a positive control. Apc has a previously documented increase in fluorescence in the presence of inorganic carbon (Guillén-García et al., 2022). The control analysis had a much lower sample size (N=3). However, there was a low variance in the data before normalisation and an even lower variance after normalisation. Despite the low variance, significant differences were not observed at all between NaCl and $NaHCO_3$ conditions in the raw data or after normalisation (Figure 16).

Analyses performed with Modified Dilution Buffer pH

For all subsequent analyses, the method was changed to include buffering the pH of every component in the reaction solution except for the protein sample. The reaction solution mainly consisted of the dialysis buffer used when purifying the proteins (30 mM Tris, 150 mM NaCl). For the first set of analyses on Cpc WT and Apc WT, the dialysis buffer pH was not tested before performing excitation-emission analysis, and the pH of the final solution would have been approximately 7.9. It was hypothesised that the high pH affected the equilibrium of $NaHCO_3$ and CO_2 in the water, resulting in a potentially lower final concentration of CO_2 in the reaction solution than desired. The pH of the dialysis buffer was modified to ensure that the final pH of NaCl and $NaHCO_3$ conditions would be between 7.40 and 7.50. However, no significant differences were observed despite a combined variance of 5.5% before and 2.3% after normalisation (Figure 17).

All previous purifications and analyses were performed in buffers composed of 30 mM Tris and 150 mM NaCl. To achieve a pH of approximately 7.40, HCl was added to buffers. To account for the risk of

inorganic carbon degassing due to HCl being added to the $NaHCO_3$ buffer, the method was changed for subsequent analysis to utilise 0.1 M MOPS buffer. The advantage of the MOPS buffer was that it had an unmodified pH of less than 5, so when modifying the pH of buffers containing $NaHCO_3$, NaOH was used to increase buffer pH, and no HCl was necessary.

Despite changing buffers and ensuring that all buffers used differed by a pH value of less than 0.1, no significant differences were observed between NaCl and $NaHCO_3$ conditions during the next analysis of Apc WT purified using IMAC alone. Additionally, five replicates of the analysis with 20 mM $NaHCO_3$ were performed, and two of these replicates displayed emission maxima approximately 15nm higher than the other three (Figure 18). The reasons for this are unknown. All protein used in this experiment was stored in the same tube before use. A likely explanation is that the mixture in the 1.5 ml microcentrifuge tube was extremely heterogeneous, and some fluorescent protein that functioned incorrectly was concentrated enough within a small region of the tube to be only detected in two out of the eight analyses run consecutively on the same date. During subsequent analyses, more emphasis was placed on thoroughly mixing protein samples using a micropipette before use. However, a more vigorous mixing method was not employed due to the relatively labile nature of PBPs.

The fluorolog could produce high-quality data. However, its major limitation was its inability to run several samples in parallel. A H4 plate reader was used instead of a fluorolog for subsequent excitation-emission analyses. The plate reader had two major advantages over the fluorolog: the 96-well plates used in the plate reader only required a total volume of 100 µl for each well, rather than the 3,000 µl needed to fill the cuvette for the fluorolog. Additionally, it would have been prohibitively expensive to use more than one fluorolog cuvette, and the cuvette had to be cleaned thoroughly between each sample analysis. Cuvette cleaning further increased the time required to run multiple analyses. The 96-well plates allowed samples to be run in parallel, with a much lower amount of time required to prepare each sample. The first Apc WT analysis run on the H4 plate reader was under the

same conditions as the last Apc run on the fluorolog. Therefore, the aim was to ensure that the results were similar rather than further optimise the experimental method. This experiment where N=5 did not result in significant differences between NaCl and $NaHCO_3$ conditions (Figure 19).

The next analysis of Apc WT on the H4 plate reader used the same purified Apc preparation as all previous Apc analyses and included more replicates (N=8). The experiment compared two different concentrations of NaCl and $NaHCO_3$: 5 mM and 20 mM. Significant differences were observed between NaCl and $NaHCO_3$ concentrations before and after normalising peak emission intensity to 610nm. A dose-dependent response was also observed, where 20 mM $NaHCO_3$ led to a significantly lower emission intensity than 5 mM $NaHCO_3$ in the normalised data (p=0.0003).

5 mM concentrations of $NaHCO_3$ appeared to lower the total emission of Apc WT while increasing the increase between emission intensity at 610 nm and the emission intensity peak compared to the NaCl control (Table 10). This could be evidence of competing mechanisms through which inorganic carbon may decrease the fluorescence of Apc monomers or individual subunits while increasing the fluorescence of Apc trimers or hexamers.

However, despite the observation of significant dose-dependent differences between NaCl and $NaHCO_3$ conditions, there were two problems with the data that were produced. Firstly, the protein was purified using IMAC only and then stored at 4^{o}C in a 30 mM Tris, 150 mM NaCl buffer for three weeks before analysis. A method for differentiating between Apc trimers and monomers based on absorbance spectra was not validated using verified Apc trimers and monomers. However, according to (MacColl, 2004), the absorbance data produced less than 24 hours before excitation-emission analysis (Figure 23) would suggest that most Apc in this sample was present as αβ monomers. It is likely that the response to $NaHCO_3$ was caused by interactions between inorganic carbon and Apc monomers.

The second limitation of this data was that the effect of inorganic carbon on Apc fluorescence previously described by the Cann group was positive, not negative. In this experiment, adding inorganic carbon resulted in a suppression of fluorescence, with a higher concentration of inorganic

carbon resulting in a greater suppression (Figure 20, Figure 21). These data suggest that interactions between inorganic carbon and Apc monomers may result in reduced fluorescence. This suppression may result from non-specific interactions involving other proteins in the crudely purified sample, or it may indicate that inorganic carbon could enhance the fluorescence of assembled Apc hexamers while suppressing the fluorescence of non-assembled Apc subunits. Unfortunately, this hypothesis cannot be tested with the available data, as there was no validated method available for quantifying the ratio of Apc subunits to hexamers.

For the next experiment, Apc K6A was used as a previously validated negative control of Apc's response to inorganic carbon due to the mutation of the positively charged K6 carbamylation site to a neutral alanine. Two fresh preparations of Apc WT and Apc K6A were expressed and purified. Despite sample sizes of N=10 for the Apc WT protein, no significant differences were observed between NaCl and $NaHCO_3$ peak emissions before or after normalising to emission at 610nm in the WT (Figure 26). For the K6A sample (N=9), significant decreases in peak emission intensity were observed in the original data (p=0.009) but not in the normalised data (Figure 25). If the K6A protein responded to inorganic carbon after normalisation, the effect could have been masked by high inter-replicate variance, as when comparing K6A NaCl to $NaHCO_3$ p=0.071. Additionally, because the K6A mutant appeared to have a greater response to inorganic carbon than the WT, it was suggested that human error may have led to the mislabelling of the samples.

The analysis was repeated on the sample labelled 'Apc WT,' and the resulting data aligned with the first analysis of the 'Apc WT' data (Figure 29). Therefore, it was concluded that if human error caused the sample labels to be swapped, the error occurred before the excitation-emission analysis began. Additionally, if the higher-than-normal emission maxima wavelengths resulted from structural imperfections such as protein misfolding, it must have occurred to the entire protein sample.

Proteins Purified Using IMAC Followed by SEC with Modified Dilution Buffer pH

SEC Used Without Differentiating Protein Fractions

The next experiment used Apc WT and Apc K6A freshly purified from the same expression batch as the analyses used to produce the figures (Figure 25, Figure 26, Figure 29). In this case, the protein samples were purified using both IMAC and SEC before analysis. The results were anomalous. Before normalising, neither the Apc WT nor the Apc K6A mutant responded significantly to inorganic carbon (Figure 34, Figure 35). However, after normalising to emission intensity at 610 nm, the K6A mutant but not the WT displayed a significant decrease in emission in the presence of $NaHCO_3$ compared to NaCl. It is important to note that even though SEC was employed during the protein preparation for this analysis, it was not used to separate Apc hexamers, trimers, monomers, and subunits. Apc monomers and subunits likely accounted for a high proportion of the protein examined.

Possible reasons for the fact that Apc K6A but not Apc WT responded to inorganic carbon are (i) both Apc WT and Apc K6A samples were mislabelled before purification, (ii) the presence of monomers and dimers in the purified solutions were responsible for the significant response of the K6A mutant (although there is no data available comparing the responses of monomers and dimers with the responses of hexamers for comparisons), or (iii) flaws with both Apc WT and Apc K6A were introduced at the stage of protein expression (which may be supported by the higher than expected emission maxima).

After the unexpected results of the previous analysis of Apc WT (Figure 29), it may have been more time-efficient to express a fresh batch of Apc WT and Apc K6A to avoid the risk of encountering more unexpected results from the other protein preparations that were expressed together. This expression batch of Apc WT and Apc K6A could not be used to draw significant conclusions, and fresh expressions of Apc WT and K6A were produced for subsequent analyses.

Purification Using SEC to Remove PBP Monomer and Subunit Fractions

A calibration curve for the SEC column was prepared to ensure that the SEC fractions used for fluorescence analysis could be separated between PBP hexamers, trimers, and monomers for subsequent analyses.

The next batch of expressed and purified Apc WT and Apc K6A was separated using SEC and analysis was performed on protein samples consisting chiefly of αβ trimers. No significant differences were observed between NaCl and $NaHCO_3$ conditions for either Apc WT or the Apc K6A mutant (Figure 40, Figure 41). To demonstrate that the lack of significant differences was not a result of instrument error, the experimental plate was analysed again three times to calculate the variance between repeat measurements for each well. The figure (Figure 42) displays the results of the repeat analysis for each replicate, and the variance between peak emission intensity for each well ranged from 0.9% to 2.0%. This repeat analysis did not control for photobleaching caused by the analysis itself, and therefore, even if the instrument had a negligible error, some variance between repeat measurements would be expected. The variance between repeat measurements of 2.0% or less suggests that instrument error did not cause the high inter-replicate variation.

To examine the effects of incubating the protein with NaCl and $NaHCO_3$, the 96-well plate used for the (Figure 40, Figure 41) analysis was stored at 4°C for approximately 60 hours and then analysed again (Figure 43, Figure 44). Both Apc WT and the K6A mutant displayed significant reductions in emission intensity after incubation with $NaHCO_3$ when compared with incubations with NaCl. The peak emission data normalised to emission intensity at 610nm displayed a significant reduction in Apc WT emission intensity after incubation with $NaHCO_3$ but not after incubation with NaCl. After normalising, the Apc K6A mutant did not display significant differences between NaCl and $NaHCO_3$ conditions. There was insufficient sample volume for accurate pH analysis.

After the 60-hour incubation, the pH of the 0.1M $NaHCO_3$ 0.1 M MOPS buffer was 7.60, and the pH of the 0.1 M MOPS buffer used for diluting samples was 7.42. Therefore, the pH of the proteins that

had been incubated for 60 hours must have been within the range of 7.40-7.60. The protein used for the previous two analyses was dialysed into buffers at pH 7.40 and pH 7.61 to measure the effects on emission intensity at those two pH values. The *t*-test of the raw data for the Apc WT sample returned p=0.057 where N=3 (Figure 45) and after normalisation p=0.80. It may be possible that a greater sample number would have produced a *p*-value low enough to demonstrate that significant differences in Apc WT fluorescence occur in the raw data due to the pH difference between 7.40 and 7.61.

The Apc K6A mutant displayed significantly greater emission intensity at pH 7.61 than at pH 7.40 before (Figure 46) and after normalisation. $NaHCO_3$ in the sample incubated with $NaHCO_3$ for 60 hours appears to have increased the pH from approximately 7.42 up to as high as 7.60 compared to the 60-hour NaCl incubations. If the increased pH increases fluorescence, while $NaHCO_3$ decreases fluorescence, it may erroneously appear that the $NaHCO_3$ does not cause a fluorescence response in Apc K6A trimers, because a positive response to the increased pH would offset a negative response to $NaHCO_3$.

The normalised data suggest that the difference between the two pH values is enough to cause significant differences in the emission of the Apc K6A mutant but not necessarily the Apc WT. While these data suggest that the results of Apc K6A incubation with $NaHCO_3$ may not be used to draw reliable conclusions, the significant reduction in emission intensity in Apc WT incubated with 20 mM $NaHCO_3$ may be a genuine effect caused by inorganic carbon. Either Apc WT is not affected by the pH difference between 7.42 and 7.60, or the emission reduction caused by 20 mM $NaHCO_3$ is not significantly offset by any pH-mediated fluorescence increase. Ideally, this experiment comparing the response of Apc to pH 7.42 and 7.60 would have been repeated to increase confidence in the results. However, repeat analyses could not be performed in the time available.

After demonstrating that incubation with $NaHCO_3$ may be used to reduce Apc WT fluorescence significantly, the modified method was applied to Cpc WT and CpcB-K36A. CpcB-K36A was modified at a putative site of carbamylation to ensure no carbamylation would occur at that site. For both

proteins analysed, SEC was used to isolate αβ hexamer fractions for analysis, and most functional Cpc in growing cyanobacteria would be in hexameric form. The initial excitation-emission analysis showed significant differences between NaCl and $NaHCO_3$ conditions in the raw data (Figure 53, Figure 54). Interestingly, the effect was an increase in fluorescence in the presence of $NaHCO_3$, not a decrease as was previously observed in Apc samples. Differences were not significant after normalising emission intensity peaks to emission intensity at 610 nm. Absorbance analyses were attempted on the purified protein. However, there was insufficient protein in the sample for accurate absorbance measurements. Therefore, in this case, absorbance peaks can't be used to indicate the presence of αβ trimers using the absorbance characteristics described by (MacColl, 2004). However, it appears that the Cpc αβ hexamers displays the expected increase in fluorescence in the presence of inorganic carbon. There is greater variance in the CpcB-K36A sample (Figure 54). However, CpcB-K36A also displays a significant increase in fluorescence in the presence of inorganic carbon. The significant increase in CpcB-K36A emission in the presence of $NaHCO_3$ suggests that the K36 site of the Cpcβ subunit is not a site of carbamylation.

After this experiment, the end of the period allocated to experiments for this project had been reached. No more data could be collected to verify the occurrence and the site of Cpc carbamylation through repeat experiments. However, the data obtained throughout this study is valuable for future analysis of fluorescent phycobilisome proteins. No analysis of Apc during this study was performed solely on αβ hexamers. Purifications of Apc using both IMAC and SEC failed to recover sufficient hexamer-containing fractions for analysis. Apc hexamers may be more labile than Cpc hexamers, *E. coli* production strains may produce lower quantities of Apc hexamers, or Apc hexamers may have dissociated during purification.

The excitation-emission figures display either no discernible differences between the emission intensity of Apc in the presence of $NaHCO_3$, or they display a suppression of emission intensity in the presence of $NaHCO_3$, compared with NaCl. Normalisation was used to determine whether the addition of $NaHCO_3$ resulted in a significantly different peak emission intensity relative to the starting

emission. The data obtained by a series of analyses of Apc and its mutants describe an inconsistent reduction in overall emission intensity in the presence of inorganic carbon. While the effect was not consistent across all experiments described, significant emission intensity reductions were observed in the raw data for the dose-dependent Apc WT analysis (Figure 20, Figure 21), the 'Apc K6A' sample where it was suggested that Apc K6A and Apc WT may have been swapped (Figure 25), and Apc WT after 60-hour incubation with $NaHCO_3$ (Figure 44).

Additionally, it should be noted that the 5 mM $NaHCO_3$ concentration (Figure 20) displayed a significant reduction in emission in the raw data but a significant increase in the emission peak data that were normalised to emission at 610 nm, compared to 5 mM NaCl. The available data cannot be used to conclude whether these reductions were simply artefacts, if non-specific interactions caused them, or if they resulted from a previously undescribed interaction between CO_2 and Apc monomers. However, inorganic carbon interacting with Apc WT monomers or subunits may cause the total fluorescence intensity to decrease while increasing the difference between emission at its emission intensity maximum (approx. 641 nm) and its emission at 610 nm. This could be an indication of opposing effects caused by the addition of inorganic carbon; non-specific interactions or interactions between CO_2 and Apc WT subunits could reduce the total emission intensity, while CO_2 could be interacting with a small amount of Apc WT hexamers or trimers to increase the emission of a small amount of assembled Apc αβ hexamers present in the sample. Inorganic carbon may increase fluorescence in assembled Apc hexamers while decreasing fluorescence in Apc monomers and αβ subunits. This would have the physiological benefit of reducing the energy transmitted by PBP monomers within the cell when the monomers are not in assembled hexameric form in the PBS. It is unclear if further study of fluorescence reduction mediated by inorganic carbon could be applied to improving the growth of cyanobacteria.

Inorganic carbon may reduce fluorescence in Apc WT and Apc K6A trimers, monomers, and subunits, while also fitting with previously reported conclusions that inorganic carbon enhances fluorescence

in Apc WT hexamers. The data above suggests that recombinant PBPs expressed in *E. coli* and purified using IMAC alone should not be used for analyses due to a high concentration of PBP monomers or subunits in such protein preparations.

The analysis of Cpc WT and CpcB-K36A (Figure 53, Figure 54) was performed on hexamer fractions isolated during SEC. The presence of hexamers in these protein samples can account for the $NaHCO_3$-mediated increase in fluorescence intensity in Cpc WT and CpcB-K36A. Where significant differences were observed in Apc and its mutants in this study, the effect had always been a suppression of emission intensity. However, this analysis achieved the aim of confirming that Cpc WT hexamers increase their fluorescence intensity in the presence of inorganic carbon, most likely through carbamylation. In order to confirm the occurrence of CO_2-mediated Cpc carbamylation, the method used previously by the Cann group on Apc could be used to measure the fluorescence quantum yield of Cpc and its mutants in its purified form and in whole organisms (Guillén-García et al., 2022). The data also suggests that the Cpcβ-K36A position is not the site of carbamylation.

Project Outcomes

The data described above agrees with the hypothesis that Cpc fluorescence is enhanced by carbamylation. The data above also suggests that Cpcβ-K36A is likely not a Cpc carbamylation site. Another outcome of this project is a potential improvement in the method for purifying recombinant His-tagged PBPs from *E. coli*. In future studies, analyses of recombinant His-tagged PBPs produced in *E. coli* should avoid:

1. A failure to measure the presence of αβ trimers and monomers using absorbance spectra as described by (MacColl, 2004).
2. A failure to fully purify αβ hexamers to separate them from αβ trimers, αβ monomers, or individual α and β subunits.

In this study the method was developed through trial and error. Trial and error method development can be very labour-intensive and slow. Purified PBP fractions consisting chiefly of αβ hexamers were

required to replicate the previously described fluorescence suppression mediated by inorganic carbon. However, most of the protein preparations analysed in this study were not believed to be composed of assembled αβ hexamers.

The unexpected decrease in PBP fluorescence that was inconsistently observed in the presence of inorganic carbon may have represented an opposing mechanism through which inorganic carbon could decrease the fluorescence of PBP trimers, monomers, or subunits. This fluorescence suppression could be useful for minimising excess energy transfer during protein assembly or lysis. While the negative effects of inorganic carbon on PBP fluorescence is an interesting avenue of study, it is unknown if knowledge of the effects of inorganic carbon on non-assembled protein *in vitro* can be used to grow cyanobacteria more efficiently.

Conclusion

This report describes the development of the method for measuring phycobiliprotein (PBP) responses to inorganic carbon. The majority of the experimental period was allocated to method development and analysis of PBPs that were not in hexameric form. Therefore, insufficient time was available to generate reproducible data and draw conclusions about the effects of CO_2 on all of the previously generated Cpc mutants. Previous claims that inorganic carbon can enhance Cpc WT fluorescence have been validated, and one previously identified putative site of Cpc carbamylation, Cpcβ-K36, was discounted as the site of Cpc carbamylation.

Bibliography

Adir, N., Bar-Zvi, S., & Harris, D. (2020). The amazing phycobilisome. *Biochimica et Biophysica Acta (BBA) - Bioenergetics*, *1861*(4), 148047. https://doi.org/10.1016/j.bbabio.2019.07.002

Aikawa, S., Nishida, A., Ho, S.-H., Chang, J.-S., Hasunuma, T., & Kondo, A. (2014). Glycogen production for biofuels by the euryhaline cyanobacteria *Synechococcus sp*. Strain PCC 7002 from an oceanic environment. *Biotechnology for Biofuels*, *7*(1), 88. https://doi.org/10.1186/1754-6834-7-88

Andersson, I., & Backlund, A. (2008). Structure and function of Rubisco. *Plant Physiology and Biochemistry*, *46*(3), 275–291. https://doi.org/10.1016/j.plaphy.2008.01.001

Basic Amino Acids. (2003). [Graphic]. http://www.biology.arizona.edu/biochemistry/problem_sets/aa/Basic.html

Berns, D. S., & MacColl, R. (1989). Phycocyanin in physical chemical studies. *Chemical Reviews*, *89*(4), 807–825. https://doi.org/10.1021/cr00094a005

Biswas, A., Vasquez, Y. M., Dragomani, T. M., Kronfel, M. L., Williams, S. R., Alvey, R. M., Bryant, D. A., & Schluchter, W. M. (2010). Biosynthesis of Cyanobacterial Phycobiliproteins in Escherichia coli: Chromophorylation Efficiency and Specificity of All Bilin Lyases from *Synechococcus sp*. Strain PCC 7002. *Applied and Environmental Microbiology*, *76*(9), 2729–2739. https://doi.org/10.1128/AEM.03100-09

Blake, L. I., & Cann, M. J. (2022). Carbon Dioxide and the Carbamate Post-Translational Modification. *Frontiers in Molecular Biosciences*, *9*. https://www.frontiersin.org/articles/10.3389/fmolb.2022.825706

Chen, H., Liu, Q., Zhao, J., & Jiang, P. (2016). Biosynthesis, spectral properties and thermostability of cyanobacterial allophycocyanin holo-α subunits. *International Journal of Biological Macromolecules*, *88*, 88–92. https://doi.org/10.1016/j.ijbiomac.2016.03.050

Choi, S. Y., Wang, J.-Y., Kwak, H. S., Lee, S.-M., Um, Y., Kim, Y., Sim, S. J., Choi, J., & Woo, H. M. (2017). Improvement of Squalene Production from CO2 in S*ynechococcus elongatus* PCC 7942 by

Metabolic Engineering and Scalable Production in a Photobioreactor. *ACS Synthetic Biology*, *6*(7), 1289–1295. https://doi.org/10.1021/acssynbio.7b00083

Cummins, E. P., Selfridge, A. C., Sporn, P. H., Sznajder, J. I., & Taylor, C. T. (2014). Carbon dioxide-sensing in organisms and its implications for human disease. *Cellular and Molecular Life Sciences*, *71*(5), 831–845. https://doi.org/10.1007/s00018-013-1470-6

Dartnell, L. R., Storrie-Lombardi, M. C., Mullineaux, C. W., Ruban, A. V., Wright, G., Griffiths, A. D., Muller, J.-P., & Ward, J. M. (2011). Degradation of Cyanobacterial Biosignatures by Ionizing Radiation. *Astrobiology*, *11*(10), 997–1016. https://doi.org/10.1089/ast.2011.0663

Davies, F. K., Work, V. H., Beliaev, A. S., & Posewitz, M. C. (2014). Engineering Limonene and Bisabolene Production in Wild Type and a Glycogen-Deficient Mutant of *Synechococcus sp*. PCC 7002. *Frontiers in Bioengineering and Biotechnology*, *2*. https://www.frontiersin.org/articles/10.3389/fbioe.2014.00021

Domínguez-Martín, M. A., Sauer, P. V., Kirst, H., Sutter, M., Bína, D., Greber, B. J., Nogales, E., Polívka, T., & Kerfeld, C. A. (2022). Structures of a phycobilisome in light-harvesting and photoprotected states. *Nature*, *609*(7928), 835–845. https://doi.org/10.1038/s41586-022-05156-4

Ducat, D. C., & Silver, P. A. (2012). Improving carbon fixation pathways. *Current Opinion in Chemical Biology*, *16*(3), 337–344. https://doi.org/10.1016/j.cbpa.2012.05.002

Farrokh, P., Sheikhpour, M., Kasaeian, A., Asadi, H., & Bavandi, R. (2019). Cyanobacteria as an eco-friendly resource for biofuel production: A critical review. *Biotechnology Progress*, *35*(5), e2835. https://doi.org/10.1002/btpr.2835

Forchhammer, K., & Selim, K. A. (2020). Carbon/nitrogen homeostasis control in cyanobacteria. *FEMS Microbiology Reviews*, *44*(1), 33–53. https://doi.org/10.1093/femsre/fuz025

Fuchs, G. (2011). Alternative Pathways of Carbon Dioxide Fixation: Insights into the Early Evolution of Life? *Annual Review of Microbiology*, *65*(1), 631–658. https://doi.org/10.1146/annurev-micro-090110-102801

Gao, Z., Zhao, H., Li, Z., Tan, X., & Lu, X. (2012). Photosynthetic production of ethanol from carbon dioxide in genetically engineered cyanobacteria. *Energy & Environmental Science*, *5*(12), 9857–9865. https://doi.org/10.1039/C2EE22675H

Ge, J., Wang, X., Bai, Y., Wang, Y., Wang, Y., Tu, T., Qin, X., Su, X., Luo, H., Yao, B., Huang, H., & Zhang, J. (2023). Engineering Escherichia coli for efficient assembly of heme proteins. *Microbial Cell Factories*, *22*(1), 59. https://doi.org/10.1186/s12934-023-02067-5

Guillén-García, A., Gibson, S. E. R., Jordan, C. J. C., Ramaswamy, V. K., Linthwaite, V. L., Bromley, E. H. C., Brown, A. P., Hodgson, D. R. W., Blower, T. R., Verlet, J. R. R., Degiacomi, M. T., Pålsson, L.-O., & Cann, M. J. (2022). Allophycocyanin A is a carbon dioxide receptor in the cyanobacterial phycobilisome. *Nature Communications*, *13*(1), Article 1. https://doi.org/10.1038/s41467-022-32925-6

Hagemann, M., Song, S., & Brouwer, E.-M. (2021). Inorganic Carbon Assimilation in Cyanobacteria: Mechanisms, Regulation, and Engineering. In *Cyanobacteria Biotechnology* (pp. 1–31). John Wiley & Sons, Ltd. https://doi.org/10.1002/9783527824908.ch1

Hsieh-Lo, M., Castillo, G., Ochoa-Becerra, M. A., & Mojica, L. (2019). Phycocyanin and phycoerythrin: Strategies to improve production yield and chemical stability. *Algal Research*, *42*, 101600. https://doi.org/10.1016/j.algal.2019.101600

Iñiguez, C., Capó-Bauçà, S., Niinemets, Ü., Stoll, H., Aguiló-Nicolau, P., & Galmés, J. (2020). Evolutionary trends in RuBisCO kinetics and their co-evolution with CO2 concentrating mechanisms. *The Plant Journal*, *101*(4), 897–918. https://doi.org/10.1111/tpj.14643

Jahn, M., Vialas, V., Karlsen, J., Maddalo, G., Edfors, F., Forsström, B., Uhlén, M., Käll, L., & Hudson, E. P. (2018). Growth of Cyanobacteria Is Constrained by the Abundance of Light and Carbon Assimilation Proteins. *Cell Reports*, *25*(2), 478-486.e8. https://doi.org/10.1016/j.celrep.2018.09.040

Janković, B. (2009). Kinetic Analysis of Isothermal Decomposition Process of Sodium Bicarbonate Using the Weibull Probability Function—Estimation of Density Distribution Functions of the

Apparent Activation Energies. *Metallurgical and Materials Transactions B*, *40*(5), 712–726. https://doi.org/10.1007/s11663-009-9271-x

Kacar, B., Hanson-Smith, V., Adam, Z. R., & Boekelheide, N. (2017). Constraining the timing of the Great Oxidation Event within the Rubisco phylogenetic tree. *Geobiology*, *15*(5), 628–640. https://doi.org/10.1111/gbi.12243

Kanno, M., Carroll, A. L., & Atsumi, S. (2017). Global metabolic rewiring for improved CO2 fixation and chemical production in cyanobacteria. *Nature Communications*, *8*(1), Article 1. https://doi.org/10.1038/ncomms14724

Khan, A. Z., Bilal, M., Mehmood, S., Sharma, A., & Iqbal, H. M. N. (2019). State-of-the-Art Genetic Modalities to Engineer Cyanobacteria for Sustainable Biosynthesis of Biofuel and Fine-Chemicals to Meet Bio–Economy Challenges. *Life*, *9*(3), Article 3. https://doi.org/10.3390/life9030054

King, D. T., Zhu, S., Hardie, D. B., Serrano-Negrón, J. E., Madden, Z., Kolappan, S., & Vocadlo, D. J. (2022). Chemoproteomic identification of CO2-dependent lysine carboxylation in proteins. *Nature Chemical Biology*, *18*(7), Article 7. https://doi.org/10.1038/s41589-022-01043-1

Korosh, T. C., Markley, A. L., Clark, R. L., McGinley, L. L., McMahon, K. D., & Pfleger, B. F. (2017). Engineering photosynthetic production of L-lysine. *Metabolic Engineering*, *44*, 273–283. https://doi.org/10.1016/j.ymben.2017.10.010

Li, X., Hou, W., Lei, J., Chen, H., & Wang, Q. (2023). The Unique Light-Harvesting System of the Algal Phycobilisome: Structure, Assembly Components, and Functions. *International Journal of Molecular Sciences*, *24*(11), 9733. https://doi.org/10.3390/ijms24119733

Lin, J.-Y., Tan, S.-I., Yi, Y.-C., Hsiang, C.-C., Chang, C.-H., Chen, C.-Y., Chang, J.-S., & Ng, I.-S. (2022). High-level production and extraction of C-phycocyanin from cyanobacteria *Synechococcus* sp. PCC7002 for antioxidation, antibacterial and lead adsorption. *Environmental Research*, *206*, 112283. https://doi.org/10.1016/j.envres.2021.112283

Lin, P.-C., Saha, R., Zhang, F., & Pakrasi, H. B. (2017). Metabolic engineering of the pentose phosphate pathway for enhanced limonene production in the cyanobacterium *Synechocysti s sp*. PCC 6803. *Scientific Reports*, *7*(1), Article 1. https://doi.org/10.1038/s41598-017-17831-y

Linthwaite, V. L., Janus, J. M., Brown, A. P., Wong-Pascua, D., O'Donoghue, A. C., Porter, A., Treumann, A., Hodgson, D. R. W., & Cann, M. J. (2018). The identification of carbon dioxide mediated protein post-translational modifications. *Nature Communications*, *9*(1), Article 1. https://doi.org/10.1038/s41467-018-05475-z

Ma, J., & Wang, P. (2021). Effects of rising atmospheric CO2 levels on physiological response of cyanobacteria and cyanobacterial bloom development: A review. *Science of The Total Environment*, *754*, 141889. https://doi.org/10.1016/j.scitotenv.2020.141889

MacColl, R. (2004). Allophycocyanin and energy transfer. *Biochimica et Biophysica Acta (BBA) - Bioenergetics*, *1657*(2), 73–81. https://doi.org/10.1016/j.bbabio.2004.04.005

Marx, A., & Adir, N. (2013). Allophycocyanin and phycocyanin crystal structures reveal facets of phycobilisome assembly. *Biochimica et Biophysica Acta (BBA) - Bioenergetics*, *1827*(3), 311–318. https://doi.org/10.1016/j.bbabio.2012.11.006

Miao, R., Liu, X., Englund, E., Lindberg, P., & Lindblad, P. (2017). Isobutanol production in *Synechocystis* PCC 6803 using heterologous and endogenous alcohol dehydrogenases. *Metabolic Engineering Communications*, *5*, 45–53. https://doi.org/10.1016/j.meteno.2017.07.003

Minato, T., Teramoto, T., Adachi, N., Hung, N. K., Yamada, K., Kawasaki, M., Akutsu, M., Moriya, T., Senda, T., Ogo, S., Kakuta, Y., & Yoon, K.-S. (2021). Non-conventional octameric structure of C-phycocyanin. *Communications Biology*, *4*(1), 1–10. https://doi.org/10.1038/s42003-021-02767-x

Montgomery, B. L. (2017). Seeing new light: Recent insights into the occurrence and regulation of chromatic acclimation in cyanobacteria. *Current Opinion in Plant Biology*, *37*, 18–23. https://doi.org/10.1016/j.pbi.2017.03.009

Novoveská, L., Nielsen, S. L., Eroldoğan, O. T., Haznedaroglu, B. Z., Rinkevich, B., Fazi, S., Robbens, J., Vasquez, M., & Einarsson, H. (2023). Overview and Challenges of Large-Scale Cultivation of Photosynthetic Microalgae and Cyanobacteria. *Marine Drugs*, *21*(8), Article 8. https://doi.org/10.3390/md21080445

Ramazi, S., & Zahiri, J. (2021). Post-translational modifications in proteins: Resources, tools and prediction methods. *Database*, *2021*, baab012. https://doi.org/10.1093/database/baab012

Raud, M., Kikas, T., Sippula, O., & Shurpali, N. J. (2019). Potentials and challenges in lignocellulosic biofuel production technology. *Renewable and Sustainable Energy Reviews*, *111*, 44–56. https://doi.org/10.1016/j.rser.2019.05.020

Shestakov, S. V., & Karbysheva, E. A. (2017). The origin and evolution of cyanobacteria. *Biology Bulletin Reviews*, *7*(4), 259–272. https://doi.org/10.1134/S2079086417040090

Shimakawa, G., Akimoto, S., Ueno, Y., Wada, A., Shaku, K., Takahashi, Y., & Miyake, C. (2016). Diversity in photosynthetic electron transport under [CO2]-limitation: The cyanobacterium *Synechococcus sp*. PCC 7002 and green alga Chlamydomonas reinhardtii drive an O2-dependent alternative electron flow and non-photochemical quenching of chlorophyll fluorescence during CO2-limited photosynthesis. *Photosynthesis Research*, *130*(1), 293–305. https://doi.org/10.1007/s11120-016-0253-y

Song, K., Tan, X., Liang, Y., & Lu, X. (2016). The potential of *Synechococcus elongatus* UTEX 2973 for sugar feedstock production. *Applied Microbiology and Biotechnology*, *100*(18), 7865–7875. https://doi.org/10.1007/s00253-016-7510-z

Terrier, P., & Douglas, D. J. (2010). Carbamino group formation with peptides and proteins studied by mass spectrometry. *Journal of The American Society for Mass Spectrometry*, *21*(9), 1500–1505. https://doi.org/10.1016/j.jasms.2010.05.008

The phycobilisome, a light-harvesting complex responsive to environmental conditions. (n.d.). https://doi.org/10.1128/mr.57.3.725-749.1993

The UniProt Consortium. (2023). UniProt: The Universal Protein Knowledgebase in 2023. *Nucleic Acids Research*, *51*(D1), D523–D531. https://doi.org/10.1093/nar/gkac1052

Wang, B., Eckert, C., Maness, P.-C., & Yu, J. (2018). A Genetic Toolbox for Modulating the Expression of Heterologous Genes in the Cyanobacterium *Synechocystis sp*. PCC 6803. *ACS Synthetic Biology*, *7*(1), 276–286. https://doi.org/10.1021/acssynbio.7b00297

Wang, L., Chen, L., Yang, S., & Tan, X. (2020). Photosynthetic Conversion of Carbon Dioxide to Oleochemicals by Cyanobacteria: Recent Advances and Future Perspectives. *Frontiers in Microbiology*, *11*. https://doi.org/10.3389/fmicb.2020.00634

Weiss, T. L., Young, E. J., & Ducat, D. C. (2017). A synthetic, light-driven consortium of cyanobacteria and heterotrophic bacteria enables stable polyhydroxybutyrate production. *Metabolic Engineering*, *44*, 236–245. https://doi.org/10.1016/j.ymben.2017.10.009